NC-1059, A CHANNEL FORMING PEPTIDE, INDUCES A REVERSIBLE CHANGE IN BARRIER FUNCTION OF EPITHELIAL MONOLAYERS

by

SUMA SOMASEKHARAN

M.S, Kasturba Medical College, India, 2000

AN ABSTRACT OF A DISSERTATION

submitted in partial fulfillment of the requirements for the degree

DOCTOR OF PHILOSOPHY

Graduate Biochemistry Group

KANSAS STATE UNIVERSITY

Manhattan, Kansas

2008

Abstract

NC-1059 is a synthetic channel-forming peptide that provides for ion transport across, and transiently reduces barrier integrity of, cultured epithelial monolayers derived from canine kidney (MDCK cells; Broughman, J. R. et al; *Am J Physiol Cell Physiol 286: C1312-23*). In this first study experiments were conducted to determine whether epithelial cells derived from other sources were similarly affected. Human (T84, Calu-3) and non-human (IPEC-J2, PVD9902) epithelial cells derived from intestinal (T84, IPEC-J2), airway (Calu-3), and genitourinary (PVD9902) tissues were grown on permeable supports. Ion transport and barrier function were assessed electrically in a modified Ussing chamber. Basal short circuit current (I_{sc}) was typically less than 3 μA cm^{-2}. Apical NC-1059 exposure caused, in all cell types, an increase in I_{sc} to >15 μA cm^{-2}, indicative of net anion secretion or cation absorption that was followed by an increase in transepithelial conductance (g_{te} in mS cm^{-2}; T-84, 1.6 to 62; PVD9902, 0.2 to 51; IPEC-J2, 0.3 to 26; Calu-3, 2.2 to 13). NC-1059 induces a concentration dependent change in the I_{sc} and g_{te} across these epithelia. The results in all cases were consistent with both a transcellular and a paracellular effect of the peptide. NC-1059 enhanced permeation of dextrans ranging from 10 kDa to 70 kDa across all epithelia tested. These results document an effect of NC-1059 on the paracellular route of epithelial barriers. Immunolabeling, confocal microscopy and immunoblotting methods were used in a second study to assess the molecular changes associated with increased paracellular permeability. NC-1059 induced a substantial reorganization of actin within 60 minutes of exposure. Confocal microscopy revealed that the changes in actin organization were accompanied by a pronounced change in the abundance and distribution of

tight junction proteins occludin and ZO-1. Immunoblotting results suggest a time and concentration dependent effect on cellular abundance of these tight junction proteins. The effects on g_{te} and junctional proteins are transient with > 85% of recovery in 24 hours post exposure and full recovery within 48 hours. The reversible modulation of the epithelial tight junctions has therapeutic potential to increase the efficiency of drug delivery across barrier membranes.

NC-1059, A CHANNEL FORMING PEPTIDE, INDUCES A REVERSIBLE CHANGE IN BARRIER FUNCTION OF EPITHELIAL MONOLAYERS

by

SUMA SOMASEKHARAN

M.S, Kasturba Medical College, India, 2000.

A DISSERTATION

submitted in partial fulfillment of the requirements for the degree

DOCTOR OF PHILOSOPHY

Graduate Biochemistry Group

KANSAS STATE UNIVERSITY

Manhattan, Kansas

2008

Approved by:

Co-Major Professor

Dr John M Tomich

Approved by:

Co-Major Professor

Dr Bruce Schultz

Copyright

Abstract

NC-1059 is a synthetic channel-forming peptide that provides for ion transport across, and transiently reduces barrier integrity of, cultured epithelial monolayers derived from canine kidney (MDCK cells; Broughman, J. R. et al; *Am J Physiol Cell Physiol 286: C1312-23*). In this first study experiments were conducted to determine whether epithelial cells derived from other sources were similarly affected. Human (T84, Calu-3) and non-human (IPEC-J2, PVD9902) epithelial cells derived from intestinal (T84, IPEC-J2), airway (Calu-3), and genitourinary (PVD9902) tissues were grown on permeable supports. Ion transport and barrier function were assessed electrically in a modified Ussing chamber. Basal short circuit current (I_{sc}) was typically less than 3 μA cm^{-2}. Apical NC-1059 exposure caused, in all cell types, an increase in I_{sc} to >15 μA cm^{-2}, indicative of net anion secretion or cation absorption that was followed by an increase in transepithelial conductance (g_{te} in mS cm^{-2}; T-84, 1.6 to 62; PVD9902, 0.2 to 51; IPEC-J2, 0.3 to 26; Calu-3, 2.2 to 13). NC-1059 induces a concentration dependent change in the I_{sc} and g_{te} across these epithelia. The results in all cases were consistent with both a transcellular and a paracellular effect of the peptide. NC-1059 enhanced permeation of dextrans ranging from 10 kDa to 70 kDa across all epithelia tested. These results document an effect of NC-1059 on the paracellular route of epithelial barriers. Immunolabeling, confocal microscopy and immunoblotting methods were used in a second study to assess the molecular changes associated with increased paracellular permeability. NC-1059 induced a substantial reorganization of actin within 60 minutes of exposure. Confocal microscopy revealed that the changes in actin organization were accompanied by a pronounced change in the abundance and distribution of tight junction proteins occludin and ZO-1. Immunoblotting results suggest a time and

concentration dependent effect on cellular abundance of these tight junction proteins. The effects on g_{te} and junctional proteins are transient with > 85% of recovery in 24 hours post exposure and full recovery within 48 hours. The reversible modulation of the epithelial tight junctions has therapeutic potential to increase the efficiency of drug delivery across barrier membranes.

Table of Contents

List of Figures

List of Tables

Acknowledgments

I have utmost gratitude towards my advisors, **Dr Bruce Schultz and Dr John Tomich** for having provided the guidance and support that has made my doctoral pursuit a truly enriching experience.

I express gratitude to **Dr. Takeo Iwamoto** who has sythesized several batches of NC-1059 and other peptides I have used thus far.

I thank my fellow lab members, **Ryan Carlin, Dr Rebecca Quesnell, Dr Pradeep Malreddy, Sarah Devlin** and all past and current members of the Schultz lab. I extend thanks to **Yasuaki Hiromasa, Gary Radke** and all other members of the Tomich lab for their assistance throughout my Ph.D.

I express utmost gratitude to **Dr. Peying Fong** for all the help she has provided.

I thank my committee members, **Dr. Lawrence Davis, Dr. Michael Kanost and Dr. John Schlup**. I am grateful to Joel **Sanemman, Dr. Philline Wangemann, Nithya Raveendran and Dr. Daniel Marcus** and his laboratory members.

I am most thankful that I have the most wonderful family and friends. I particularly like to thank my brothers **Sujit** and **Sudeep**, my husband **Hari**, and dear friends and other family members for their love and support without which all of this would not have been possible.

Dedication

I dedicate my doctorate to my **parents** Soumini Somasekharan and late M.G.Somasekharan Pillai, for their sacrifices, unconditional love and constant support that they have provided throughout my life. My parents have been a source of inspiration, strength and guidance to me.

CHAPTER 1 - Background

Overview:

This section will start at the level of the epithelium and will focus on the pathway between cells (i.e., the paracellular pathway) that solutes and solvent might traverse to move between mucosal (apical) and serosal (basolateral) solutions. The paracellular pathway will be examined first from an electrical perspective to provide a foundation for the measurement techniques employed in this research project. A morphological and molecular perspective of the paracellular pathway will then be presented. The types of cell-cell contacts in epithelial tissues, the types of proteins that are involved in forming these contacts and their functions will be described. The final component of this section will introduce mechanisms that are employed to modify the paracellular pathway and this section will include an introduction to synthetic channel-forming peptides that were discovered and initially described by members of this laboratory.

Epithelia: Epithelial tissues are made up of tightly packed cells that are arranged in one or more layers that line internal and external body surfaces including the skin, nasopharyngeal, gastrointestinal, genitourinary tracts and organs of the body. Epithelial cells have diverse shapes, sizes, and morphological characteristics such as the presence of cilia, which give them unique capabilities. Epithelial layers, irrespective of location serve as selective barriers to the flow of molecules. These tissues protect the underlying tissue from exposure to harmful chemicals and organisms and also maintain the composition of the compartments that they separate. There are two major routes for the movement of solutes across epithelial layers; transcellular and paracellular. The transcellular route allows the movement of hydrophobic molecules. Epithelial

cell membranes have a variety of channels, carriers and pumps that help in the movement or uptake of hydrophilic molecules that would otherwise be excluded. The paracellular pathway also shows charge and size selectivity and therefore limits the movement of most hydrophilic molecules. The movement of charged solutes across an epithelial barrier can be measured electrically with a scheme as depicted in Fig 1.1.

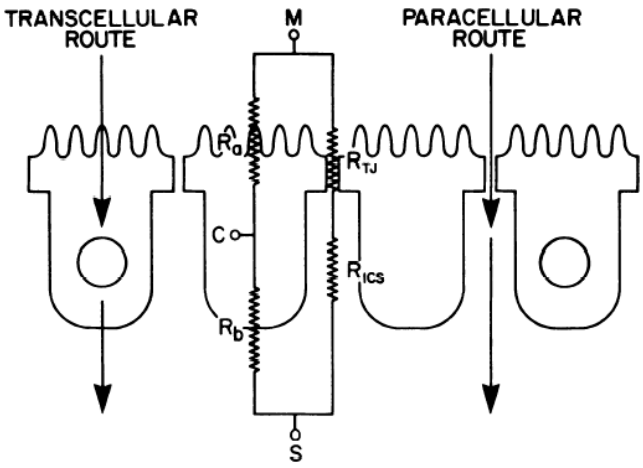

Figure 1.1: Representation of an epithelium as a simplified electrical circuit.

Two pathways for solute movement across epithelia are depicted, i.e., transcellular and paracellular. The electrical circuit represents the epithelium as a series of resistors. M denotes the mucosal or apical node and S the serosal or basolateral node. R_a and R_b are the resistances across apical and basolateral membranes, respectively and R_{tj} and R_{ics} are the resistances across the tight junctions and lateral intercellular space, respectively. C indicates the cellular node. (The figure is adapted from, Powell, 1981)

Transepithelial electrical conductance (g_{te}) is commonly used as a measure of epithelial barrier integrity. The epithelium shows characteristic electrical properties and can be modeled

mathematically as an electrical circuit. In Fig. 1.1 is a simplified representation of this electrical circuit (Powell, 1981). In the circuit, the apical and basolateral membrane resistances, R_a and R_b are in series and R_c is the transcellular resistance = $R_a + R_b$. The paracellular resistance R_s, is the sum of the tight junction (R_{tj}) and intercellular space resistances (R_{ics}) (i.e., $R_s = R_{tj} + R_{ics}$). R_s is modeled in parallel with R_c. Hence the transepithelial resistance (R_{te}) can be determined (i.e., $R_{te} = (R_c)(R_s)/R_c + R_s$). Since conductance ($g$) is inversely proportional to the resistance (according to Ohm's law g=1/R) the information provided in Fig. 1.1 can also be presented in terms of electrical conductance, g. The transcellular conductance, g_c is the sum of the reciprocals of the apical membrane conductance (g_a) and the basolateral membrane conductance (g_b). g_s represents the paracellular conductance, which likewise is the sum of the reciprocal of the conductance across the tight junction (g_{tj}) and the conductance associated with the lateral intercellular space (g_{is}). g_{te}, which can be readily measured in the laboratory, is the sum of g_c and g_s. In commonly studied epithelia the g_c is small as compared to the g_s and hence a dramatic change in g_{te} most often reflects an increase in g_s (Cereijido & Anderson, 2001).

Several factors influence g_{te} including the density of the paracellular route, which depend on size and shape of the individual epithelial cells as shown in Fig. 1.2 (Cereijido & Anderson, 2001). Hence, epithelia that differ in morphology can vary greatly in basal g_{te}. Epithelia that have a high g_{te} are called "leaky" and epithelia with a low g_{te} are referred to as "tight" (Cereijido & Anderson, 2001). In several epithelia, large changes in g_{te} can reflect a change in g_s, and are an indicator that the integrity of the tight junctions and intercellular spaces as a barrier to solute flow are compromised. The integrity of the paracellular route is maintained by a complex network of junctional and cytosolic proteins.

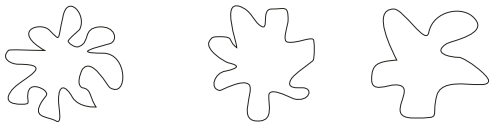

Figure 1.2: Epithelial cell shape can influence the density of intercellular spaces and hence g_{te}.

As the ratio of lateral surface area to cross sectional area increases, density or linear amount of intercellular space per unit area of epithelium will increase (Cereijido & Anderson, 2001).

Ultrastructure of the intercellular space: Electron microscopy images of intercellular junctions in various epithelia were described by Farqhuar and Palade as "tripartite complexes" that were divided into three intercellular regions from apical to basolateral: *zonula occludens* (tight junctions); *zonula adherens* (adheren junctions); and *macula adherens* (desmosomes; Fig. 1.3) (Farquhar & Palade, 1963). In observations made with electron micrographs of several different tissues (Farquhar & Palade, 1963) the *zonula occludens* extended from apical to basolateral by 0.2 to 0.5 μm (Fig. 1.4). The electron micrographs also revealed that the intercellular lumen is wider at the level of the *zonula adherens*, than at the *zona occludens* Fig. 1.4A. The overall adheren junction appears to be 25 nm wide and extend by ~ 0.3 to 0.5 μm along the intercellular space (Farquhar & Palade, 1963). The desmosomes lie below the adheren junction and are surrounded by filaments called intermediate filaments (Fig 1.3 and 1.4A) (Farquhar & Palade, 1963).

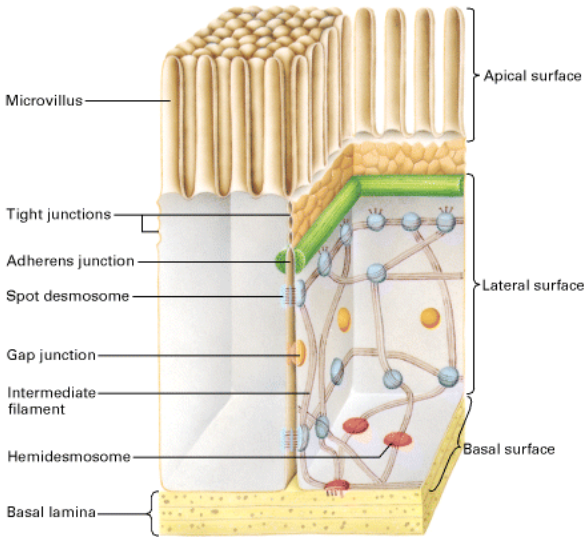

Figure 1.3: An idealized perspective of cell-cell contacts and the intercellular space.

Tight junctions form a continuous band between adjacent cells near the apical boundary of contact. Adheren junctions lie below (i.e., basal) to the tight junctions and are followed by the desmosomes, which are associated with intermediate filaments. Additionally the adjoining cells communicate through gap junctions. (Adapted from Molecular Cell Biology, Lodish et al., 1995).

Ultrastructure of the tight junctions: Farqhuar and Palade named the tight junctions *zonula occludens,* which translates as "closing belt" in Latin, based on their observations that, at the level of the tight junctions, the lumen was extremely narrow, being only ~ 11 nm wide (Farquhar & Palade, 1963). Electron micrographs of tight junctions revealed two outer membranes and two inner membranes that appose each other but at some regions, the inner membranes were so close

together that they appeared as one membrane. These regions of focal contacts are informally called “kisses” (Fig. 1.4B) (Lodish et al., 1995). Freeze fracture replicas of the “kisses” show a network of anastamosing strands that are partitioned onto the protoplasmic leaflet (P face) of the freeze fracture and show corresponding grooves on the exoplasmic leaflet (E face; Fig. 1.5) (Staehelin, 1973). Immunogold labeling of the freeze fracture tissue shows that integral membrane proteins that constitute a part of the junctional multimolecular complex are localized along these strands, which are mostly on the P face. The distribution of these strands onto the P face is attributed to strong links of these integral membrane proteins to cytoplasmic and cytoskeletal proteins (Cereijido & Anderson, 2001).

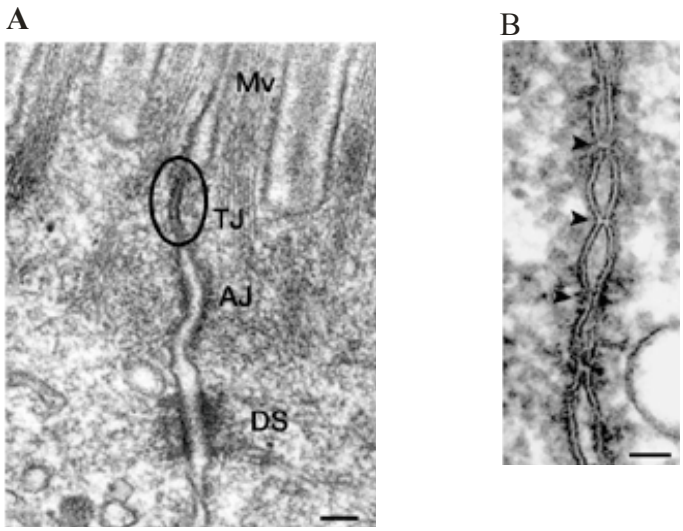

Figure 1.4: Electron micrographs of intercellular spaces between epithelia.

Electron micrograph of intercellular spaces between epithelia showing tight junctions (TJ), adheren junctions (AJ) and desmosomes (DS) along with the intercellular space. Microvilli (Mv) extend from the apical face of the cells. Panel B is an enlargement of the tight junctions where the arrowheads indicate points of focal contacts or "kisses". Scale bar is 200 nm in Fig. A and 50 nm in Fig. B (Adapted from Tsukita, Furuse & Itoh, 2001)

Figure 1.5: Freeze fracture replicas of epithelial cell focal contacts or tight junctions.

Freeze fracture replicas of tight junctions between epithelial cells clearly showing 'strands' or 'kisses'. The left figure is the P face and the right is the E face with strands in the P face and corresponding grooves in the E face (Figure adapted from Staehelin, 1973).

Tight junctions:

Tight junctions are “multimolecular complexes” that include integral membrane proteins, plaque proteins and several cytosolic proteins (Fig. 1.6).

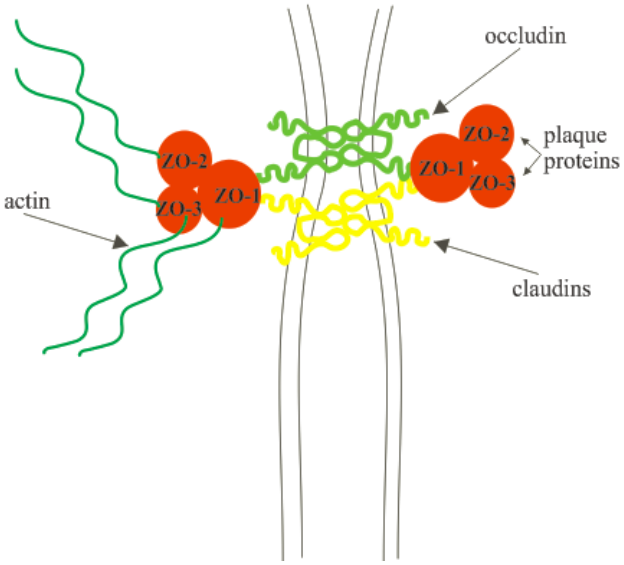

Figure 1.6: Organization of junctional proteins and the molecules involved in their regulation.

The figure represents the organization of proteins at the tight junctions. a single focal contact or “kiss” is depicted. The transmembrane proteins occludin and claudins associate with with the plaque proteins ZO-1, ZO-2 and ZO-3. The figure also shows actin, which binds the plaque proteins. (Figure modified from Mitic & Anderson, 1998).

The major integral membrane proteins, occludin, claudin family proteins and junction adhesion molecules (JAM), are localized at the most apical region of the paracellular route. The plaque proteins serve as a link between the integral membrane proteins and the actin cytoskeleton,

predominantly through specific binding sequences known as PDZ domains. The major plaque proteins are ZO-1, 2 and 3 (Fig. 1.6), multi-PDZ domain protein-1 (MUPP-1), membrane associated guanylate kinase inverted proteins (MAGI-1, 2 and 3), and the partitioning defective proteins (PAR-3 and 6) (Schneeberger & Lynch, 2004). The tight junctions also include a large number of cytosolic molecules including tumor suppressors, regulatory proteins and transcriptional factors. These cytosolic proteins interact directly or indirectly with the plaque proteins.

Transmembrane proteins at the tight junctions:

Occludin: Occludin was first identified in rat liver extract and found to be localized at the tight junctions (Furuse et al., 1993). Immunoblotting has shown several bands for occludin that range in mobility from 58 kDa to 82 kDa based on degree of phosphorylation (Sakakibara et al., 1997). The predicted topology of the protein, as shown in Fig. 1.7, reveals that the N-terminal half has 4 membrane spanning regions and the C-terminus is a large cytosolic domain.

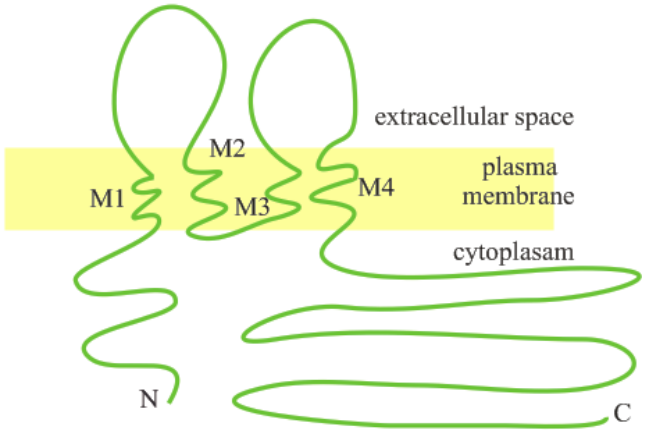

Figure 1.7: Predicted membrane topology of occludin.

M1 –M4 represent the membrane spanning domains of occludin. (Modified from Furuse et al., 1993).

A second occludin isoform, occludin 1B, contains 56 additional residues in the amino-terminal cytosolic tail and exhibits a similar expression pattern (Schneeberger & Lynch, 2004). Regardless of isoform, the membrane spanning regions, M1-M2 and M3-M4, form extracellular loops (Fig. 1.7). In the M1-M2 loop 25% of the residues are tyrosine and 36.4% residues are glycine. In the M3-M4 loop 18% of the residues are tyrosine. These tyrosine residues are potential targets for several protein kinases (Furuse et al., 1993). It is suggested that occludin exists in a hyperphosphorylated form at the tight junctions (Sakakibara et al., 1997). Most of the C-terminal half is conserved among species and has several charged residues. The midsection of the cytoplasmic domain is populated by basic residues whereas the tip of the C-terminus is not conserved and has several acidic residues. The C-terminus is a target for protein kinases. The tip of the C-terminus is involved in protein-protein interactions with guanlylate kinase (GUK) domains of ZO-1, ZO-2 and ZO-3, F-actin and cingulin (Furuse et al., 1994; Li et al., 2005; Paris et al., 2007). The C-terminus of occludin is proposed to be responsible for the localization of occludin at the tight junctions (Furuse et al., 1994). The role of occludin at the tight junctions is poorly understood. Over expression of occludin resulted in a decrease in transepithelial conductance, but surprisingly there was an increase in paracellular permeability as determined using mannitol, which is a hydrophilic molecule that can only permeate the paracellular route (Balda et al., 1996). Furthermore, occludin knockdown did not prevent the formation of functional tight junctions or affect g_{te} but affected the kind of claudins that were expressed (Cereijido & Anderson, 2001). Although evidence indicates that occludin contributes to the regulation of paracellular permeation, its fundamental role is not yet defined.

Junction adhesion molecules (JAMs): JAM-1 or JAM-A is one of four JAMs identified so far. JAM-1 is a 42 kDa glycoprotein that belongs to the large immunoglobulin family. It has one transmembrane domain and two IgG-like folds in the extracellular domain (Fig 1.8; Schneeberger & Lynch, 2004) JAM-1 has PDZ binding sites in its cytosolic tail and interacts with the PDZ domain of ZO-1, MUPP-1 and several other membrane associated guanylate kinase (MAGUK) proteins (Schneeberger & Lynch, 2004). JAM-1 plays a role in maintaining cell morphology and are involved in the assembly of junctional proteins and polarization of epithelia.

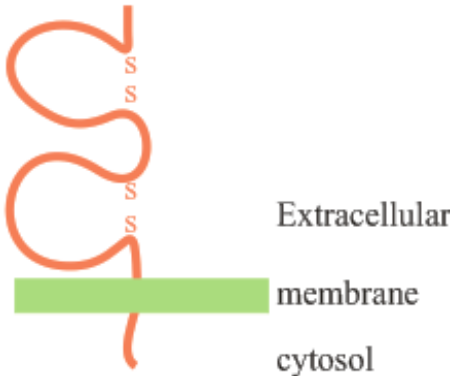

Figure 1.8: Membrane topology of JAM-1.

JAM-1 has two IgG folds in the extracellular domain. (Figure adapted from Schneeberger & Lynch, 2004).

Claudins: Twenty four isoforms of claudin have been identified thus far. Claudins-1 and 2 were identified first as ~22 kDa bands from chicken liver fraction that was enriched with junctional proteins (Furuse et al., 1998). Claudin isoforms are now attributed to be the predominant proteins

in the anastamosing strands in freeze fractures replicas (see Fig. 1.5) (Cereijido & Anderson, 2001). The sequence of claudin-1 and 2 derived from chicken liver extract suggested that they were transmembrane proteins with 4 membrane spanning regions (Furuse et al., 1998). The predicted membrane topology of claudins (Fig. 1.9) includes 2 extracellular loops of which one loop is larger. The loops of several claudins have charged residues and these extracellular loops vary greatly in net charge. Hence each loop has a distinct isoelectric point (Turksen & Troy, 2004).

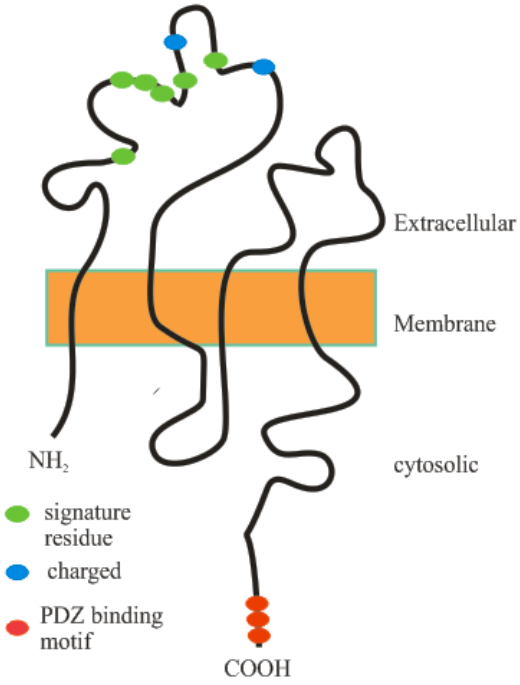

Figure 1.9: Membrane topology of claudins.

The distribution of signature residue motifs (WWCC) and charged residues depicted in the first extracellular loop is distinct for each claudin isoform. The COOH terminus has a conserved PDZ binding motif as shown. (Figure modified from Van Itallie & Anderson, 2004).

The claudins are speculated to form ion selective pores in the tight junction and also implicated in size selectivity, thus regulating paracellular permeability (Fig. 1.10; Turksen & Troy, 2004). The replacement of a basic residue in the extracellular loop of claudin-4 decreased paracellular permeability for Na^+ versus Cl^- without affecting the permeation of uncharged molecules through the paracellular route whereas replacing the acidic residues in the extracellular loop of claudin-15 shifted the permeability ratio to favor Cl^- instead of Na^+ (Colegio et al., 2002). These results suggest that claudins might form channels that confer ion selectivity to the paracellular route as depicted in Fig. 1.10 and expression of specific combination of claudins might be the basis for differences in g_{te} in different epithelia. MDCK I cells, which were considered to be "tight" epithelia as indicated by a very low g_{te}, when transfected with claudin-2 that is usually lacking in this epithelia became "leaky" (Furuse et al., 2001), which again suggested that the g_{te} in this epithelial model might be influenced by the type of claudins that are expressed.

The cytosolic portion of claudins is mostly conserved with the exception of a portion of the cytoplasmic C-terminal tail, which shows significant divergence among different claudin isoforms. There is a YV sequence at the COOH-terminus of most claudins that is the site of interaction with the PDZ domains of ZO-1, 2 and 3 that link the claudins to the cytoskeleton (Itoh et al., 1999). The cytoplasmic tail reportedly is observed to be necessary for proper targeting of claudins to the apical cell junctions (Turksen & Troy, 2004).

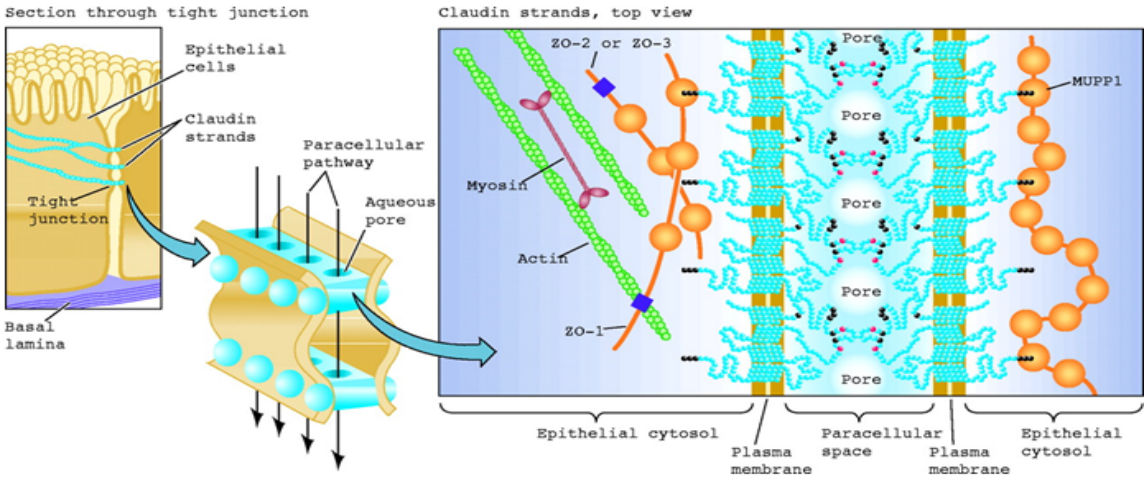

Van Itallie, C. M. et al. Physiology 19: 331-338 2004;
doi:10.1152/physiol.00027.2004

Figure 1.10: Claudins are speculated to form ion channels in the paracellular space.

The left panel is an idealized cross-sectional view of the tight junctions. Claudin strands are predicted to polymerize and form homo-and hetero-dimers along the junctional space in such a way as to form pores as depicted in the middle panel. The right panel is a representation of claudins forming ion selective pores at the tight junctions. The figure also shows the association of claudins with the plaque proteins ZO-1, ZO-2 and ZO-3 and also another plaque protein MUPP-1. The plaque proteins associate with actin as shown in the figure. (Figure adapted from Van Itallie & Anderson, 2004).

Claudins are differentially expressed in various epithelia and endothelia. Claudin-5 has been observed only in the endothelium. Clauidin-11 is restricted to the myelin sheath of oligodendrocytes. Claudin-16 is exclusively expressed in the thick ascending limb of the loop of Henle, the distal tubules and collecting duct in the kidneys. The genetic disease familial hypomagnesemia with hypercalcuria is associated with mutations in claudin-16 and characterized by defective re-absorption of Mg^{2+} and Ca^{2+}. Claudin-14 is expressed only in the organ of corti in the inner ear (Turksen & Troy, 2004). Most epithelia express more than one isoform of claudin. Based on experiments where L cells were transfected with more than one

kind of claudin, it has been proposed that the tight junctions constitute linear co-polymers of occludin and claudins. Claudins from adjacent cells show both homophilic and heterophilic interactions (Furuse, Sasaki & Tsukita, 1999).

Plaque proteins: Plaque proteins are adaptors for cytosolic proteins involved in cell signaling and also form complexes with other cytosolic proteins in order to establish apical-basolateral polarity and bring about tight junction assembly (Furuse et al., 1994; McNeil, Capaldo & Macara, 2006). Among all the plaque proteins mentioned above, the most prominent and first to be identified is ZO-1. ZO-1 and the related plaque proteins, ZO-2 and ZO-3 have significant interactions with most junctional proteins (Paris et al., 2007; Schneeberger & Lynch, 2004).

ZO-1: ZO-1 is a 225 kDa plaque protein that belongs to the MAGUK protein family (Fanning et al., 1998). The N-terminal half of ZO-1 is homologous to other MAGUKS and has 3 PDZ domains, an SH3 domain, and an inactive GUK domain as shown in Fig. 1.11 (Funke, Dakoji & Bredt, 2005). The C-terminal half has a unique proline rich region (Fanning et al., 1998; Fanning, Ma & Anderson, 2002). Splice variants of ZO-1 may be differentially distributed in epithelial and endothelial tissue (Mitic & Anderson, 1998; Schneeberger & Lynch, 2004). ZO-1 is as a scaffold protein that has several protein-protein interaction domains. The PDZ domains of ZO-1 interact with several junctional proteins including ZO-2, claudins and JAM-1 (Funke et al., 2005). The GUK domain and the adjacent region rich in acidic residues associates with the C-terminus of occludin (Li et al., 2005). ZO-1 also interacts with actin through its proline rich region (Fanning et al., 1998; Fanning et al., 2002). ZO-1 also associates with several actin binding proteins (Schneeberger & Lynch, 2004)

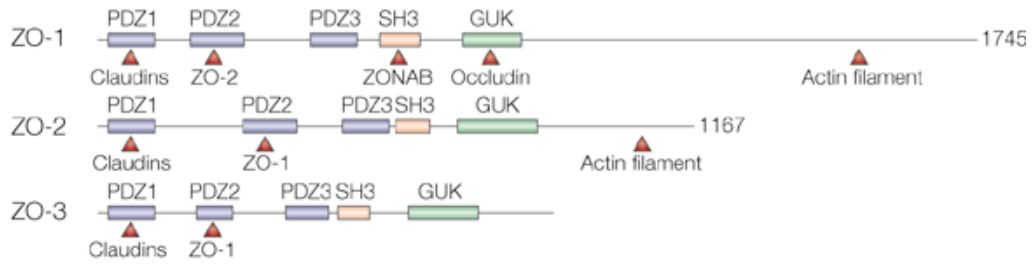

Figure 1.11: A modular representation of the various protein domains in ZO-1, ZO-2 and ZO-3.

These domains are sites of protein-protein interactions and below each individual figure are indicated the proteins that bind these domains. (Adapted from Tsukita, Furuse & Itoh, 2001)

ZO-2 and ZO-3: ZO-2 is a 160 kDa protein that has ~51% homology with ZO-1 and also binds several tight junction proteins, adheren junction proteins and actin. ZO-3 is a 130 kDa and is least similar of the three ZO proteins (Funke et al., 2005). All three proteins share the PDZ, SH3 and GUK domains that are characteristic of most MAGUKS (Fig. 1.11; Schneeberger & Lynch, 2004; Tsukita, Furuse & Itoh, 2001).

Adheren junctions: Adheren junctions are formed primarily by the interactions of cadherin and catenin families of proteins. The cadherin that is present in epithelial cells is called E-cadherin (epithelial cadherin). The cadherin and interacting catenins along with several regulatory molecules play a significant role to maintain cell adhesions. The adheren junction molecules regulate cytoskeletal rearrangements necessary for cell turnover and cell migration in cases such as wound healing (Gumbiner, 2005).

E-cadherin belongs to the superfamily of cadherin proteins and specifically to the sub family of classical cadherins (Cavallaro & Christofori, 2004; Gumbiner, 2005; Hartsock & Nelson, 2007). E-cadherin is a glycoprotein with a single transmembrane domain. It has 5 extracellular repeat

domains (EC-1-5; Fig. 1.12) that are stabilized by Ca^{2+} (Gumbiner, 2005). This region is followed by the transmembrane domain (TM). The juxtamembrane domain (JMD) and the cytoplasmic catenin binding domain (CMD) are the two catenin binding domains. E-cadherin is organized as dimers at the adheren junction and form homophilic interactions with the cadherins of adjacent cells. The CBD interacts with β-catenin and the JMD interacts with the p120 catenin and the E-3 ubiquitin ligase, Hakai (Fig. 1.12; Cavallaro & Christofori, 2004; Hartsock & Nelson, 2007).

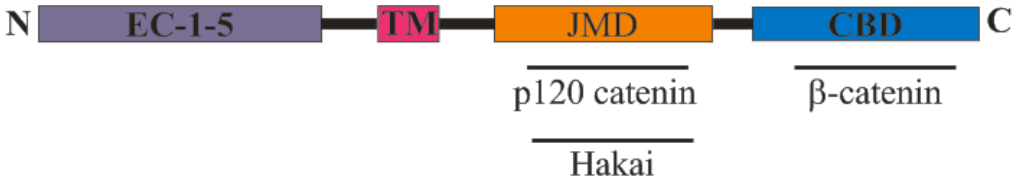

Figure 1.12: Modular representation of the domains in E-cadherin and interacting molecules.

The extracellular domains (EC), is followed by the transmembrane domain (TM) and the cytosolic domains include the juxtamembrane domain (JMD) and the catenin binding domain (CBD). (Figure modified from Hartsock & Nelson, 2007).

Catenins are involved in connecting cadherins to the cytoskeleton (Gumbiner, 2005). β-catenin is an armadillo repeat protein. The protein is so described, after the same domain found in the drosophila protein armadillo. The armadillo repeats are 40 residue sequences that assemble as helices and are present in signalling molecules. The core of the protein is made of helices of

armadillo repeat sequences that are assembled into a superhelix. This superhelix has a positively charged groove that is involved in interactions with several proteins and also subject to regulation by several kinases (Daugherty & Gottardi, 2007). β-catenin binds α-catenin, which in turn associates with actin and thus serves to link E-cadherin to the cytoskeleton (Daugherty & Gottardi, 2007). The other major catenin that associates with E-cadherin is the p120 catenin.

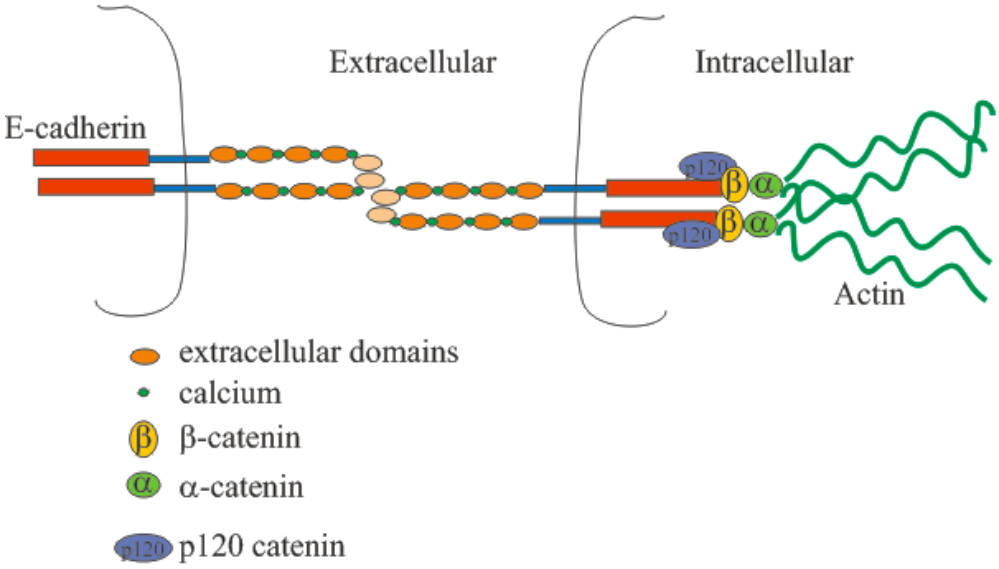

Figure 1.13: Interaction of E-cadherin, catenins and actin.

E-cadherin forms homodimers that associate with the homodimers of adjacent cells through the extracellular domains. The α, β and p120 catenins associate directly or indirectly with E-cadherin and actin. (Figure was modified from Cavallaro & Christofori, 2004).

The interaction between E-cadherin and β-catenin is subject to regulation by several kinases. The serine phosphorylation of E-cadherin by glycogen synthase kinase 3β (GSK3β) and casein kinase 2 (CK2) increases the affinity of interaction with β-catenin by several fold whereas serine

phosphorylation by CK1 decreases the affinity (Daugherty & Gottardi, 2007). Tyrosine phosphorylation of both E-cadherin and β-catenin decreases the affinity of interaction between the two proteins (Daugherty & Gottardi, 2007). The interaction of β-catenin with E-cadherin is necessary to prevent E-cadherin from being degraded (Daugherty & Gottardi, 2007). It has been shown that tyrosine phosphorylation targets E-cadherin for rapid degradation. The E-3 ligase, Hakai (Fig. 1.12), has been implicated in the proteosomal degradation of E-cadherin (Fujita et al., 2002).

GSK3β and CK1 are also involved in regulation of β-catenin. Phosphorylation by these kinases targets β-catenin for proteosomal degradation (Daugherty & Gottardi, 2007). However, activation of a serine-threonine phosphatase, PP1 by wnt signalling prevents degradation of β-catenin (Cavallaro & Christofori, 2004; Daugherty & Gottardi, 2007). Activation of this cascade by wnt increases cytosolic β-catenin protein levels, which then enters the nucleus where it activates several transcription factors. Hence β-catenin is involved in cell proliferation and also tumorogenesis (Daugherty & Gottardi, 2007).

The GTPases, Rho and Rac, of the small G protein family that are involved in regulating F-actin organization are also involved in the localization of E-cadherin to the adheren junctions. Inhibition of Rac and Rho has been reported to decrease E-cadherin immunoreactivity (Braga et al., 1997). It is speculated that these GTPases act together to regulate localization of E-cadherin at the intercellular junctions. E-cadherin and β-catenin associate with ZO-1 and are observed to be early players in the assembly of tight junctions (Gumbiner, Stevenson & Grimaldi, 1988; Rajasekaran et al., 1996). Hence the functional roles of E-cadherin and β-catenin involve cytoskeletal rearrangements to mediate changes in cell shape and regulate cell migration, turnover and proliferation. They might also be necessary to promote tight junction assembly.

Actin cytoskeleton: Actin is a 42-45 kDa, abundant protein encoded by a gene family that is highly conserved. In humans, six genes code for actin. Four α actin isoforms are expressed predominantly in muscle cells and the β and γ actin isoforms are expressed in non-muscle cells. Actin exists in 2 physical forms in cellular cytoplasm, a monomeric globular form called G-actin and a polymeric filamentous form called F-actin. F-actin is formed by the polymerization of G-actin (Lodish et al., 1995).

Actin filaments are distributed throughout the cell and are an integral component of the cell cytoskeleton. Most of the F-actin in the cell exists in the form of microfilaments. Microfilaments are short actin filaments that associate with certain actin binding proteins that help associate microfilaments into specific structures. Microfilaments are arranged as bundles or networks based on localization and function. Bundles are formed by the parallel arrangement of microfilaments that are stabilized and connected to each other through short cross-linking proteins. Networks are formed by the association of microfilaments with long cross-linking proteins. In epithelial cells, the microfilaments are present in microvilli, the cortex, and in stress fibers. Microvilli are found along the apical surface of the cells and have longitudinal bundles of microfilaments. The cortex is a region just below the plasma membrane. The cortical actin cytoskeleton is a dense network of microfilaments (Lodish et al., 1995). Stress fibers are formed by bundles of microfilaments and are present either at the leading edges of migrating cells or lying at the basal portion of adherent cells (Lodish et al., 1995). The apical junctional complexes, the tight junctions and adheren junctions, associate with actin filaments that circumscribe the cell. These actin filaments associate with myosin II and form the perijunctional actomyosin II complex (Lodish et al., 1995). The perijunctional actomyosin ring circumscribes the cell at the region of the *zonula adherens* (Lodish et al., 1995).

Polymerization of actin: G-actin has a cleft in the middle that separates its two lobes and in this cleft is an ATP binding site. Both G and F-actin are associated with ATP or ADP. The ATP bound monomers of G-actin polymerize and after polymerization, the ATP is hydrolyzed to ADP. Thus, most of the F-actin consists of ADP-G-actin monomers. The process of polymerization depicted in Fig. 1.14, does not necessarily require ATP hydrolysis although the rate of polymerization is greater in the presence of ATP. The ATP bound cleft is called the (+) end and the other end of the monomer is the (-) end. G-actin monomers add on to the growing filament, preferably towards the + end and hence the filament grows more rapidly from its (+) end than the (-) end (Lodish et al., 1995). The polymerization is reversible. G and F-actin exist in equilibrium at a certain critical concentration (Lodish et al., 1995).

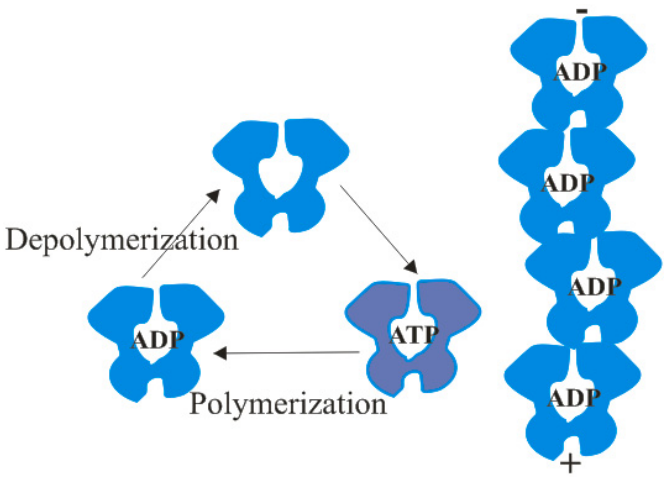

Figure 1.14: Polymerization of actin.

Figure modified from www.cytochemistry.net (Childs, 2001).

Compounds that disrupt the equilibrium between G-actin and F-actin can increase the rate of depolymerization of F-actin. Cytochalasin is a compound that binds to the (+) end of F-actin and prevents the addition of G-actin monomers. Latrunculin A is a toxin secreted by sponges that binds to G-actin and prevents polymerization. Phalloidin, a toxin derived from the mushroom *Amantia phalloides*, binds F-actin such that F-actin cannot depolymerize (Lodish et al., 1995). Based on this property, phalloidin linked to fluorescent dyes is commonly used to visualize actin in cells.

In non-migrating cells, the network of actin is responsible for maintaining the cytoplasm in a gel like state. In migrating cells, the cytoplasm is in a solution state allowing for easy movement of the cell. The transition between the "gel" and "sol" state is mediated by the proteins gelsolin and clofilin. These proteins are actin severing proteins that break actin filaments into smaller fragments and prevent re-polymerization by remaining bound to the (+) end of the fragments (Lodish et al., 1995).

Signalling pathways regulate the tight and adheren junctions: The family of small GTP proteins that include Rho, Rac and Cdc42 are modulators of the actin cytoskeleton. These proteins play a significant role in actin-based activities such as cell migration and cytoskeletal rearrangements. Rearrangements of the cytoskeletal proteins, especially actin, are increasingly associated with regulation of epithelial and endothelial junctional proteins (Bruewer et al., 2004; Jou, Schneeberger & Nelson, 1998). Both constitutively active and dominant negative mutants of Rho, Rac and Cdc42 cause reorganization of F-actin and either induction or loss of stress fibers (Bruewer et al., 2004). Toxins from *Clostridium* species that ADP-ribosylate or glucosylate Rho reduce Rho GTPase activity and hence cause depolymerization of actin filaments (Bruewer et al.,

2004; Hecht et al., 1992; Moore et al., 1990). Changes in the activity of these GTPases, in most cases, result in an increase in g_{te} and paracellular permeability associated with a disruption of junctional proteins (Bruewer et al., 2004). Rho family proteins, particularly Rho A, play a significant role in modulating actin organization (Fig. 1.15). Rho affects actin organization through Rho kinase (also known as ROCK), which can cause a direct or indirect phosphorylation of myosin light chain (MLC) (Riento & Ridley, 2003). Decreased Rho activity is associated with a decrease in phosphorylation status of MLC. Both phosphorylation and dephosphorylation of MLC alter actin organization (Riento & Ridley, 2003; Turner et al., 1997). Activation of myosin light chain kinase (MLCK) causes an increase in MLC phosphorylation, g_{te} and paracellular permeability, primarily by a reorganization of actin cytoskeleton (Clayburgh et al., 2004). Physiological events such as increased sodium glucose uptake through SGLT-1 (Turner et al., 1997), hyperosmotic stress and hyperpolarization enhance g_{te} and paracellular permeability by increasing MLC phosphorylation (Di Ciano-Oliveira et al., 2003; Szaszi et al., 2005). Hence MLCK activity and RhoA/ROCK activity are associated with increased ppMLC (dual phosphorylated myosin light chain). However it must be noted that events that are associated with MLC dephosphorylation such as ATP depletion and benzylkonium chloride exposure (a surfactant used to enhance corneal permeability) also cause a reorganization of actin and increased permeability involving a loss in localization of one or more junctional proteins (Bacallao et al., 1994; Guo et al., 2007; Mandel, Doctor & Bacallao, 1994). Disruption of actin is often associated with changes in junction protein organization and paracellular permeability. Moreover the junctional proteins associate directly or indirectly with the perijunctional actin ring. Hence it is proposed that changes in contractility of the perijunctional actomyosin ring might regulate paracellular permeability (Madara, 1998).

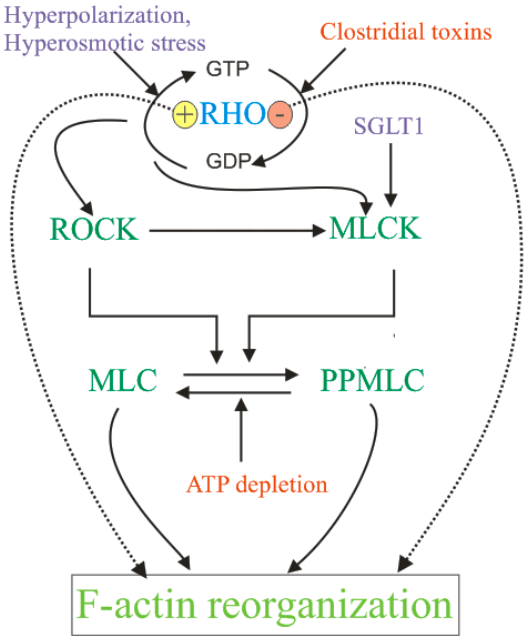

Figure 1.15: Regulation of F-actin organization by the Rho signaling pathway.

Tight junction proteins are phosphorylated or dephosphorylated by several serine threonine and tyrosine kinases or phosphatases that can either cause redistribution of these proteins away from the cell-cell contact regions or promote assembly of the junction. Several protein kinase C (PKC) isoforms are involved in regulation of the junctional proteins. The role of PKC in modulating the junctional proteins varies based on cell type and isoform as shown in Fig. (1.16).

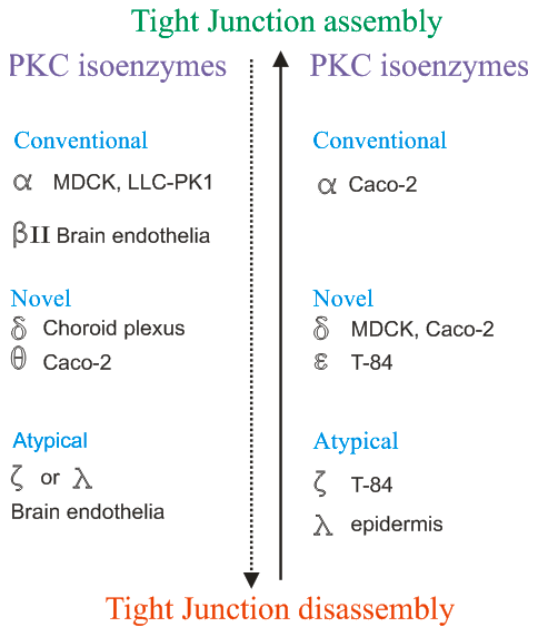

Figure 1.16: PKC isoenzymes in various cell types and their role in regulation of tight junction assembly.

(figure modified from Gonzalez-Mariscal, Tapia & Chamorro, 2007)

Oxidative stress, extracellular and intracellular Ca^{2+} and toxins such as zona occludens toxin (ZOT) and toxin A from *Clostridium difficle* are among the triggers for the activation of a PKC isoform that mediates reorganization of the actin cytoskeleton and also causes the disruption of tight junction proteins. Several other serine threonine kinases (e.g. MAPK) and phosphatases (PP1a and PP2), receptor and non receptor tyrosine kinases such as c-src, WNK-4 and c-yes also

influence tight junction permeability by phosphorylation or dephosphorylation of occludin, ZO-1 and claudins (Gonzalez-Mariscal, Tapia & Chamorro, 2007).

Extracellular molecules that modulate paracellular permeability:

The multimolecular complex that regulates paracellular permeability is a target for several extracellular molecules that modulate barrier function. These include molecules that mediate physiological events, toxins that have pathological effects and therapeutic molecules that are designed to enhance paracellular permeability. Several bacterial and fungal toxins disrupt epithelial barriers. A few examples include the enterotoxin produced by *Clostridium perifringens* and the fungal toxin, Ochratoxin A, which cause degradation of claudin-4 (Schneeberger & Lynch, 2004), (McLaughlin et al., 2004). ZOT (zona occludens toxin), which is derived from *Vibrio cholerae*, induces time-and dose-dependent rearrangement of F-actin, possibly through a PKCα dependent mechanism (Fasano et al., 1995). *Clostridium difficile* toxins A and B disrupt GTPase activity of Rho family proteins by UDP-glucosylation (Richard et al., 1999). They increase paracellular permeability by causing the disorganization of apical and basal F-actin and eventually ZO-1, 2 and occludin. *Bactrioides fragilis* toxin (BFT) is a metalloprotease that cleaves E-cadherin and also causes a reorganization of F-actin (Richard et al., 1999; Wu et al., 1998; Wu et al., 2007; Wu et al., 2006), thereby changing cell morphology and increasing barrier function.

Several charged molecules such as protamines, chitosans and polylysines also increase g_{te} and paracellular permeability. Protamine is an arginine rich polycationic peptide that affects barrier integrity of epithelial monolayers (Peterson & Gruenhaupt, 1992). Confocal images of MDCK I cells exposed to protamine showed condensation of the F-actin microfilaments and reduced

occludin immunoreactivity in a concentration dependent manner (Peixoto & Collares-Buzato, 2005).

Therapeutic modulation of paracellular permeability:

There is a strong link between permeability of solutes across the paracellular route and the arrangement of actin and various junctional proteins. Moreover several signalling pathways are involved in modulating the localization and organization of these proteins. Molecules that can disrupt this fine equilibrium and induce transient changes in permeability are useful in opening the paracellular pathway to solutes and provide a means to deliver therapeutic molecules across these selective epithelial barriers.

A variety of techniques is being investigated currently to selectively and transiently circumvent the barrier function of epithelia and endothelia. Methods are being developed to reduce epithelial tight junctions enough to allow large molecules to diffuse to the interstitial space. ZOT provides a naturally occurring alternative for increasing the permeability of small intestine epithelia (Fasano et al., 1997). ZOT and its eukaryotic homologue, zonulin, interact with an epithelial membrane receptor that leads to a reduction in epithelial resistance, presumably by activation of PKCα (Fasano, 2000; Fasano et al., 1995). The effects of ZOT are rapid in onset (< 20 minutes) and readily reversible on washout (Fasano, 2000). Thus ZOT is an excellent candidate as an adjunct to standard therapy to increase oral bioavailability of large molecules (Fasano & Uzzau, 1997). In fact, ZOT has been used to increase the permeation of anticonvulsant drugs across epithelial monolayers (Karyekar et al., 2003), to increases the uptake of PEG 4000 from rabbit small intestine (Salama et al., 2003), and increase intestinal permeability to insulin and immunoglobulins (Fasano & Uzzau, 1997). In diabetic rats, the bioavailability of oral insulin was sufficient to control blood glucose to the same degree as parenteral administration when co-

adminstered with ZOT (Fasano & Uzzau, 1997). However, ZOT has some drawbacks as a more generalized therapeutic in that it is a large peptide (399 A.A.) and its effects are observed only in the small intestine where distinct receptors are present (Uzzau et al., 2001). Small peptides derived from ZOT (e.g. AT1002, a six residue peptide) have shown promise in enhancing drug delivery (Song, Fasano & Eddington, 2007a; Song, Fasano & Eddington, 2007b).

Peptides corresponding to the first and second extracellular loops of occludin have been tested as tight junction modulators. The earliest occludin peptides synthesized were ~ 44 amino acid sequences that had a sequence based on that of the first and second extracellular domains of chick occludin. The peptides were tested on A6 cells (derived from *Xenopus*) and the peptide corresponding to the second extracellular loop resulted in a five fold increase in the g_{te} after 5 days of exposure. The peptide allowed for permeation of large dextrans (up to 40 kDa) after 36 hours of exposure and the effect of the peptide was reversible (Wong & Gumbiner, 1997). The second set of peptides studied also had sequences based on chick occludin extracellular loops. These peptides increased g_{te} in minutes (Lacaz-Vieira et al., 1999). Synthetic peptides, based on the sequence of the second extracellular loop of rat occludin tested on the rat sertoli cells resulted in an increase in g_{te} after 4 to 5 days (Chung et al., 2001). Peptides based on the sequence of the first and second extracellular loops of human occludin were tested on the Caco-2 cells, which are derived from human colon. A 24 amino acid peptide corresponding to the first extracellular loop was effective in increasing g_{te} and allowed for permeability of small molecules such as mannitol. The peptides were effective from the basolateral side and took more than six hours to increase paracellular permeability significantly (Tavelin et al., 2003). In order to have effect from the apical side, occludin peptides modified by the addition of chemical groups such as lipoamino

acid have been designed and are showing promise in increasing permeability (Everett et al., 2006; Tavelin et al., 2003).

Channel forming peptides and modulation of paracellular permeability:

A series of channel forming peptides have been synthesized in this laboratory with the ultimate goal of generating a compound that can enhance apical Cl^- conductance and serve as a substitute for endogenous Cl^- channels that are defective in diseases such as cystic fibrosis. M2GlyR is a 23 residue peptide based on the sequence of the second transmembrane segment M2 of the glycine receptor (GlyR), which is a Cl^- selective channel (Reddy et al., 1993). M2GlyR increased Cl^- conductance across lipid bilayers with single channel conductance matching that of the glycine receptor (Reddy et al., 1993). However, the aqueous solubility of this peptide was poor and proved to be a limitation to test the peptide in epithelial monolayers. Solubility was enhanced by the addition of four lysine residues at the C-terminus of M2GlyR generating the peptide CK_4-M2GlyR (PARVGLGITTVLTMTTGSSGSRAKKKK; Tomich et al., 1998; Wallace et al., 1997). CK_4-M2GlyR increased anion secretion across epithelial monolayers and the secretion was inhibited by a Cl^- channel blocker, diphenylamine-2-carboxylate (Wallace et al., 1997). The addition of four lysines at the N-terminus of M2GlyR to generate NK_4-M2GlyR (KKKKPARVGLGITTVLTMTTGSSGSRA) resulted in a peptide that elicited an indicator of short circuit current (I_{sc}), an indicator of anion secretion or cation absorption that was 50% greater than its CK_4 counterpart (Broughman et al., 2001). Further studies revealed that in the lysine residues at the C-terminus (CK_4) masked a nucleation site by forming a capping structure and limited the oligomerization of this peptide (Broughman et al., 2002a) an effect not observed with the amino lysine residues (NK_4). These results suggested that the C-terminal portion of the peptide was involved in aggregation. Furthermore the removal of C-terminus residues resulted in

a decrease in aggregation and removal of 11 residues from the C-terminus virtually eliminated aggregation (Broughman et al., 2002b). The effect of the truncated peptide on I_{sc} remained unaltered until the removal of 5 residues from the C-terminus and I_{sc} progressively decreased with subsequent removal of C-terminus residues (Broughman et al., 2002b). Taken together the results suggested that the C-terminus was responsible for aggregation and that only the N-terminus residues might be necessary to form ion channels. Hence, a peptide that has a sequence based on the N-terminal half of NK4-M2 GlyR was designed. The peptide is palindromic around the central leucine. The final sequence, KKKKAARVGLGITTVLVTTIGLGVRAA was named NC-1059 (Broughman et al., 2002b).

NC-1059 increased anion secretion and g_{te} across MDCK monolayers in a concentration dependent manner (Broughman et al., 2004). NC-1059 induced increase in g_{te} reached a peak value and remained elevated even after the I_{sc} declined (Broughman et al., 2004). This suggested that in addition to an increase in transcellular conductance, NC-1059 also increased paracellular conductance. Dextran molecules can only permeate the paracellular route. Hence various sizes of dextran were used to determine whether the permeation through the paracellular route was enhanced by NC-1059 and also to establish the size selectivity of the enhanced paracellular flux. NC-1059 enhanced the permeation of molecules as large as 9.5 kDa but not 77 kDa (Broughman et al., 2004). This established that NC-1059 enhanced paracellular permeability in a size selective manner. The increase in g_{te} was reversible and the monolayers returned to pretreatment g_{te} and permeation within 48 hours (Broughman et al., 2004). These results demonstrated that NC-1059 is a compound that can reversibly alter the barrier function of epithelial monolayers and enhance paracellular permeation of hydrophilic molecules. Hence NC-1059 holds potential to be developed as a co-therapeutic to aid in drug delivery across epithelia.

The next two chapters build on observations regarding NC-1059 that has been presented above. Experiments were conducted to determine if the effects of NC-1059 can be generalized to epithelia derived from a variety of tissue sources and the underlying molecular changes that accompany the effects on paracellular permeability. Experiments detailed in chapter 2 were designed to determine whether the permeability enhancing effects of NC-1059 can be generalized to epithelial cell models that are derived from other sources. Chapter 3 focuses on molecular mechanisms that account for the changes in paracellular permeability that were reported. Particular attention was paid to the location and abundance of actin and the junctional proteins ZO-1 and occludin. Chapter 4 provides a brief summary of the observations along with concluding remarks.

References:

Bacallao, R., Garfinkel, A., Monke, S., Zampighi, G., Mandel, L.J. 1994. ATP depletion: a novel method to study junctional properties in epithelial tissues. I. Rearrangement of the actin cytoskeleton. *J Cell Sci* **107 (Pt 12):**3301-13

Balda, M.S., Whitney, J.A., Flores, C., Gonzalez, S., Cereijido, M., Matter, K. 1996. Functional dissociation of paracellular permeability and transepithelial electrical resistance and disruption of the apical-basolateral intramembrane diffusion barrier by expression of a mutant tight junction membrane protein. *J Cell Biol* **134:**1031-49

Braga, V.M., Machesky, L.M., Hall, A., Hotchin, N.A. 1997. The small GTPases Rho and Rac are required for the establishment of cadherin-dependent cell-cell contacts. *J Cell Biol* **137:**1421-31

Broughman, J.R., Brandt, R.M., Hastings, C., Iwamoto, T., Tomich, J.M., Schultz, B.D. 2004. Channel-forming peptide modulates transepithelial electrical conductance and solute permeability. *Am J Physiol Cell Physiol* **286:**C1312-23

Broughman, J.R., Mitchell, K.E., Sedlacek, R.L., Iwamoto, T., Tomich, J.M., Schultz, B.D. 2001. NH(2)-terminal modification of a channel-forming peptide increases capacity for epithelial anion secretion. *Am J Physiol Cell Physiol* **280:**C451-8

Broughman, J.R., Shank, L.P., Prakash, O., Schultz, B.D., Iwamoto, T., Tomich, J.M., Mitchell, K. 2002a. Structural implications of placing cationic residues at either the NH2- or COOH-terminus in a pore-forming synthetic peptide. *J Membr Biol* **190:**93-103

Broughman, J.R., Shank, L.P., Takeguchi, W., Schultz, B.D., Iwamoto, T., Mitchell, K.E., Tomich, J.M. 2002b. Distinct structural elements that direct solution aggregation and membrane assembly in the channel-forming peptide M2GlyR. *Biochemistry* **41:**7350-8

Bruewer, M., Hopkins, A.M., Hobert, M.E., Nusrat, A., Madara, J.L. 2004. RhoA, Rac1, and Cdc42 exert distinct effects on epithelial barrier via selective structural and biochemical modulation of junctional proteins and F-actin. *Am J Physiol Cell Physiol* **287:**C327-35

Cavallaro, U., Christofori, G. 2004. Cell adhesion and signalling by cadherins and Ig-CAMs in cancer. *Nat Rev Cancer* **4:**118-32

Cereijido, M., Anderson, J. *Tight Junctions* Boca Raton CRC Press 2001

Childs, G.V. 2001. The Actin Cytoskeleton.

Chung, N.P., Mruk, D., Mo, M.Y., Lee, W.M., Cheng, C.Y. 2001. A 22-amino acid synthetic peptide corresponding to the second extracellular loop of rat occludin perturbs the blood-testis barrier and disrupts spermatogenesis reversibly in vivo. *Biol Reprod* **65:**1340-51

Clayburgh, D.R., Rosen, S., Witkowski, E.D., Wang, F., Blair, S., Dudek, S., Garcia, J.G., Alverdy, J.C., Turner, J.R. 2004. A differentiation-dependent splice variant of myosin light chain kinase, MLCK1, regulates epithelial tight junction permeability. *J Biol Chem* **279:**55506-13

Colegio, O.R., Van Itallie, C.M., McCrea, H.J., Rahner, C., Anderson, J.M. 2002. Claudins create charge-selective channels in the paracellular pathway between epithelial cells. *Am J Physiol Cell Physiol* **283:**C142-7

Daugherty, R.L., Gottardi, C.J. 2007. Phospho-regulation of Beta-catenin adhesion and signaling functions. *Physiology (Bethesda)* **22:**303-9

Di Ciano-Oliveira, C., Sirokmany, G., Szaszi, K., Arthur, W.T., Masszi, A., Peterson, M., Rotstein, O.D., Kapus, A. 2003. Hyperosmotic stress activates Rho: differential involvement in Rho kinase-dependent MLC phosphorylation and NKCC activation. *Am J Physiol Cell Physiol* **285:**C555-66

Everett, R.S., Vanhook, M.K., Barozzi, N., Toth, I., Johnson, L.G. 2006. Specific modulation of airway epithelial tight junctions by apical application of an occludin peptide. *Mol Pharmacol* **69:**492-500

Fanning, A.S., Jameson, B.J., Jesaitis, L.A., Anderson, J.M. 1998. The tight junction protein ZO-1 establishes a link between the transmembrane protein occludin and the actin cytoskeleton. *J Biol Chem* **273:**29745-53

Fanning, A.S., Ma, T.Y., Anderson, J.M. 2002. Isolation and functional characterization of the actin binding region in the tight junction protein ZO-1. *FASEB J* **16:**1835-7

Farquhar, M.G., Palade, G.E. 1963. Junctional complexes in various epithelia. *J Cell Biol* **17:**375-412

Fasano, A. 2000. Regulation of intercellular tight junctions by zonula occludens toxin and its eukaryotic analogue zonulin. *Ann N Y Acad Sci* **915:**214-22

Fasano, A., Fiorentini, C., Donelli, G., Uzzau, S., Kaper, J.B., Margaretten, K., Ding, X., Guandalini, S., Comstock, L., Goldblum, S.E. 1995. Zonula occludens toxin modulates tight junctions through protein kinase C-dependent actin reorganization, in vitro. *J Clin Invest* **96:**710-20

Fasano, A., Uzzau, S. 1997. Modulation of intestinal tight junctions by Zonula occludens toxin permits enteral administration of insulin and other macromolecules in an animal model. *J Clin Invest* **99:**1158-64

Fasano, A., Uzzau, S., Fiore, C., Margaretten, K. 1997. The enterotoxic effect of zonula occludens toxin on rabbit small intestine involves the paracellular pathway. *Gastroenterology* **112:**839-46

Fujita, Y., Krause, G., Scheffner, M., Zechner, D., Leddy, H.E., Behrens, J., Sommer, T., Birchmeier, W. 2002. Hakai, a c-Cbl-like protein, ubiquitinates and induces endocytosis of the E-cadherin complex. *Nat Cell Biol* **4:**222-31

Funke, L., Dakoji, S., Bredt, D.S. 2005. Membrane-associated guanylate kinases regulate adhesion and plasticity at cell junctions. *Annu Rev Biochem* **74:**219-45

Furuse, M., Fujita, K., Hiiragi, T., Fujimoto, K., Tsukita, S. 1998. Claudin-1 and -2: novel integral membrane proteins localizing at tight junctions with no sequence similarity to occludin. *J Cell Biol* **141:**1539-50

Furuse, M., Furuse, K., Sasaki, H., Tsukita, S. 2001. Conversion of zonulae occludentes from tight to leaky strand type by introducing claudin-2 into Madin-Darby canine kidney I cells. *J Cell Biol* **153:**263-72

Furuse, M., Hirase, T., Itoh, M., Nagafuchi, A., Yonemura, S., Tsukita, S. 1993. Occludin: a novel integral membrane protein localizing at tight junctions. *J Cell Biol* **123:**1777-88

Furuse, M., Itoh, M., Hirase, T., Nagafuchi, A., Yonemura, S., Tsukita, S. 1994. Direct association of occludin with ZO-1 and its possible involvement in the localization of occludin at tight junctions. *J Cell Biol* **127:**1617-26

Furuse, M., Sasaki, H., Tsukita, S. 1999. Manner of interaction of heterogeneous claudin species within and between tight junction strands. *J Cell Biol* **147:**891-903

Gonzalez-Mariscal, L., Tapia, R., Chamorro, D. 2007. Crosstalk of tight junction components with signaling pathways. *Biochim Biophys Acta*

Gumbiner, B., Stevenson, B., Grimaldi, A. 1988. The role of the cell adhesion molecule uvomorulin in the formation and maintenance of the epithelial junctional complex. *J Cell Biol* **107:**1575-87

Gumbiner, B.M. 2005. Regulation of cadherin-mediated adhesion in morphogenesis. *Nat Rev Mol Cell Biol* **6:**622-34

Guo, Y., Satpathy, M., Wilson, G., Srinivas, S.P. 2007. Benzalkonium chloride induces dephosphorylation of Myosin light chain in cultured corneal epithelial cells. *Invest Ophthalmol Vis Sci* **48:**2001-8

Hartsock, A., Nelson, W.J. 2007. Adherens and tight junctions: Structure, function and connections to the actin cytoskeleton. *Biochim Biophys Acta*

Hecht, G., Koutsouris, A., Pothoulakis, C., LaMont, J.T., Madara, J.L. 1992. Clostridium difficile toxin B disrupts the barrier function of T84 monolayers. *Gastroenterology* **102:**416-23

Itoh, M., Furuse, M., Morita, K., Kubota, K., Saitou, M., Tsukita, S. 1999. Direct binding of three tight junction-associated MAGUKs, ZO-1, ZO-2, and ZO-3, with the COOH termini of claudins. *J Cell Biol* **147:**1351-63

Jou, T.S., Schneeberger, E.E., Nelson, W.J. 1998. Structural and functional regulation of tight junctions by RhoA and Rac1 small GTPases. *J Cell Biol* **142:**101-15

Karyekar, C.S., Fasano, A., Raje, S., Lu, R., Dowling, T.C., Eddington, N.D. 2003. Zonula occludens toxin increases the permeability of molecular weight markers and chemotherapeutic agents across the bovine brain microvessel endothelial cells. *J Pharm Sci* **92:**414-23

Lacaz-Vieira, F., Jaeger, M.M., Farshori, P., Kachar, B. 1999. Small synthetic peptides homologous to segments of the first external loop of occludin impair tight junction resealing. *J Membr Biol* **168:**289-97

Li, Y., Fanning, A.S., Anderson, J.M., Lavie, A. 2005. Structure of the conserved cytoplasmic C-terminal domain of occludin: identification of the ZO-1 binding surface. *J Mol Biol* **352:**151-64

Lodish, H., Baltimore, D., Berk, A., Zipursky, L.S., Matsudara, P., Darnell, J. *Molecular Cell Biology* New YorK W. H Freeman and Company 1995.

Madara, J.L. 1998. Regulation of the movement of solutes across tight junctions. *Annu Rev Physiol* **60:**143-59

Mandel, L.J., Doctor, R.B., Bacallao, R. 1994. ATP depletion: a novel method to study junctional properties in epithelial tissues. II. Internalization of Na+,K(+)-ATPase and E-cadherin. *J Cell Sci* **107 (Pt 12):**3315-24

McLaughlin, J., Padfield, P.J., Burt, J.P., O'Neill, C.A. 2004. Ochratoxin A increases permeability through tight junctions by removal of specific claudin isoforms. *Am J Physiol Cell Physiol* **287:**C1412-7

McNeil, E., Capaldo, C.T., Macara, I.G. 2006. Zonula occludens-1 function in the assembly of tight junctions in Madin-Darby canine kidney epithelial cells. *Mol Biol Cell* **17:**1922-32

Mitic, L.L., Anderson, J.M. 1998. Molecular architecture of tight junctions. *Annu Rev Physiol* **60:**121-42

Moore, R., Pothoulakis, C., LaMont, J.T., Carlson, S., Madara, J.L. 1990. C. difficile toxin A increases intestinal permeability and induces Cl- secretion. *Am J Physiol* **259:**G165-72

Paris, L., Tonutti, L., Vannini, C., Bazzoni, G. 2007. Structural organization of the tight junctions. *Biochim Biophys Acta*

Peixoto, E.B., Collares-Buzato, C.B. 2005. Protamine-induced epithelial barrier disruption involves rearrangement of cytoskeleton and decreased tight junction-associated protein expression in cultured MDCK strains. *Cell Struct Funct* **29:**165-78

Peterson, M.W., Gruenhaupt, D. 1992. Protamine interaction with the epithelial cell surface. *J Appl Physiol* **72:**236-41

Powell, D.W. 1981. Barrier function of epithelia. *Am J Physiol cell Physiol* **241:**G275-88

Rajasekaran, A.K., Hojo, M., Huima, T., Rodriguez-Boulan, E. 1996. Catenins and zonula occludens-1 form a complex during early stages in the assembly of tight junctions. *J Cell Biol* **132:**451-63

Reddy, G.L., Iwamoto, T., Tomich, J.M., Montal, M. 1993. Synthetic peptides and four-helix bundle proteins as model systems for the pore-forming structure of channel proteins. II. Transmembrane segment M2 of the brain glycine receptor is a plausible candidate for the pore-lining structure. *J Biol Chem* **268:**14608-15

Richard, J.F., Petit, L., Gibert, M., Marvaud, J.C., Bouchaud, C., Popoff, M.R. 1999. Bacterial toxins modifying the actin cytoskeleton. *Int Microbiol* **2:**185-94

Riento, K., Ridley, A.J. 2003. Rocks: multifunctional kinases in cell behaviour. *Nat Rev Mol Cell Biol* **4:**446-56

Sakakibara, A., Furuse, M., Saitou, M., Ando-Akatsuka, Y., Tsukita, S. 1997. Possible involvement of phosphorylation of occludin in tight junction formation. *J Cell Biol* **137:**1393-401

Salama, N.N., Fasano, A., Lu, R., Eddington, N.D. 2003. Effect of the biologically active fragment of zonula occludens toxin, delta G, on the intestinal paracellular transport and oral absorption of mannitol. *Int J Pharm* **251:**113-21

Schneeberger, E.E., Lynch, R.D. 2004. The tight junction: a multifunctional complex. *Am J Physiol Cell Physiol* **286:**C1213-28

Song, K.H., Fasano, A., Eddington, N.D. 2007a. Effect of the six-mer synthetic peptide (AT1002) fragment of zonula occludens toxin on the intestinal absorption of cyclosporin A. *Int J Pharm*

Song, K.H., Fasano, A., Eddington, N.D. 2007b. Enhanced nasal absorption of hydrophilic markers after dosing with AT1002, a tight junction modulator. *Eur J Pharm Biopharm*

Staehelin, L.A. 1973. Further observations on the fine structure of freeze-cleaved tight junctions. *J Cell Sci* **13:**763-86

Szaszi, K., Sirokmany, G., Di Ciano-Oliveira, C., Rotstein, O.D., Kapus, A. 2005. Depolarization induces Rho-Rho kinase-mediated myosin light chain phosphorylation in kidney tubular cells. *Am J Physiol Cell Physiol* **289:**C673-85

Tavelin, S., Hashimoto, K., Malkinson, J., Lazorova, L., Toth, I., Artursson, P. 2003. A new principle for tight junction modulation based on occludin peptides. *Mol Pharmacol* **64:**1530-40

Tomich, J.M., Wallace, D., Henderson, K., Mitchell, K.E., Radke, G., Brandt, R., Ambler, C.A., Scott, A.J., Grantham, J., Sullivan, L., Iwamoto, T. 1998. Aqueous solubilization of transmembrane peptide sequences with retention of membrane insertion and function. *Biophys J* **74:**256-67

Tsukita, S., Furuse, M., Itoh, M. 2001. Multifunctional strands in tight junctions. *Nat Rev Mol Cell Biol* **2:**285-93

Turksen, K., Troy, T.C. 2004. Barriers built on claudins. *J Cell Sci* **117:**2435-47

Turner, J.R., Rill, B.K., Carlson, S.L., Carnes, D., Kerner, R., Mrsny, R.J., Madara, J.L. 1997. Physiological regulation of epithelial tight junctions is associated with myosin light-chain phosphorylation. *Am J Physiol cell Physiol* **273:**C1378-85

Uzzau, S., Lu, R., Wang, W., Fiore, C., Fasano, A. 2001. Purification and preliminary characterization of the zonula occludens toxin receptor from human (CaCo2) and murine (IEC6) intestinal cell lines. *FEMS Microbiol Lett* **194:**1-5

Van Itallie, C.M., Anderson, J.M. 2004. The molecular physiology of tight junction pores. *Physiology (Bethesda)* **19:**331-8

Wallace, D.P., Tomich, J.M., Iwamoto, T., Henderson, K., Grantham, J.J., Sullivan, L.P. 1997. A synthetic peptide derived from glycine-gated Cl- channel induces transepithelial Cl- and fluid secretion. *Am J Physiol Cell Physiol* **272:**C1672-9

Wong, V., Gumbiner, B.M. 1997. A synthetic peptide corresponding to the extracellular domain of occludin perturbs the tight junction permeability barrier. *J Cell Biol* **136:**399-409

Wu, S., Lim, K.C., Huang, J., Saidi, R.F., Sears, C.L. 1998. Bacteroides fragilis enterotoxin cleaves the zonula adherens protein, E-cadherin. *Proc Natl Acad Sci U S A* **95:**14979-84

Wu, S., Rhee, K.J., Zhang, M., Franco, A., Sears, C.L. 2007. Bacteroides fragilis toxin stimulates intestinal epithelial cell shedding and gamma-secretase-dependent E-cadherin cleavage. *J Cell Sci* **120:**1944-52

Wu, S., Shin, J., Zhang, G., Cohen, M., Franco, A., Sears, C.L. 2006. The Bacteroides fragilis toxin binds to a specific intestinal epithelial cell receptor. *Infect Immun* **74:**5382-90

CHAPTER 2 - Epithelial Barrier Modulation by a Channel Forming Peptide

Suma Somasekharan, Robert Brandt, Takeo Iwamoto, John M. Tomich, and Bruce D. Schultz*.

SS, RB, TI, JMT: Department of Biochemistry, Kansas State University, Manhattan, KS 66506

BDS: Department of Anatomy & Physiology, Kansas State University, Manhattan KS 66506

*Corresponding author: Dr Bruce D Schultz, Kansas State University Department of Anatomy and Physiology, 1600 Denison Avenue, Coles Hall 228, Manhattan, KS-66506

Phone numbers: 785-532-4839 (office), 785-532-4557 (fax).

Email: bschultz@vet.ksu.edu

This chapter has been submitted in this format for review to a peer reviewed journal.

Abstract:

NC-1059 is a synthetic channel-forming peptide that provides for ion transport across, and transiently reduces barrier integrity of, cultured epithelial monolayers derived from canine kidney (MDCK cells)(Broughman et al., 2004). Experiments were conducted to determine whether epithelial cells derived from other sources were similarly affected. Epithelial cells derived from human intestine (T-84), airway (Calu-3), porcine intestine (IPEC-J2) and reproductive duct (PVD9902) were grown on permeable supports. Basal short circuit current (I_{sc}) was typically less than 3 μA cm^{-2} for most epithelia. Apical NC-1059 exposure caused, in all cell types, an increase in I_{sc} to >15 μA cm^{-2}, indicative of net anion secretion or cation absorption that was followed by an increase in transepithelial conductance (in mS cm^{-2}; T-84, 1.6 to 62; PVD9902, 0.2 to 51; IPEC-J2, 0.3 to 26; Calu-3, 2.2 to 13). These results are consistent with the peptide affecting transcellular ion movement with a likely effect also on the paracellular route. NC-1059 exposure increased dextran permeation when compared to basal permeation, which documents an effect on the paracellular pathway. In order to evaluate membrane ion channels, experiments were conducted to study the dose dependence and stability of the NC-1059-induced membrane conductance in *Xenopus laevis* oocytes. NC-1059 induced a dose dependent increase in oocyte membrane conductance that remained stable for greater than 2 hours. The results demonstrate that NC-1059 increases transcellular conductance and paracellular permeation in a wide range of epithelia. These effects might be exploited to promote drug delivery across barrier epithelia.

Key words: Transepithelial conductance, Short circuit current, Dextran Permeability, MDCK, PVD9902, IPEC-J2, Calu-3.

Introduction:

NK_4-M2GlyR (KKKKPARVGLGITTVLTMTTGSSGSRA) is a synthetic channel forming peptide whose sequence is based on the second transmembrane segment (M2) of the glycine receptor (GlyR) alpha-subunit (Broughman et al., 2001; Tomich et al., 1998; Wallace et al., 1997). Lysine residues were added to the N-terminus of M2GlyR to increase aqueous solubility. It was shown subsequently that sequential removal of C-terminus residues from NK_4-M2GlyR reduced aggregation of the peptide in solution and peptides truncated up to five residues from the C-terminus retained ion transport properties (Broughman et al., 2002b). Hence a palindromic peptide consisting of the 11 N-terminal residues from M2GlyR followed by a central leucine and then an inverse sequence of the N-terminal segment, was synthesized to maximize channel-forming activity (Broughman et al., 2002b). Proline residues were replaced with alanines to improve the chemical synthesis to arrive at the final sequence KKKKAARVGLGITTVLVTTIGLGVRAA, which was named NC-1059.

Apical exposure of MDCK cell monolayers to NC-1059 caused a concentration dependent increase in short circuit current (I_{sc}) (Broughman et al., 2004), a measure of net ion transport. Furthermore, the apparent dissociation constant, k_{app}, was reported to be 50 μM, which is four fold lower than the originally designed NK_4-M2GlyR. In these studies, transepithelial electrical conductance (g_{te}) began to increase with I_{sc} and continued to increase even after I_{sc} reached peak value and began to decline. Exposure of MDCK cell monolayers to NC-1059 also increased permeation of 9.5 kDa fluorescein isothiocynate (FITC)-conjugated dextran suggesting that a paracellular route was opened by NC-1059 (Broughman et al., 2004). g_{te} returned to pretreatment values within 2 days after NC-1059 exposure, the shortest time point tested (Broughman et al., 2004). These observations were very encouraging, as there is a tremendous impetus to identify

molecules that may serve as "absorption enhancers" to augment delivery of hydrophilic and large uncharged therapeutics across epithelial barriers (Kondoh & Yagi, 2007).

Tight junctions are multimolecular complexes between apical intercellular regions of epithelial cells that regulate paracellular permeability. Several techniques are being investigated to selectively and transiently reduce barrier function of epithelia or endothelia to allow the diffusion of therapeutic molecules to the interstitial space. Calcium chelators and surfactants disrupt barrier integrity but have unacceptable side effects including changes in cell function and diminished cell adhesion (Thompson, Cavitt & Audus, 1994). Peptides corresponding to first and second extracellular loops of occludin, a tight junction protein, increased paracellular permeability, but required several hours to show significant effects (Chung et al., 2001; Lacaz-Vieira et al., 1999; Tavelin et al., 2003; Wong & Gumbiner, 1997). More recently, a modified occludin peptide was shown to be effective at high concentrations (1 mM) in enhancing permeability across airway epithelia (Everett et al., 2006). The zonula occludens toxin of *Vibrio cholerae* (ZOT) provides a natural alternative to increase the permeability of small intestine epithelia (Fasano & Uzzau, 1997). ZOT has a rapid onset (< 20 minutes) and is reversible. Yet, ZOT has drawbacks as a more generalized co-therapeutic agent in that it is a large peptide (399 amino acids) dependent on the presence of a membrane receptor that may not be present in all epithelia (Fasano et al., 1995).

NC-1059 has the potential to be developed into a co-therapeutic that can increase bioavailability of various drugs. NC-1059 is a small peptide that can be readily synthesized. Additionally, we hypothesize that NC-1059 can modulate barrier function of epithelia derived from varied sources. The goal of the study presented in this paper is to determine the effect of NC-1059 on epithelial cell lines derived from a variety of tissues. This study evaluates the differences in I_{sc}

response, changes in g_{te} and paracellular permeation between different epithelia when exposed to various concentrations of NC-1059. Additionally, studies were conducted using *Xenopus laevis* oocytes to isolate and characterize effects of NC-1059 on membrane conductance independent of effects on cell-cell interactions.

Methods:

Peptide Synthesis: NC-1059 was synthesized by solid phase peptide synthesis using 9-fluorenylmethoxycarbonyl chemistries and purified as described previously (Broughman et al., 2002a).

Chemicals and stock solutions: 1-ethyl-2-benzimidazolinone (1-EBIO) was purchased from Acros (Fisher Scientific, Pittsburgh, PA). Unless specified otherwise, all other chemicals used were purchased from Sigma Aldrich (St. Louis, MO). NC-1059 was prepared as a 5 mM stock in deionized water immediately before addition to the experimental chamber.

Cell Culture: T-84 Cells were obtained from Dr. Daniel Devor (University of Pittsburgh, Pittsburgh, PA) and maintained in culture as described previously (Broughman et al., 2004; Broughman et al., 2001). Cells were grown on 25 cm^2 flasks (Corning Incorporated, Corning, NY) with a medium containing a 1:1 mixture of Dulbecco's modified Eagle medium (DMEM) and Nutrient F12 (Gibco, Invitrogen, Carlsbad, CA), 5% heat inactivated fetal bovine serum (FBS; Atlanta Biologicals, Atlanta, GA) and 1% penicillin and streptomycin (Gibco). Approximately $5*10^5$ cells were seeded onto 1.13 cm^2 permeable supports (Snapwell, Costar, Corning Incorporated). The medium was refreshed every other day until used for experimentation with the last medium change occurring one day prior to analysis. All other cell types were maintained using similar techniques, with some exceptions noted below.

IPEC-J2 cells were provided by Dr. Anthony Blikslager (North Carolina State University, Raleigh, NC) and were grown in a medium containing 1:1 mixture of DMEM and Nutrient F12, 5% heat inactivated FBS, 1% insulin-transferrin-selenium and 1% penicillin and streptomycin.

PVD9902 (Carlin et al., 2006) cells were grown in a medium containing DMEM, 10% heat inactivated FBS, and 1% penicillin and streptomycin. The PVD9902, IPEC-J2 and T-84 cells were grown on the permeable supports, typically for 14 days prior to experimental evaluation.

Calu-3 cells were grown with a medium containing a 1:1 mixture of DMEM and Nutrient F12, 15% heat inactivated FBS, 2 mM glutamine and 1% penicillin and streptomycin. Cells were grown on the permeable supports for 28-34 days. The apical medium was removed on the second day and cells were cultured without medium on the apical surface thereafter until evaluation.

Electrical Measurements: I_{sc} and transepithelial electrical potential were measured using a modified Ussing chamber (model DCV9, Navicyte, San Diego, CA) as described previously (Broughman et al., 2004; Broughman et al., 2001). Monolayers were bathed symmetrically with Ringer solution (in mM: 120 NaCl, 25 $NaHCO_3$, 3.3 KH_2PO_4, 0.8 K_2HPO_4, 1.2 $MgCl_2$, and 1.2 $CaCl_2$) that was prepared fresh daily, maintained at 37ºC, and bubbled with 5% CO_2 / 95% O_2 to maintain pH and to provide mixing. Monolayers were clamped to 0 mV using a voltage clamp apparatus (model 558C-5, University of Iowa, Dept. of Bioengineering, Iowa City, IA). A 5 s bipolar pulse was applied every 100 s to allow for g_{te} assessment. Data acquisition was performed at 1 Hz with an Intel based computer using Aqknowledge software (v. 3.2.6, BIOPAC Systems, Santa Barbara, CA) and MP100A-CE interface. The current measured in response to the voltage pulse was used to calculate g_{te} using Ohms law, $g_{te} = \Delta I/\Delta V$.

Xenopus oocyte isolation: Oocytes were isolated as described previously (Broughman et al., 2004) from human chorionic gonadotropin treated *Xenopus laevis* (Xenopus One, Ann Arbor, MI) that were housed individually at 17ºC. All procedures involving animals were conducted in compliance with American Physiological Society guidelines and the procedure were approved by the university IACUC. The follicular layer of the oocytes was removed using collagenase and

trypsin inhibitor in ND-96 that was nominally Ca^{2+} free (in mM: 96 NaCl, 1 KCl, 1 $MgCl_2$, 5 HEPES, pH=7.5). Oocytes were washed subsequently with nominally Ca^{2+} free ND-96 and incubated in a hypotonic solution (0.1 M K_2HPO_4 and 0.1% bovine serum albumin) for 1 hour with gentle rolling at 15 minute intervals. Oocytes were then maintained in modified Barth's solution (in mM: 88 NaCl, 1 KCl, 0.3 $Ca(NO_3)_2$, 0.41 $CaCl_2$, 0.82 $MgSO_4$, 2.4 $NaHCO_3$, 10 HEPES, pH=7.5) containing penicillin and streptomycin at 17ºC until used.

Membrane conductance measurements: Oocyte membrane conductance was measured as described previously (Broughman et al., 2004) using a two electrode voltage clamp technique. Recordings were conducted in ND-96 (in mM: 96 NaCl, 1 KCl, 1 $MgCl_2$, 1.8 $CaCl_2$, 5 HEPES,). Briefly, the oocytes were impaled with glass pipettes having a Ag/AgCl electrode filled with 1 M KCl. The electrodes were connected to a voltage clamp amplifier (Gene Clamp 500B, Axon Instruments, Foster City, CA) and an analog to digital converter (DigiData 1200, Axon Instruments). The software used for data acquisition and analysis was pClamp 9.0 (Axon Instruments). Oocyte recordings were carried out using 2 voltage clamp protocols. In the first repeating 'diary' protocol, oocytes were sequentially held at -30 mV for 128 ms and then held at -90 mV, -30 mV, 0 mV, and 30 mV for a duration of 1000 ms each (total protocol duration = 4.128 s). The protocol was repeated throughout the recording to assess the stability of the membrane conductance for the entire duration of the experiment. The second 'step' protocol was employed to determine with greater accuracy the slope conductance of the oocyte. The protocol included nine 2048 ms sweeps consisting of an initial 548 ms at -30 mV followed by 1000 ms at the step potential and ending with 500 ms at -30 mV. The step potential ranged from -100 mV to +60 mV at 20 mV increments. A mean current from the middle 250 ms of each step potential

was used to construct a current-voltage relationship (I-V plot). Data were fitted by a linear regression and slope conductance was obtained from the fit.

The dose dependence of the NC-1059-induced changes in *Xenopus laevis* oocyte conductance was determined by making bolus additions of NC-1059 to a flowing bath. Doses of increasing size ranging from 1.25 to 20 nmoles of NC-1059 were added to the bath (~0.5 mL bath with 0.5 mL/min flow rate). Each addition was made after the current reached a plateau following the previous exposure and the slope conductance had been determined using the protocol described above. To determine if the NC-1059-induced conductance remains stable for a long duration, oocytes were exposed to 5 nmoles of NC-1059 and, once the membrane conductance reached a stable value, the step protocol was conducted to determine the slope conductance. The step protocol was repeated periodically thereafter with the entire recording lasting 2 hours.

Dextran permeability assay: Dextran permeation through the monolayer was measured as described previously (Broughman et al., 2004). Media were removed and the monolayers were washed with warm PBS. In untreated and NC-1059 exposed monolayers, Ringer solution was added to the basolateral (1 mL) and apical (200 μL) compartments in the Snapwell culture system. NC-1059 was added to the Ringer solution on the apical side of the monolayers to result in a final concentration of 200 μM NC-1059. Monolayers were also exposed symetrically to 5 mM EDTA in hypotonic Ringer solution (diluted 1:1 with deionized H_2O). FITC conjugated-dextran (0.5 mg of 10, 20, 40 or 70 kDa) was added to the apical compartment of all treatments. After incubation at 37ºC for 1 hour, samples were taken from the basolateral compartment for determination of fluorescence intensity (Fluorskan Ascent FL, Labsystems). A series of dilutions of each size of dextran was prepared and fluorescence determined as a function of concentration.

A linear regression was used to derive the slope and to calculate the amount of dextran that permeated the monolayer.

Data analysis: All results are reported as mean ± SEM. All graphs and regression fits were completed using Sigmaplot (v 6.0, SPSS Inc, Richmond, CA) or Excel (v 11.8, Microsoft Corp, Redmond, WA). The student's t-test (Sigmaplot) and ANOVA (Excel) were used for statistical analysis where required. Concentration dependence was determined using the maximal I_{sc} recorded following exposure to each concentration of NC-1059. Kinetic parameters for concentration dependence were determined by fitting the following modified Hill equation (Eqn. 1) to each data set.

$$I_{sc} = I_{sc\,\min} + \frac{\Delta I_{sc\,\max} \times [NC-1059]^{b}}{(k_{app})^{b} + [NC-1059]^{b}} \qquad \textbf{Eqn. 1}$$

In the above equation $I_{sc\ \min}$ is the basal I_{sc} prior to peptide addition. $\Delta I_{sc\ \max}$ is the greatest increase in I_{sc} observed during exposure to a given concentration of NC-1059. The apparent K_D (k_{app}) is the concentration required to achieve half maximal I_{sc} and b is the Hill coefficient.

The time course for NC-1059 induced changes in g_{te} was determined by fitting with a sigmoidal function (Eqn. 2) to values of g_{te} that were calculated every one hundred seconds throughout each experiment using the time of NC-1059 exposure as the starting point for data acquisition.

$$g_{te} = g_{te\min} + \frac{\Delta g_{te\max}}{1 + e^{-\left[\frac{t-t_0}{b}\right]}} \qquad \textbf{Eqn. 2}$$

In Eqn. 2, $g_{te\ \min}$ is the baseline conductance and $\Delta g_{te\ \max}$ is the peak change in conductance reached during the recording for each concentration. b is inversely proportional to the slope at half $\Delta g_{te\ \max}$. The data used for the fit were restricted to ~300 s after the peak g_{te} was reached.

Results:

NC-1059 induces a change in electrical parameters for all epithelia that were tested. Experiments were conducted to determine if the concentration dependent changes observed in I_{sc} and g_{te} with MDCK cells exposed apically to NC-1059 can be generalized to epithelia derived from different tissues and species. Typical and summarized results for each cell type are presented in Figs. 1 - 4.

T-84 cells derived from human colon: NC-1059 caused a concentration dependent increase in I_{sc} and g_{te} across T-84 cell monolayers. Fig. 1A shows the recording from a typical experiment in which an epithelial cell monolayer was exposed apically to NC-1059 (60 μM). An initial I_{sc} of 2 μA cm^{-2} was measured. The monolayer was exposed to 1-EBIO (300 μM) prior to peptide exposure as indicated by the solid bar. 1-EBIO activates Ca^{2+} sensitive K^+ channels, IK and SK (Devor et al., 1996b), hyperpolarizing the cells and thus increasing the electrochemical driving force for anion secretion. 1-EBIO can also activate the cystic fibrosis transmembrane regulator (CFTR) anion channel (Devor et al., 1996a), although at concentrations higher than required to activate K^+ channels. The concentration of 1-EBIO was selected because it is reported to produce a maximal activation of K^+ channels and below the half-maximal concentration for CFTR activation. Exposure of the T-84 cells to 1-EBIO resulted in a variable increase in I_{sc} that was consistent with SK or IK activation and transient activation of CFTR channels. Once the I_{sc} attained a constant value, the monolayer was exposed to NC-1059. Exposure to the peptide was associated with a characteristic rapid increase in I_{sc} within 4 min from 4 to 38 μA cm^{-2}. Subsequently I_{sc} declined toward baseline, but remained elevated at ~17 μA cm^{-2} for more than 30 minutes. The magnitude of the current change generated in response to the bipolar pulse applied across the monolayers (represented by the vertical deflections in the I_{sc} trace) was used to

calculate g_{te}. Initially, g_{te} was 0.5 mS cm^{-2} and increased to 0.75 mS cm^{-2} with exposure to 1-EBIO. g_{te} further increased immediately upon NC-1059 exposure along with the I_{sc}, which is expected with the introduction of ion channels in the apical membrane. At peak I_{sc}, g_{te} was 2.5 mS cm^{-2}. However, g_{te} continued to increase even after peak I_{sc} was attained and during the decline in I_{sc}. By the end of the recording presented in Fig. 1A, g_{te} had increased to 21 mS cm^{-2}. The results for concentration dependent effects of NC-1059 on I_{sc} are summarized from 6 experiments in Fig. 1B. Prior to NC-1059 exposure, I_{sc} was 6.5 ± 1.5 μA cm^{-2} and maximal $I_{sc,}$ with 200 μM NC-1059, was 65.8 ± 5.2 μA cm^{-2} (n=6). The solid line represents the best fit of Eqn. 1 to the data set. Results of the fit are presented in Table 1. It is noteworthy that the fit employed a Hill coefficient that was greater than unity, which suggests a complex reaction scheme and could be indicative of the peptide's assembly into oligomeric conductive pores. The average change in the g_{te} for each concentration as a function of time is provided in Fig. 1C. The graph revealed that the conductance increased with peptide exposure from a value of ~1 mS cm^{-2} to a maximal value in about 30 minutes and remained elevated throughout the experiment. A significant increase in g_{te} was observed with 30 μM and maximal g_{te} increased with concentration, reaching a maximal value at 100 μM. The peptide at 200 μM did not elicit a response greater than that observed with 100 μM. Parameters derived when Eqn. 2 was fitted to the data sets for 100 and 200 μM are reported in Table 2. The results indicate that the half-maximal response occurred more quickly with exposure to 200 μM than 100 μM, although the maximal conductances were nearly identical. The time to reach half-maximal g_{te} (t_0) was greatest with 30 μM NC-1059 (17.1 ± 0.1 min) and decreased with increasing concentration suggesting a concentration dependent effect on the lag time to reach half maximal change in $g_{te.}$ Additionally, the slope ($1/b$) was greater for 200 μM as compared to 100 μM, further suggesting a

concentration dependent effect on the rate of change in g_{te}. The peak conductance as a function of concentration is provided in Fig. 1D. Little change in g_{te} was observed with 10 μM NC-1059 as compared to untreated monolayers. The g_{te} was significantly greater following exposure to 30 μM NC-1059 and a maximal g_{te} value of ~58 mS cm^{-2} was observed with both 100 μM and 200 μM. The maximal g_{te} that is reported approached the limit that the system can detect reliably.

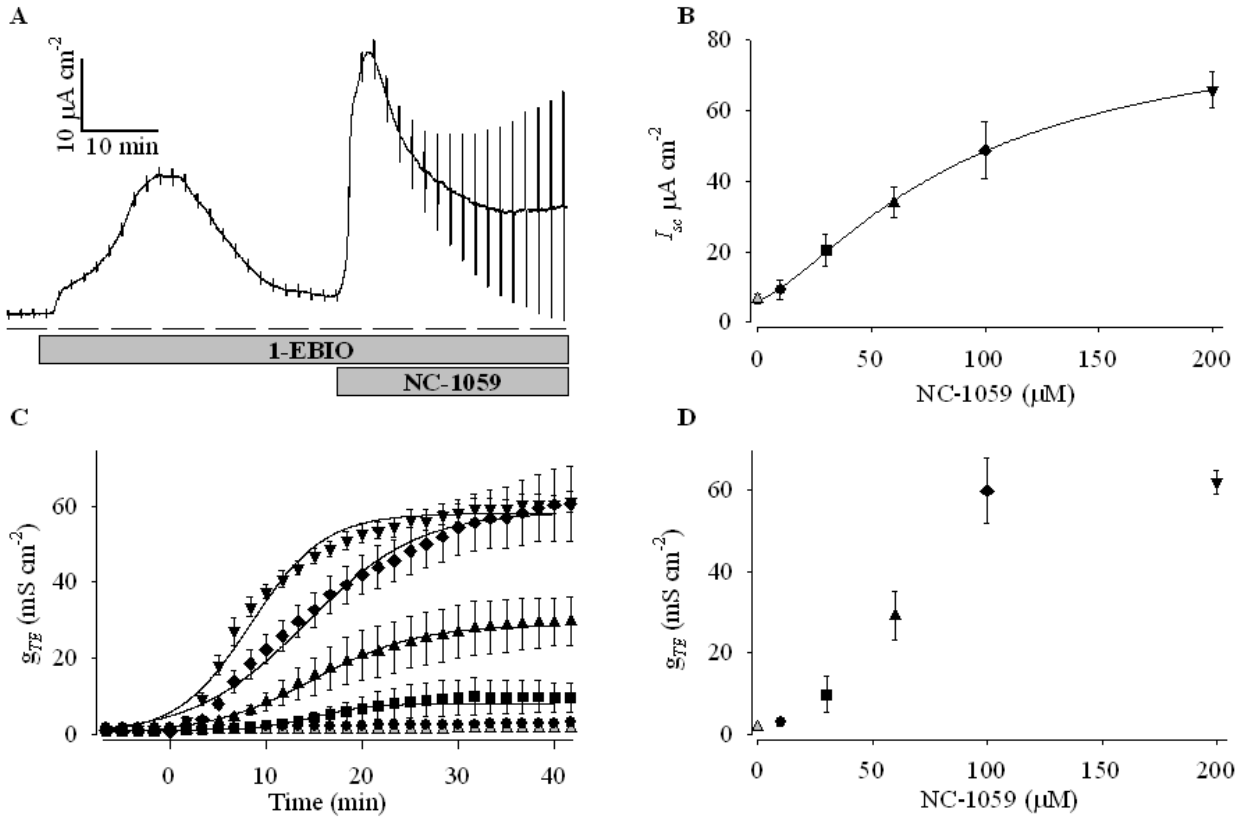

Figure 2.1: NC-1059 induces a concentration dependent elevation in I_{sc} and g_{te} across T-84 monolayers.

A) A representative trace of I_{sc} measured from a T-84 monolayer using a modified Ussing chamber. The shaded bars indicate the presence of 1-EBIO (300 µM) and apical exposure to NC-1059 (60 µM). **B**) Maximal I_{sc} as a function of concentration. The symbols represent the maximal I_{sc} at the concentrations tested. The solid line represents a best fit of Eqn. 1 to the data set and parameters of the fit are presented in Table 1. **C**) g_{te} vs. time for untreated (▲), 10 (●), 30 (■), 60 (▲), 100 (♦), 200 (▼) µM NC-1059. The solid lines represent the best fit to Eqn. 2 for the data set for 30, 60, 100 and 200 µM. **D**) The maximum g_{te} as a function of concentration is plotted. Panels B, C and D represent data summarized from six observations for each concentration.

PVD9902 cells derived from porcine vas deferens: Fig. 2A shows a typical recording of a PVD9902 monolayer exposed to 60 μM NC-1059. Exposure to 300 μM 1-EBIO resulted in a small change in I_{sc} but little change in $g_{te.}$ Subsequent exposure to 60 μM NC-1059 was associated with an increase in I_{sc} from 5 to 15 μA cm^{-2}. I_{sc} reached a peak in less than 2 minutes and declined to a lower, but still elevated level. There was an increase in g_{te} from 0.17 to 1.2 mS cm^{-2} and g_{te} remained elevated throughout the recording. Average maximal I_{sc} as a function of concentration is summarized from 6 experiments in Fig. 2B. In PVD9902 cell monolayers, the average I_{sc} prior to NC-1059 exposure, but after exposure to 1-EBIO, was 4.0 ± 0.4 μA cm^{-2} and a significant effect of the peptide on I_{sc} was observed at 60 μM with greater responses at 100 μM and 200 μM. The change in I_{sc} did not show any indication of a plateau within this concentration range of NC-1059 and hence the fit to Eqn. 1 was constrained to a maximal I_{sc} of 100 μA cm^{-2}. The solid line represents the best fit of the data with Eqn. 1 (see Table 1). Fig. 2C provides the concentration dependent changes in g_{te} as a function of time with PVD9902 monolayers exposed to various concentrations of NC-1059. On the scale shown, no observable change in g_{te} was seen with either 30 or 60 μM. A significant change in g_{te} was observed at 100 μM and g_{te} was nearly three-fold greater with 200 μM. The parameters derived from the fit of Eqn. 2 (Table 2) showed that PVD9902 monolayers exposed to 200 μM NC-1059 reached half maximal g_{te} more rapidly than at 100 μM with a difference that was nearly 10 min. Also the slope ($1/b$) derived from the fit was steeper for 200 μM than 100 μM. The g_{te} began to decline gradually which limited the duration of the fit. The peak conductance as a function of concentration in PVD9902 is provided in Fig. 2D. Again no significant differences in g_{te} were observed for concentrations ≤ 60 μM. As shown in Fig. 2C and D, substantial increases in g_{te} occurred following exposure to 100 μM NC-1059 with even greater effect at 200 μM.

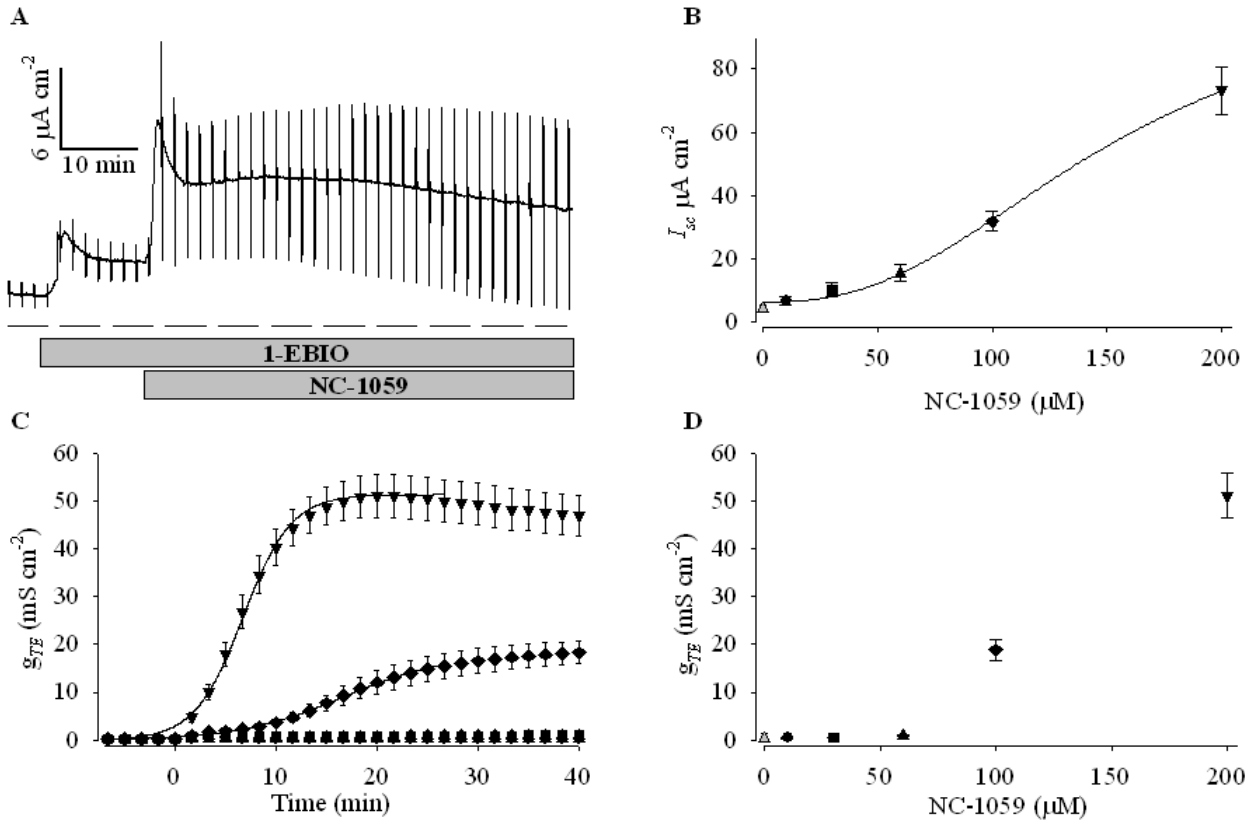

Figure 2.2: NC-1059 induces a concentration dependent elevation in I_{sc} and g_{te} across PVD9902 monolayers.

A) A representative trace of I_{sc} measured from a PVD9902 monolayer using a modified Ussing chamber. The shaded bars indicate the presence of 1-EBIO (300 μM) and apical exposure to NC-1059 (60 μM). **B**) Maximal I_{sc} as a function of concentration. The symbols represent the maximal I_{sc} at the concentrations tested. The solid line represents the best fit of Eqn. 1 to the data set. Parameters of the function are presented in Table 1. **C**) g_{te} vs. time for untreated (▲), 10 (●), 30 (■), 60 (▲), 100 (♦), 200 (▼) μM NC-1059. The solid lines represent the best fit to Eqn. 2 for the data set of 100 and 200 μM. **D**) The maximum g_{te} as a function of concentration is plotted. Panels B, C and D represent data summarized for six observations at each concentration.

.

IPEC-J2 cells derived from porcine jejunum: Fig. 3 provides typical and summarized results for concentration dependent effects of NC-1059 on IPEC-J2 monolayers. Fig. 3A is a trace of an IPEC-J2 monolayer exposed to 60 μM NC-1059. When exposed to 300 μM 1-EBIO the monolayer exhibited no change in I_{sc}. Peptide exposure resulted in an increase of I_{sc} from a basal value of less than 1.0 to 5.5 μA cm^{-2}. I_{sc} increased to a maximal value and then declined, but not to baseline. The g_{te} increased to reach a peak value of 2.34 mS cm^{-2} and returned towards baseline within 30 minutes of peptide addition. Fig. 3B provides a summary of the concentration dependent effects of NC-1059 on maximal I_{sc} from 6 experiments. IPEC-J2 cells showed significant increases in maximal I_{sc} at 60 μM and greater change at 100 μM and 200 μM. The increase in maximal I_{sc} between 30 μM to 200 μM was almost linear with a nearly three-fold difference between 100 and 200 μM. The I_{sc} did not appear to reach a maximal value within the tested concentration range. Hence, Eqn. 1 was fitted to the data with the maximal I_{sc} constrained to100 μA cm^{-2} (Table 1). IPEC-J2 cells showed a significant increase in g_{te} with 100 and 200 μM NC-1059 and the g_{te} reached a peak in 20 minutes or less and then began to decline towards baseline (Fig. 3C). This rapid decline in g_{te} after reaching a peak value was a common pattern observed with all concentrations of NC-1059 tested in IPEC-J2 monolayers. Although there is a modest decline in g_{te} in PVD9902, a pronounced decline is observed only in IPEC-J2 monolayers. The average time to reach half maximal g_{te} (t_0), derived from the best fit with Eqn. 2 (Table 2) was several minutes greater for 100 μM as compared to 200 μM and slope was less for 100 μM when compared to 200 μM. The calculated constants from the fit (Table 2) suggest a concentration dependent change in g_{te}. The peak change in g_{te} as a function of concentration in IPEC-J2 is shown in Fig. 3D. The change in g_{te} was nearly three-fold greater at 200 μM as compared to 100 μM. The difference in peak g_{te} between 100 and 200 μM was similar to the

pattern observed with PVD9902 monolayers, but the peak g_{te} after exposure to NC-1059 is at least 50% lower than other epithelia for each concentration. It is also noteworthy that the graph does not reach a plateau for the concentrations tested indicating that with higher concentration of peptide a response comparable to other epithelia may be attained.

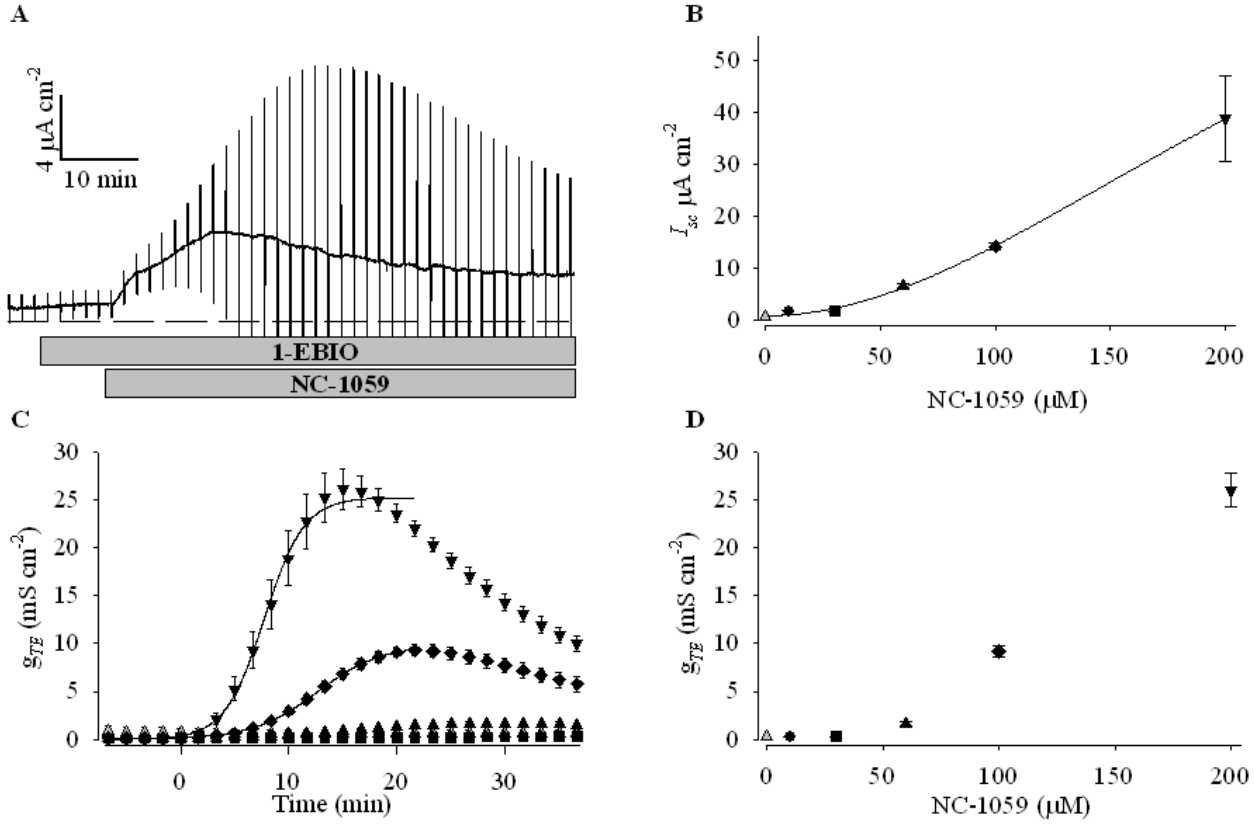

Figure 2.3: NC-1059 induces a concentration dependent change in I_{sc} and g_{te} across IPEC-J2 monolayers.

A) A representative trace of I_{sc} measured from IPEC-J2 monolayers using a modified Ussing chamber. The shaded bars indicate the presence of 1-EBIO (300 μM) and apical exposure to NC-1059 (60 μM). **B**) Maximal I_{sc} as a function of concentration. The symbols represent the maximal I_{sc} at the concentrations tested. The solid line represents a best fit of Eqn. 1 to the data set. Parameters of the function are presented in Table 1. **C**) g_{te} vs. time for untreated (▲), 10 (●), 30 (■), 60 (▲), 100 (♦), 200 (▼) μM NC-1059. The solid lines represent the best fit to Eqn. 2 for the data set of 100 and 200 μM. **D**) The maximum g_{te} as a function of concentration is plotted. Panels B, C and D represent data summarized for six observations at each concentration.

.

Calu-3 cells from human airway: In Fig. 4A, a Calu-3 monolayer was exposed to 300 μM 1-EBIO and this resulted in a 30 μA cm^{-2} increase in I_{sc} that declined only modestly. Subsequent exposure to 60 μM NC-1059 increased the I_{sc} by only 7 μA cm^{-2} and there is no significant change in g_{te}. The average I_{sc} across Calu-3 monolayers after exposure to 1-EBIO and prior to addition of NC-1059 was 22 ± 5.0 μA cm^{-2} and after exposure to 100 μM NC-1059, the average I_{sc} reached 29 ± 6.5 μA cm^{-2} and 37 ± 5.5 μA cm^{-2} at 200 μM (n=6; Fig. 4B). A fit of Eqn.1 to the data set was not feasible as there was a very small change in the I_{sc} over the concentration range tested. Calu-3 cells showed an increase in g_{te} (Fig. 4C) after addition of NC-1059 that was relatively small when compared to the change in g_{te} observed for the other epithelia that have been studied. The parameters derived from the sigmoidal fits showed small differences in t_0 for 100 and 200 μM NC-1059 and the values for slope, were indistinguishable. The average peak g_{te} as a function of concentration is shown in Fig. 4D. The g_{te} at 200 μM was variable and therefore not significantly different than the g_{te} at 100 μM.

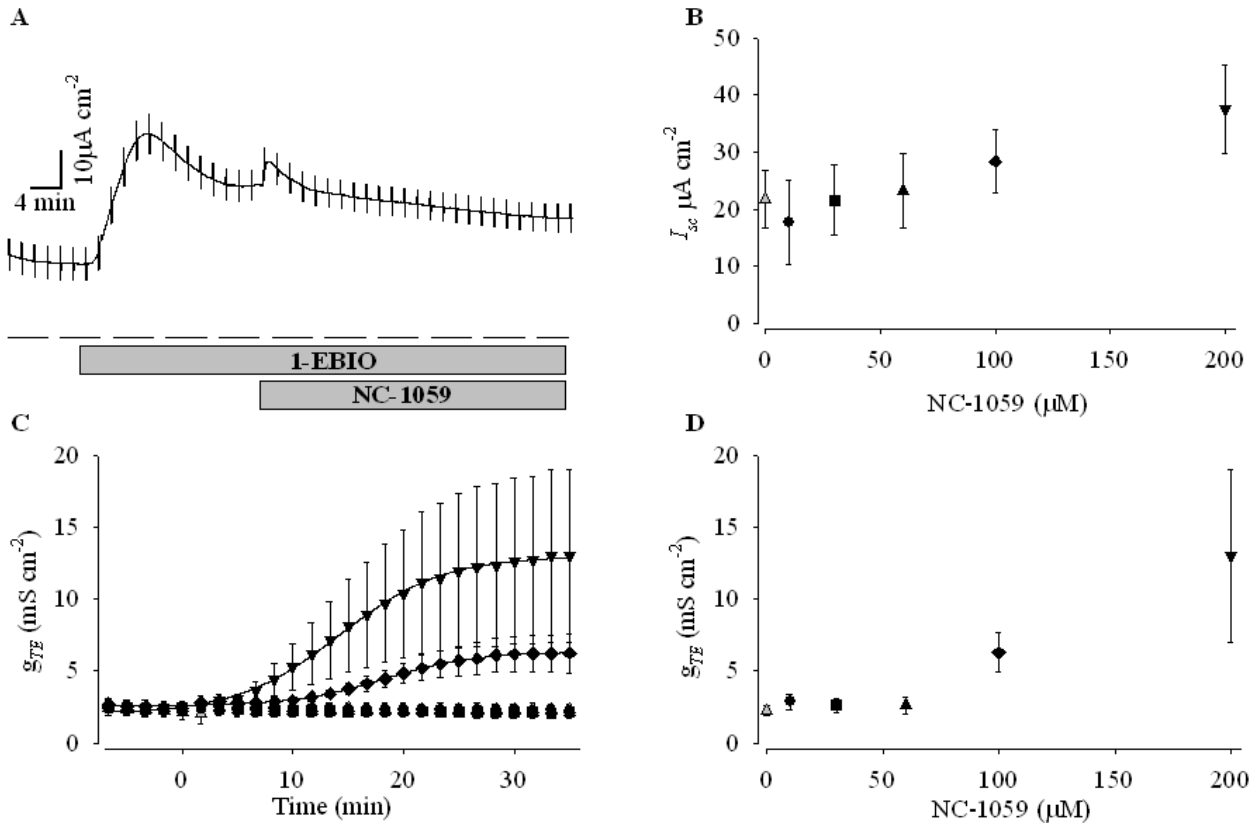

Figure 2.4: NC-1059 induces a change in I_{sc} and g_{te} in Calu-3 monolayers.

A) A representative trace of I_{sc} measured from Calu-3 monolayers using a modified Ussing chamber. The shaded bars indicate the presence of 1-EBIO (300 μM) and apical exposure to NC-1059 (60 μM). **B**) Maximal I_{sc} as a function of concentration. The symbols represent the maximal I_{sc} at the concentrations tested. **C**) g_{te} vs. time for untreated (▲), 10 (●), 30 (■), 60 (▲), 100 (♦), 200 (▼) μM NC-1059. The solid lines represent a best fit of Eqn. 2 for the data set of 100 and 200 μM. **D**) The maximum g_{te} as a function of concentration is plotted. The figures B, C and D represent data summarized from six experiments.

Table 1: Parameters derived from the fit of the modified Hill equation.

Cell line	Initial Values		Following 1-EBIO		Parameters derived with Eqn. 1		
	I_{sc} (μA)	g_{te} (mS)	I_{sc} (μA)	g_{te} (mS)	$\Delta I_{sc\ max}$ (μA)	k_{app} (μM)	Hill coefficient
T-84	2.32 ± 0.38	0.87 ± 0.24	6.56 ± 1.50	1.65 ±0.67	79.1± 31.8	91.1 ± 54.8	1.4 ± 0.7
PVD9902	1.99 ± 0.25	0.17 ± 0.02	3.98 ± 1.10	0.23 ±1.05	*100 ± 52	152 ± 73	2.5 ± 1.1
IPEC-J2	0.82 ± 0.05	0.14 ± 0.01	0.70 ± 0.44	0.29±0.06	*100 ±324	256 ± 743	2.0 ± 2.0
Calu-3	7.56 ± 2.45	2.33 ± 0.40	21.76 ± 5.03	2.26 ±0.33			

* values constrained during fitting

Table 2: Parameters derived from the sigmoidal fit of g_{te} as a function of time for each concentration.

Tissue	Max g_{te} (mS) 100μM	Max g_{te} (mS) 200μM	b (min) 100μM	b (min) 200μM	t_0 (min) 100μM	t_0 (min) 200μM
T-84	58.6 ± 5.3	58.1 ± 1.9	5.8 ± 1.2	3.8 ± 0.3	14.2 ± 1.2	8.4 ± 0.4
PVD9902	18.1 ± 1.5	51.3 ± 2.4	5.2 ± 1.07	2.4 ± 0.4	16.7 ± 1.1	6.7 ± 0.4
IPEC-J2	9.8 ± 0.4	25.2 ± 1.3	3.0 ± 0.3	1.8 ± 0.3	12.6 ± 0.3	7.7 ± 0.4
Calu-3	2.0 ± 0.7	11.0 ± 3.1	4.1 ± 1.84	4.7 ± 3.4	18.2 ± 2.0	14.2 ± 1.9

* Parameters refer to Equation 2

NC-1059 allows for the permeation of variously sized dextran through different epithelial monolayers. The increase in g_{te} reported above might suggest an increase in paracellular permeability. However the electrical parameter cannot differentiate transcellular versus paracellular conductance. Hence, dextran of various sizes was used to assess permeation through the paracellular pathway. Additionally, since there were distinct differences in the g_{te} before and after exposure to NC-1059, variously sized dextran was used to observe if these differences are reflected in the size selectivity to uncharged solutes.

The effects of NC-1059 on g_{te} of the various epithelia studied suggest a reduction in the paracellular barrier properties of these epithelia. MDCK monolayers treated with 100 μM NC-1059 showed an increase in permeation of 9.5 kDa, but not 77 kDa dextran by about 5-fold (Broughman et al., 2004). EDTA, an agent that disrupts epithelial monolayers, showed a much greater enhancement of permeation. In order to test the effect of NC-1059 on the paracellular route of additional cell types, the permeation of 10, 20, 40 and 70 kDa dextran was determined over a duration of 1 hour across several different epithelia (Fig. 5). Permeation across monolayers exposed to 200 μM NC-1059, 5 mM EDTA or vehicle control was measured. The permeable support was freely permeable to all sizes of dextran tested (Broughman et al., 2004). NC-1059 and EDTA enhanced permeation to various sizes of dextran in all cell types tested. The epithelia differed in the amount of dextran that permeated in each case and in the pattern of permeation relative to solute size. Results specific to each cell type are presented below. Results presented are summarized from 3 experiments for each cell type.

T-84: In untreated T-84 monolayers, the permeation of dextran decreased with an increase in size. Based on Fick's law, this pattern of permeation cannot be attributed solely to diffusion rate and might be influenced by geometric constraints based on composition and length of the

intercellular space as suggested to be the case with MDCK monolayers (Spring, 1998; Spring & Hope, 1978). The permeation of dextran (all sizes tested), was significantly greater across T-84 monolayers when treated with NC-1059 as compared to untreated monolayers. The average permeation of 10 kDa dextran in the presence of NC-1059 was greater by 4-fold relative to untreated monolayers and was comparable with previously published observations with MDCK monolayers (Broughman et al., 2004). Permeation of 20, 40 and 70 kDa dextran was 4 to 9-fold greater in NC-1059 treated monolayers than in untreated monolayers. EDTA exposure allowed for permeation of all sizes of dextran, although the relative permeation was increased less than 2-fold for 10 kDa dextran and about 4-fold for 20 kDa dextran. There was a modest effect of EDTA on the permeation of 10 and 20 kDa dextran as compared to permeation after exposure to NC-1059. However the permeation of 40 and 70 kDa dextran was much greater in the presence of EDTA as compared to NC-1059.

PVD9902: Permeation for all sizes of dextran tested in untreated PVD9902 monolayers was similar. In the PVD9902 monolayers exposed to NC-1059, the average permeation of 10 kDa dextran was 12-fold greater and for 20 kDa dextran, 27-fold greater than in untreated monolayers. It should be noted that the permeation of 20 kDa across untreated monolayers was less than half of the other dextran sizes; hence the fold change observed was much greater. Permeation of 40 and 70 kDa dextran was 4-fold and 3-fold greater in peptide treated than untreated monolayers respectively. NC-1059 induced a significant increase in permeation of all sizes of dextran. Although the permeation was enhanced for all sizes of dextran in NC-1059 treated monolayers, the absolute and relative permeation decreased with size. This suggests that there is finite limit to the size of solute that can permeate the paracellular pathway when PVD9902 monolayers are exposed to NC-1059. Permeation for all sizes of dextran was increased

to a greater extent across EDTA treated monolayers than with NC-1059 treatment. This is consistent with EDTA induced disruption of the tight junctions.

IPEC-J2: The permeation across untreated IPEC-J2 monolayers was comparable to PVD9902 for 10 and 20 kDa dextran and less than the rates reported for all sizes of dextran across T-84 monolayers. NC-1059 treatment increased the permeation of dextran across IPEC-J2 monolayers of 10 and 20 kDa dextran, by ~4-fold (Fig. 5C inset). The permeation of 40 kDa dextran was increased ~3-fold in peptide treated when compared to untreated monolayers and no NC-1059 associated difference was observed with 70 kDa dextran. Although average permeation for most sizes of dextran tested in the presence of NC-1059 was enhanced several fold, the results did not achieve statistical significance. There was a very large increase in permeation for all sizes of dextran in the presence of EDTA, the largest of all cell types tested in both absolute and relative permeation. The results suggested that the size of the dextran molecule was the rate limiting factor in the permeation across NC-1059 treated monolayers. The net increase in permeation for 20, 40 and 70 kDa dextran in IPEC-J2 monolayers treated with NC-1059 was relatively smaller when compared to the incremental change with PVD9902 and T-84 monolayers.

Calu-3: Calu-3 cells allowed for substantially greater permeation of dextran molecules in basal conditions than the other epithelia in this study (Fig. 5D), which is consistent with the high g_{te} observed in these monolayers. Since basal permeation of all sizes of dextran is relatively high, the average permeation of all sizes of dextran tested was enhanced only ~2-fold by NC-1059 exposure. A significant increase in permeation as compared to untreated monolayers was observed only in the case of 40 kDa dextran (Fig. 5D inset). Like all other epithelia studied, EDTA enhanced permeation for all sizes of dextran by several fold across Calu-3 cells.

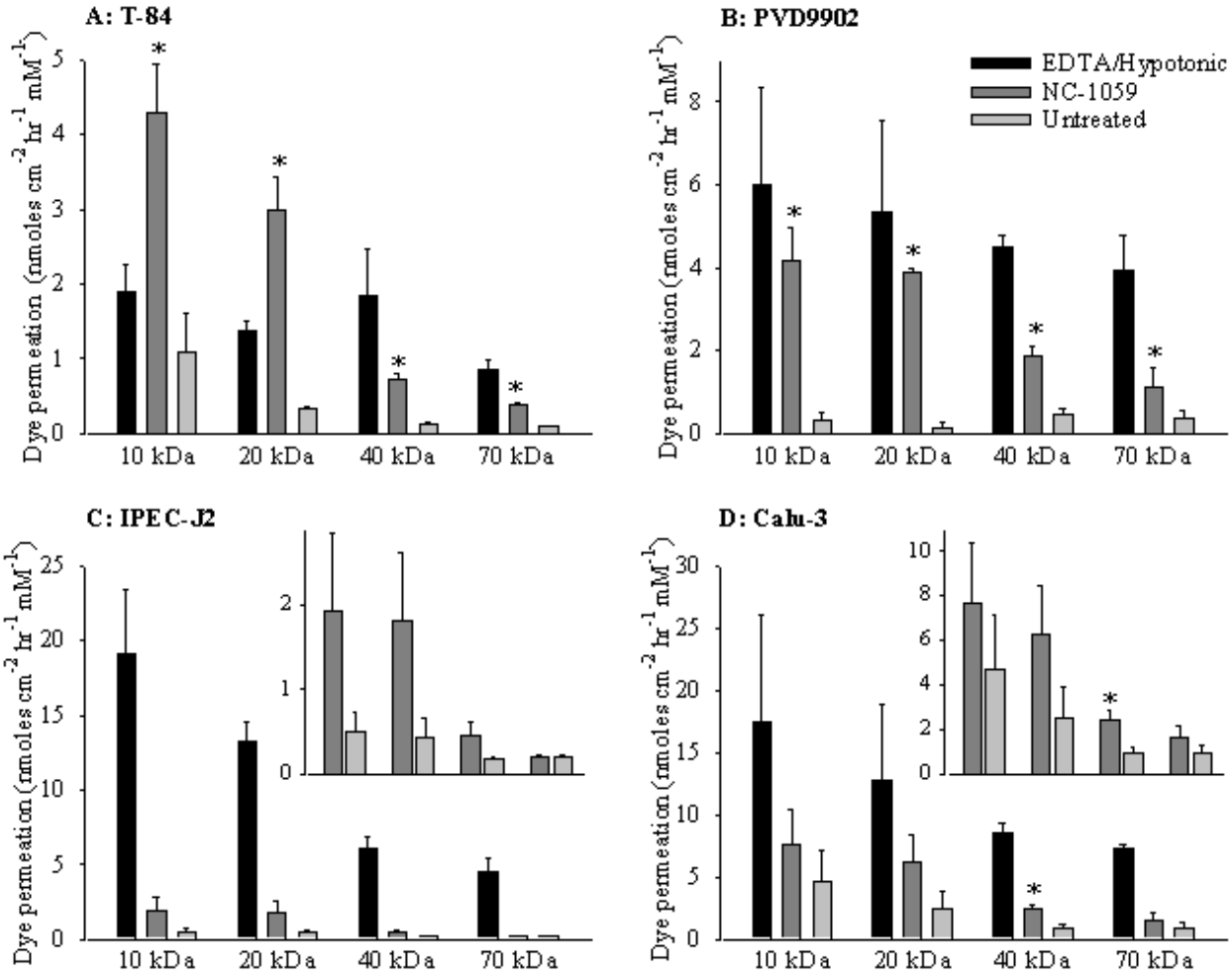

Figure 2.5: NC-1059 allows for the movement of uncharged molecules across epithelial monolayers derived from a variety of mammalian sources.

FITC conjugated dextran of 10, 20, 40 and 70 kDa was added to the apical compartment and appearance of fluorescence in the basolateral compartment was quantified in the presence of one of three treatments (EDTA solution, NC-1059 and vehicle control as described in methods). In addition, dye permeation across the permeable support was quantified in the absence of cells (not shown). Dextran permeation was studied in the four different epithelia: T-84, PVD9902, IPEC-J2 and Calu-3. The insets in the bottom panel show the dextran permeation for untreated and NC-1059 treated across IPEC-J2 and Calu-3 on a different scale. The figures A, B, C and D represent data summarized from three experiments (* $p < 0.05$ for t-test comparing untreated versus NC-1059 treated).

Taken together the results show that NC-1059 enhances the permeation of 10 to 70 kDa dextran across epithelial monolayers with different tissues of origin. That g_{te} continued to increase even after the I_{sc} had reached a peak value and had begun to decline suggested an increase in paracellular conductance. The dextran permeation results corroborate the conclusion that NC-1059 enhances paracellular conductance in addition to the transcellular conductance. However, this simultaneous change in the transcellular and paracellular conductances across epithelial monolayers makes it difficult to isolate and quantify the changes in apical membrane conductance using an Ussing chamber. Therefore the two electrode voltage clamp technique was used to study the membrane conductance induced by NC-1059, using *Xenopus laevis* oocytes.

NC-1059 increases membrane conductance in Xenopus laevis oocytes in a dose dependent manner and remains associated with the oocyte membrane for more than 2 hours. The dose dependent effect of NC-1059 on *Xenopus laevis* oocyte membranes was determined. A typical trace showing the dose dependent changes in oocyte membrane conductance is presented in Fig. 6A. The basal conductance was 5.81 μS. Exposure to 1.25 nmoles of NC-1059 resulted in a pronounced increase in the membrane conductance. Once the conductance reached a plateau, the addition of 2.5 nmoles NC-1059 to the flowing bath solution resulted in the membrane conductance increasing by greater than 2-fold when compared to 1.25 nmoles. Further addition of 5 nmoles resulted in only a small increment in conductance. The incremental change in membrane conductance with each dose was relatively small until exposure to 10 nmoles. Addition of 10 nmoles of NC-1059 increased the oocyte membrane conductance substantially to 199 μS. The addition of 20 nmoles of NC-1059, after the conductance reached a plateau, did not elicit a marked change. The data summarized from this experiment and 4 additional experiments (Fig. 6B) show an overall trend that follows the profile described for this typical trace. Slope

conductance increased from 31.8 ± 17.0 μS for 1.25 nmoles to 243.5 ± 71.2 μS at 20 nmoles (n=5).

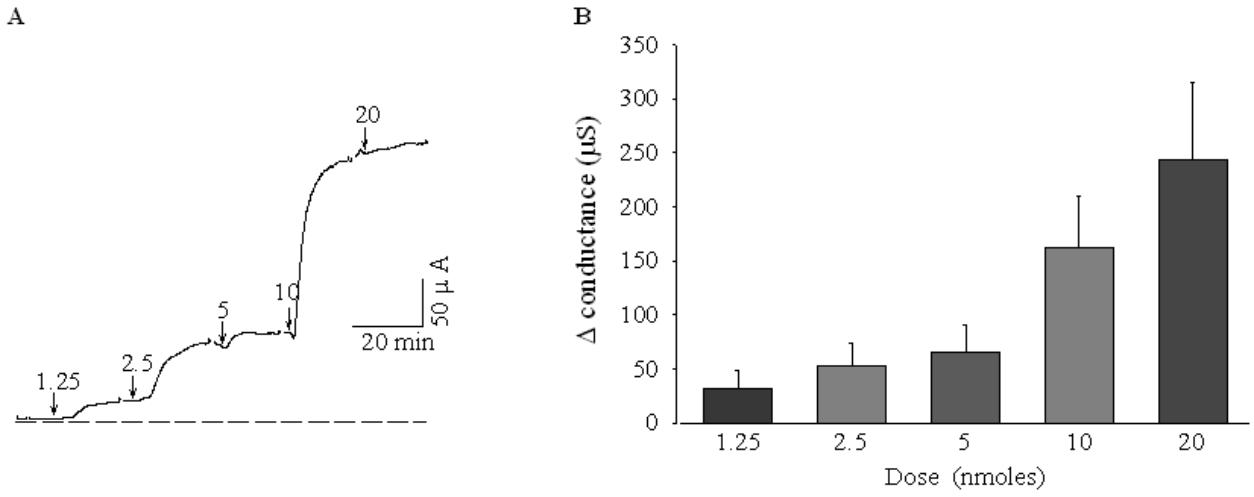

Figure 2.6: NC-1059 induces a dose dependent change in *Xenopus laevis* oocyte membrane conductance.

A) A typical trace showing that NC-1059 induces a dose dependent change in *Xenopus laevis* oocyte membrane conductance. The arrows indicate time of addition of NC-1059 to the perfusion solution. **B)** NC-1059 induces a dose dependent change in *Xenopus laevis* oocyte membrane conductance. The recordings were made in a constantly perfused bath and bolus additions of the peptide were made to the bath as indicated. Slope conductance was calculated using linear regression of current voltage plots obtained when the current reached a plateau after each bolus addition. Each bar shows the average change in slope conductance from baseline (mean ± SEM for n=5).

NC-1059 had a dose dependent effect on *Xenopus laevis* oocytes similar to the observation that there was a concentration dependent effect of NC-1059 in epithelial monolayers. Thus, a second set of experiments was conducted to observe the stability of the NC-1059 induced conductance in the oocyte membrane. A typical trace showing the effect of NC-1059 on membrane conductance is represented in Fig. 7A. Peptide (5 nmoles) was added to the perfusion solution after determining the basal conductance. The conductance increased to 150 μS, and after reaching a plateau, the conductance remained at an elevated value during the rest of the recording. Data are summarized from three experiments in Fig. 7B to show that membrane conductance increased upon exposure to NC-1059 and then remained stable during the entire recording period of 2 hours. This outcome suggests that the dose dependent change in membrane conductance induced by NC-1059 was caused by formation of ion channels in the membrane. Membrane conductance reflects the aggregate value for the number of actively gating channels (n), the single channel conductance (g_i) and the open channel probability (p_o) of these channels ($g_{membrane} = g_i \cdot n \cdot p_o$). Although these individual properties were not determined, the aggregate value was stable over the duration of the recording.

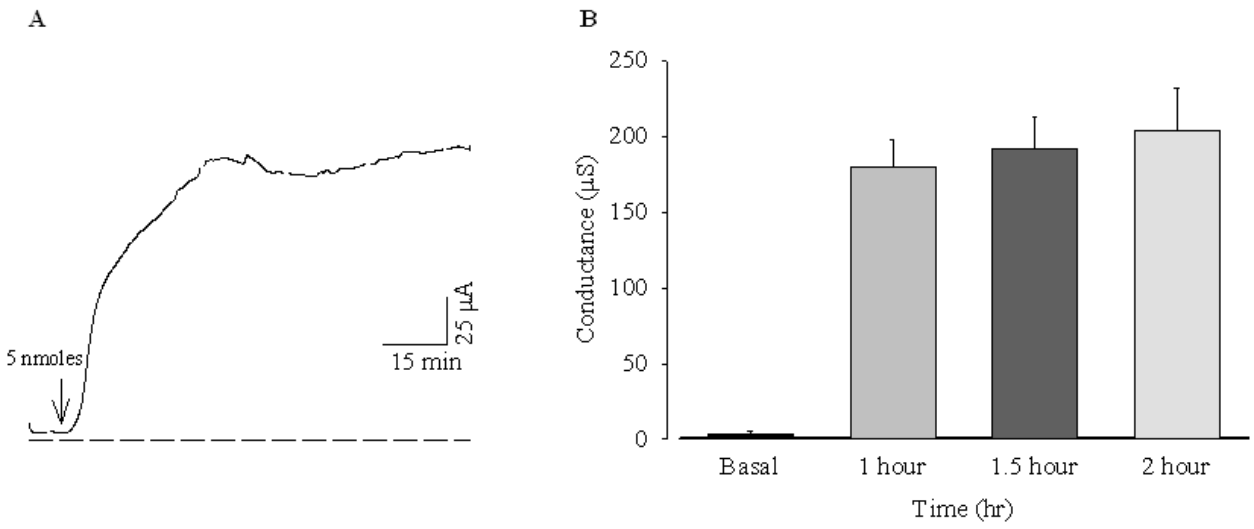

Figure 2.7: NC-1059 induces a stable change in *Xenopus laevis* oocyte conductance, lasting longer than 2 hours.

A) A typical trace of NC-1059 induced *Xenopus laevis* oocyte membrane conductance as a function of time. **B**) NC-1059 induces a stable change in *Xenopus laevis* oocyte conductance, lasting longer than 2 hours. Recordings were conducted in a constantly perfused bath. The bars represent average (mean ± SEM for n=3) slope conductance prior to addition of peptide, slope conductance after 1 hour ,1.5 hours and 2 hours of peptide addition.

Discussion:

The results demonstrate that NC-1059, a synthetic channel forming peptide, increased ion transport and solute permeation across epithelial monolayers derived from a variety of sources. The pattern of change in I_{sc} and g_{te} as a function of NC-1059 concentration was different in magnitude and stability for each cell type tested. Also, NC-1059 induced permeation of 10, 20, 40 and 70 kDa dextran across the various epithelia showed distinct patterns in terms of amount and size of dextran that permeated. NC-1059 increased oocyte membrane conductance in a dose dependent manner and the induced change in conductance remained elevated for the duration of the recording. Taken together the results suggest that NC-1059 associates with cell membranes to form stable active ion channels. The results further demonstrate that the NC-1059 induced increase in permeation across epithelial barriers, especially through the paracellular route is not limited to MDCK monolayers, and can be generated in a variety of epithelia derived from different tissues and species.

Epithelia were chosen to represent organs where efficient drug delivery is of clinical significance. The epithelia also represent a broad spectrum in terms of the degree of "tightness" (Furuse et al., 2001) as indicated by basal g_{te}. The epithelia used in the study can be arranged in the degree of electrical tightness as IPEC-J2 > PVD9902 > T-84 > Calu-3 (see Table 1). The change in I_{sc} and g_{te} showed characteristically distinct patterns in the four epithelial monolayers in terms of k_{app}, Hill coefficient, and time taken to reach half maximal g_{te}, slope and the magnitude of g_{te} at different NC-1059 concentrations. The changes in I_{sc} and g_{te} observed at various peptide concentrations in T-84 monolayers are quantitatively and qualitatively similar to MDCK cells and, like MDCK cells, the k_{app} was less than 100 μM with T-84 cells (Broughman et al., 2004). However, in PVD9902 cell monolayers the I_{sc} did not appear to reach a maximal

value within the concentration range tested. Hence the k_{app} may be greater than 100 μM. In the case of IPEC-J2 as well, the k_{app} may be greater than the reported value. Hill coefficients were greater than 1 for T-84 cells and greater than 2 for IPEC-J2 and PVD9902 cells. Both k_{app} and Hill coefficients follow this trend, IPEC-J2 > PVD9902 > T-84. Based on the constants derived from the fit of Eqn. 2, the effect of NC-1059 on g_{te} also follows the trend IPEC-J2 > PVD9902 > T-84. Hence it appears that the response to NC-1059 might be influenced by basal g_{te}. Lipid composition of membranes, particularly negatively charged lipids and cholesterol, have been shown to influence activity of synthetic channel forming peptides (Bell & Miller, 1984; Lin & Kagan, 2002), which might explain differences in the response between epithelia.

NC-1059 increased epithelial dextran permeation, indicating that a paracellular route was accessed. In T-84 and PVD9902 monolayers, the NC-1059 induced increment in dextran permeation was greater for the smaller dextrans (10 and 20 kDa). Nevertheless permeation for all sizes of dextran was enhanced relative to untreated monolayers. IPEC-J2 cells exhibited less permeation when compared to other cell types. This is consistent with the observation that g_{te} is nearly 50% less across IPEC-J2 as compared to PVD9902 and T-84 monolayers. Also, g_{te} declined rapidly in IPEC-J2 monolayers as compared to a more sustained response observed in other epithelia. Since enhancing permeability of intestinal epithelia can be associated with a risk of infection, absorption enhancers must have a transient effect. Therefore, limited and transient enhancement in permeation by NC-1059 across the IPEC-J2 monolayers is a useful property associated with the peptide in these cells derived from the small intestine. The sustained effect with T-84 cells however, demonstrates that this observation cannot be extended to all intestinal cell types. Clearly, additional studies are required to define effects of NC-1059 on additional intestinal cell types and on native tissue.

NC-1059 produced a modest effect on ion transport across Calu-3 cell monolayers. The large and sustained effect of 1-EBIO supports the conclusion that CFTR is abundant and active in the apical membrane of unstimulated Calu-3 cells (Shen et al., 1994) and the apical conductance is not rate limiting for ion transport. Thus a negligible effect of NC-1059 on I_{sc} is not unexpected. Nonetheless, 100 and 200 μM NC-1059 increased g_{te}, which we interpret as an increase in paracellular permeability. Ultimately, the amount of dextran that permeated Calu-3 monolayers in the presence of NC-1059 was comparable to that observed in the other epithelia studied. The ability of NC-1059 to enhance permeation by 10 to 20 kDa molecules across Calu-3 monolayers suggests that it might be used to enhance delivery of drugs in nasal sprays or inhalers.

NC-1059 increased paracellular passage of dextrans up to 70 kDa, although permeation was quite low. Larger molecules were not tested in this study. Earlier work in MDCK cells, however, showed no passage of 2.5 MDa dextran (Broughman et al., 2004). Taken together, the results suggest that permeation of small molecules (e.g., vancomycin) will be enhanced by NC-1059. Permeation of larger molecules such as insulin (~4 kDa) will also likely be enhanced by NC-1059, but molecules such as albumin (67 kDa) would be expected to have limited permeability. Permeability of larger and potentially harmful structures such as bacteria and virus particles would also be expected to remain negligible.

Epithelial cells differ in size and hence the monolayers may differ in the number of lateral intercellular spaces. Additionally, epithelia may differ in the composition, distribution and expression of the junctional proteins that maintain the integrity of the paracellular route (Acharya et al., 2004; Heiskala, Peterson & Yang, 2001). Both of these factors can contribute to the differences observed in the epithelia studied. Tight junctions are “multimolecular complexes” comprised of integral membrane proteins and plaque proteins. These plaque proteins are

associated with several cytosolic proteins and also connect the integral membrane proteins and perijunctional-actin cytoskeleton (Schneeberger & Lynch, 2004). These proteins have an integral role in regulating paracellular permeability (Anderson & Van Itallie, 1995; Furuse et al., 1996; McCarthy et al., 1996). Disruption of actin and the localization of junctional proteins by toxins such as ZOT (Fasano, 2000) reportedly resulted in increased paracellular permeability. Results in this paper show that NC-1059 enhances permeation through the paracellular space. The results suggest that, in addition to supporting ion transport across epithelial cells, NC-1059 transiently affects the stability or distribution of tight junction proteins.

NC-1059 induces a rapid and dose dependent increase in membrane conductance in *Xenopus laevis* oocytes. It is noteworthy that the membrane conductance consistently changed in small increments until the 5 nmole dose and addition of 10 nmoles caused a more substantial change in conductance. Exposure to a higher dose inconsistently caused a modest change in membrnae conductance that did not achieve statistical significance. A possible explanation is that 10 nmoles establishes a critical concentration in the membrane at which individual peptide molecules are sufficiently close to assemble into the greatest number of functional channels and possibly to saturate the membrane such that further peptide exposure does not enhance conductance.

NC-1059 induced an increase in membrane conductance that remained stable in *Xenopus* oocytes as opposed to the transient effect on I_{sc} observed in mammalian epithelial monolayers. This suggests that there is a secondary event in the epithelial monolayers responsible for the decrease in I_{sc} (i.e., results suggest that channel-forming peptides can remain resident in the cell membrane). One possibility is that NC-1059 forms channels that cause depolarization. The decrease in I_{sc} may occur when cellular mechanisms are not sufficient to maintain electrochemical driving forces to sustain net ion transport at the peak level. Long stable

recordings with both mammalian cell monolayers and *Xenopus* oocytes, however, demonstrate that the peptide does not induce cell lysis.

The predominant obstacle to the permeation of clinically relevant therapeutics across epithelial barriers is the degree of hydrophilicity and size for many of these molecules. Systemic drug delivery for such compounds requires larger doses of drugs and therefore is associated with increased costs and the potential for undesirable effects in some cases (Torchilin, 2000). Several oral antibiotics and antivirals have limited permeability across intestinal epithelia because of their hydrophilic nature and size (Peppas, Wood & Blanchette, 2004). Colonic, airway and corneal / conjuctival epithelia are barriers to the absorption of drugs specifically targeted to these tissues. The conditions that afflict the anterior portion of the eye such as glaucoma and keratitis are treated with drugs that must permeate through corneal or conjuctival epithelia (Edward & Prausnitz, 2001; Zhang, Prausnitz & Edwards, 2004). The nasal or airway epithelium is another major target for drug delivery as an alternative to injections of drugs such as insulin (Gonzalez et al., 2006; Turker, Onur & Ozer, 2004). Results presented in this paper show that NC-1059 enhanced the permeation of molecules as large as 10 and 20 kDa across colonic (T-84), small intestine (IPEC-J2) and airway (Calu-3) epithelial monolayers. NC-1059 also enhanced permeation across kidney (MDCK) (Broughman et al., 2004) and reproductive duct (PVD9902) epithelial monolayers. Hence NC-1059 has potential to be developed as an absorption enhancer for therapeutic agents.

Acknowledgments: We thank Gary Radke and Ryan Carlin for their technical assistance. This article is contribution # 08-76-J from the Kansas Agriculture experiment station, Manhattan, KS-66506.

This study is supported in part by PHS grants GM 066620 (JMT) and GM 074096 (JMT).

References:

Acharya, P., Beckel, J., Ruiz, W.G., Wang, E., Rojas, R., Birder, L., Apodaca, G. 2004. Distribution of the tight junction proteins ZO-1, occludin, and claudin-4, -8, and -12 in bladder epithelium. *Am J Physiol Renal Physiol* **287:**F305-18

Anderson, J.M., Van Itallie, C.M. 1995. Tight junctions and the molecular basis for regulation of paracellular permeability. *Am J Physiol Cell Physiol* **269:**G467-75

Bell, J.E., Miller, C. 1984. Effects of phospholipid surface charge on ion conduction in the K+ channel of sarcoplasmic reticulum. *Biophys J* **45:**279-87

Broughman, J.R., Brandt, R.M., Hastings, C., Iwamoto, T., Tomich, J.M., Schultz, B.D. 2004. Channel-forming peptide modulates transepithelial electrical conductance and solute permeability. *Am J Physiol Cell Physiol* **286:**C1312-23

Broughman, J.R., Mitchell, K.E., Sedlacek, R.L., Iwamoto, T., Tomich, J.M., Schultz, B.D. 2001. NH(2)-terminal modification of a channel-forming peptide increases capacity for epithelial anion secretion. *Am J Physiol Cell Physiol* **280:**C451-8

Broughman, J.R., Shank, L.P., Prakash, O., Schultz, B.D., Iwamoto, T., Tomich, J.M., Mitchell, K. 2002a. Structural implications of placing cationic residues at either the NH2- or COOH-terminus in a pore-forming synthetic peptide. *J Membr Biol* **190:**93-103

Broughman, J.R., Shank, L.P., Takeguchi, W., Schultz, B.D., Iwamoto, T., Mitchell, K.E., Tomich, J.M. 2002b. Distinct structural elements that direct solution aggregation and membrane assembly in the channel-forming peptide M2GlyR. *Biochemistry* **41:**7350-8

Carlin, R.W., Sedlacek, R.L., Quesnell, R.R., Pierucci-Alves, F., Grieger, D.M., Schultz, B.D. 2006. PVD9902, a porcine vas deferens epithelial cell line that exhibits neurotransmitter-stimulated anion secretion and expresses numerous HCO3(-) transporters. *Am J Physiol Cell Physiol* **290:**C1560-71

Chung, N.P., Mruk, D., Mo, M.Y., Lee, W.M., Cheng, C.Y. 2001. A 22-amino acid synthetic peptide corresponding to the second extracellular loop of rat occludin perturbs the blood-testis barrier and disrupts spermatogenesis reversibly in vivo. *Biol Reprod* **65:**1340-51

Devor, D.C., Singh, A.K., Bridges, R.J., Frizzell, R.A. 1996a. Modulation of Cl^- secretion by benzimidazolones. II. Coordinate regulation of apical G_{Cl} and basolateral G_K. *American Journal of Physiol Lung Cell Mol Physiol* **271:**L785-95

Devor, D.C., Singh, A.K., Frizzell, R.A., Bridges, R.J. 1996b. Modulation of Cl^- secretion by benzimidazolones. I. Direct activation of a Ca^{2+}-dependent K^+ channel. *American Journal of Physiol Lung Cell Mol Physiol* **271:**L775-84

Devor, D.C., Singh, A.K., Lambert, L.C., DeLuca, A., Frizzell, R.A., Bridges, R.J. 1999. Bicarbonate and chloride secretion in Calu-3 human airway epithelial cells. *J Gen Physiol* **113:**743-60

Edward, A., Prausnitz, M.R. 2001. Predicted permeability of the cornea to topical drugs. *Pharm Res* **18:**1497-508

Everett, R.S., Vanhook, M.K., Barozzi, N., Toth, I., Johnson, L.G. 2006. Specific modulation of airway epithelial tight junctions by apical application of an occludin peptide. *Mol Pharmacol* **69:**492-500

Fasano, A. 2000. Regulation of intercellular tight junctions by zonula occludens toxin and its eukaryotic analogue zonulin. *Ann N Y Acad Sci* **915:**214-22

Fasano, A., Fiorentini, C., Donelli, G., Uzzau, S., Kaper, J.B., Margaretten, K., Ding, X., Guandalini, S., Comstock, L., Goldblum, S.E. 1995. Zonula occludens toxin modulates tight junctions through protein kinase C-dependent actin reorganization, in vitro. *J Clin Invest* **96:**710-20

Fasano, A., Uzzau, S. 1997. Modulation of intestinal tight junctions by Zonula occludens toxin permits enteral administration of insulin and other macromolecules in an animal model. *J Clin Invest* **99:**1158-64

Furuse, M., Fujimoto, K., Sato, N., Hirase, T., Tsukita, S. 1996. Overexpression of occludin, a tight junction-associated integral membrane protein, induces the formation of intracellular multilamellar bodies bearing tight junction-like structures. *J Cell Sci* **109 (Pt 2):**429-35

Furuse, M., Furuse, K., Sasaki, H., Tsukita, S. 2001. Conversion of zonulae occludentes from tight to leaky strand type by introducing claudin-2 into Madin-Darby canine kidney I cells. *J Cell Biol* **153:**263-72

Gonzalez, C., Kanevsky, D., De Marco, R., Di Girolamo, G., Santoro, S. 2006. Non-invasive routes for insulin administration: current state and perspectives. *Expert Opin Drug Deliv* **3:**763-70

Heiskala, M., Peterson, P.A., Yang, Y. 2001. The roles of claudin superfamily proteins in paracellular transport. *Traffic* **2:**93-8

Kondoh, M., Yagi, K. 2007. Progress in absorption enhancers based on tight junction. *Expert Opin Drug Deliv* **4:**275-86

Lacaz-Vieira, F., Jaeger, M.M., Farshori, P., Kachar, B. 1999. Small synthetic peptides homologous to segments of the first external loop of occludin impair tight junction resealing. *J Membr Biol* **168:**289-97

Lin, M.C., Kagan, B.L. 2002. Electrophysiologic properties of channels induced by Abeta25-35 in planar lipid bilayers. *Peptides* **23:**1215-28

McCarthy, K.M., Skare, I.B., Stankewich, M.C., Furuse, M., Tsukita, S., Rogers, R.A., Lynch, R.D., Schneeberger, E.E. 1996. Occludin is a functional component of the tight junction. *J Cell Sci* **109 (Pt 9):**2287-98

Peppas, N.A., Wood, K.M., Blanchette, J.O. 2004. Hydrogels for oral delivery of therapeutic proteins. *Expert Opin Biol Ther* **4:**881-7

Schneeberger, E.E., Lynch, R.D. 2004. The tight junction: a multifunctional complex. *Am J Physiol Cell Physiol* **286:**C1213-28

Shen, B.Q., Finkbeiner, W.E., Wine, J.J., Mrsny, R.J., Widdicombe, J.H. 1994. Calu-3: a human airway epithelial cell line that shows cAMP-dependent Cl- secretion. *Am J Physiol* **266:**L493-501

Spring, K.R. 1998. Routes and mechanism of fluid transport by epithelia. *Annu Rev Physiol* **60:**105-19

Spring, K.R., Hope, A. 1978. Size and shape of the lateral intercellular spaces in a living epithelium. *Science* **200:**54-8

Tavelin, S., Hashimoto, K., Malkinson, J., Lazorova, L., Toth, I., Artursson, P. 2003. A new principle for tight junction modulation based on occludin peptides. *Mol Pharmacol* **64:**1530-40

Thompson, S.E., Cavitt, J., Audus, K.L. 1994. Leucine enkephalin effects on paracellular and transcellular permeation pathways across brain microvessel endothelial cell monolayers. *J Cardiovasc Pharmacol* **24:**818-25

Tomich, J.M., Wallace, D., Henderson, K., Mitchell, K.E., Radke, G., Brandt, R., Ambler, C.A., Scott, A.J., Grantham, J., Sullivan, L., Iwamoto, T. 1998. Aqueous solubilization of transmembrane peptide sequences with retention of membrane insertion and function. *Biophys J* **74:**256-67

Torchilin, V.P. 2000. Drug targeting. *Eur J Pharm Sci* **11 Suppl 2:**S81-91

Turker, S., Onur, E., Ozer, Y. 2004. Nasal route and drug delivery systems. *Pharm World Sci* **26:**137-42

Wallace, D.P., Tomich, J.M., Iwamoto, T., Henderson, K., Grantham, J.J., Sullivan, L.P. 1997. A synthetic peptide derived from glycine-gated Cl- channel induces transepithelial Cl- and fluid secretion. *Am J Physiol Cell Physiol* **272:**C1672-9

Wong, V., Gumbiner, B.M. 1997. A synthetic peptide corresponding to the extracellular domain of occludin perturbs the tight junction permeability barrier. *J Cell Biol* **136:**399-409

Zhang, W., Prausnitz, M.R., Edwards, A. 2004. Model of transient drug diffusion across cornea. *J Control Release* **99:**241-58

CHAPTER 3 - NC-1059, a Channel Forming Peptide, Induces a Reversible Redistribution of Actin and Junctional Proteins.

Suma Somasekharan, Takeo Iwamoto, John M. Tomich, and Bruce D. Schultz*.

SS, TI, JMT: Department of Biochemistry, Kansas State University, Manhattan, KS 66506

BDS: Department of Anatomy & Physiology, Kansas State University, Manhattan KS 66506

Corresponding author: Dr Bruce D Schultz, Kansas State University Department of Anatomy and Physiology, 1600 Denison Avenue, Coles Hall 228, Manhattan, KS-66506

Phone numbers: 785-532-4839 (office), 785-532-4557 (fax).

Email:bschultz@vet.ksu.edu

Running title: NC-1059 redistributes junctional proteins.

This chapter will be submitted for peer review in this format.

Abstract:

The goal of this study is to identify the mechanism(s) by which NC-1059, a synthetic channel forming peptide, increases epithelial paracellular permeability. Apical exposure to NC-1059 (60 μM) increased short circuit current, transepithelial electrical conductance (g_{te}) and enhanced the permeation of dextrans (10-70 kDa) across MDCK monolayers, both of which returned to pretreatment levels within 48 hours after washout (1). MDCK monolayers in this study showed a large increase in g_{te} and enhanced permeation of 40 and 70 kDa dextran. MDCK monolayers exposed to 100 and 200 μM NC-1059 for 60 min showed a substantial recovery in g_{te} at 24 hours and returned to pretreatment values within 48 hours. MDCK monolayers exposed to NC-1059, when subjected to immunolabeling and confocal microscopy, revealed a concentration dependent reorganization or loss of actin, ZO-1 and occludin over 60 min. NC-1059 also causes a decrease in abundance of E-cadherin and β-catenin over 60 min. Effects of NC-1059 exposure were reversible with progressive recovery of immunoreactivity at the apical cell junction for occludin and ZO-1 observed 24 and 48 hour post exposure. The modulation of the epithelial tight junctions in a reversible manner indicates that NC-1059 has therapeutic potential to increase the efficiency of drug delivery across barrier membranes.

Key words: Occludin, ZO-1, Actin, Paracellular permeability, Transepithelial conductance, Madin Darby Canine Kidney cells

Introduction:

NK_4-M2GlyR (KKKKPARVGLGITTVLTMTTGSSGSRA) is a channel forming peptide that was synthesized by adding four lysine residues to the second transmembrane segment (M2) of the glycine receptor (GlyR) alpha-subunit (2, 32, 35) and was shown to increase anion secretion by epithelial monolayers. However, the subsequent removal of up to five C-terminus residues of NK_4-M2GlyR reduced aggregation of the peptide in aqueous solution while retaining ion transport properties (2). Based on the hypothesis that only the N-terminus half of the peptide was necessary for its ion transport properties, a palindromic peptide was designed with 11 residues from the N-terminal half of NK_4-M2GlyR. The final sequence, KKKKAARVGLGITTVLVTTIGLGVRAA, was termed NC-1059.

NC-1059 enhances ion transport and reduces barrier function of epithelial monolayers. MDCK monolayers that were exposed to NC-1059 apically showed a concentration dependent increase in short circuit current (I_{sc}) demonstrating an increase in anion secretion or cation absorption. The transepithelial conductance (g_{te}), a measure of epithelial barrier function, also increased in a concentration dependent manner (1). Furthermore, NC-1059 enhanced the permeation of 9.5 kDa dextran, showing that a paracellular route was opened (1). The effect of the peptide on g_{te} and paracellular solute movement was reversed within 48 hours of returning the monolayers to fresh media. The cell monolayers regained responsiveness to subsequent treatments with the peptide (1). Thus the effects of NC-1059 on epithelial monolayers are reversible and repeatable.

Epithelial cell layers act as barriers to the movement of hydrophilic or uncharged molecules. The intercellular contacts between epithelial cells are called tight junctions and play a critical role in the barrier function. Tight junctions are “multimolecular complexes” located between the apical intercellular regions of both epithelial and endothelial cells that regulate paracellular

permeability (29). Occludin, claudins, junctional adhesion molecule-1 (JAM-1) and zona occludens protein-1 (ZO-1), along with other proteins form the tight junctions (29). The tight junction complex associates with the perijunctional actomyosin ring and this complex is proposed to be involved in regulation of the movement of solutes through the paracellular route (18). Compounds such as bacterial and fungal toxins (e.g., *Clodtridium difficle* toxins, ochratoxin), positively charged molecules (e.g., protamine) and chitosans are amongst several molecules observed to cause an increase in g_{te} through an effect on actin organization and /or localization of junctional proteins (20, 22, 25, 28). Peptides corresponding to the first and second extracellular loops of occludin also increased paracellular permeability. However they required several hours to produce significant effects (5, 36). More recently, a modified occludin peptide reportedly enhanced permeability across airway epithelia and caused a more rapid loss in localization of occludin at the tight junctions (31). The zonula occludens toxin of *Vibrio cholerae* (ZOT) is a naturally occurring peptide that increases the permeability of small intestine epithelia (10). ZOT is rapid in onset (< 20 min) and reversible. ZOT causes reorganization of actin and a change in the localization of ZO-1 (9). VP8, a rotavirus surface protein, enhances paracellular permeability by causing a redistribution of occludin, ZO-1 and claudin-3 at the tight junctions in MDCK monolayers (23). These results suggest that the actin cytoskeleton and the proteins comprising the tight junctions can be modulated either in distribution or abundance to affect epithelial barrier function.

Adheren junctions also contribute to the epithelial barrier. E-cadherin is a transmembrane adheren junction protein that associates with the actin cytoskeleton through β-catenin. These interactions are important in maintaining cell morphology and paracellular permeability (15). Additionally E-cadherin and β-catenin are important players in the assembly of the tight

junctions (14, 26). Disruption of E-cadherin is associated with an increase in paracellular permeability with an associated change in F-actin organization and organization of other junctional proteins (37-39). Hence a pronounced reorganization in F-actin might involve a change in distribution of E-cadherin and β-catenin.

The focus of this study is to establish the underlying microscopic mechanisms by which NC-1059 enhances the permeability across MDCK monolayers. We hypothesized that NC-1059 alters the localization of one or more junctional proteins. Also, since the actin cytoskeleton plays a significant role in regulating paracellular permeability, NC-1059 may induce changes in permeability by altering actin organization. This study determined the effects of selected NC-1059 concentrations on actin organization and the localization or abundance of occludin and ZO-1 over time. The study also evaluated the effects of NC-1059 on localization and abundance of adheren junction molecules E-cadherin and β-catenin. Finally the study also assessed the time course of recovery in the g_{te} and the pattern of the localization of the junctional proteins as the g_{te} recovered.

Methods:

Peptide Synthesis: NC-1059 was synthesized as described previously, by solid phase synthesis using 9-fluorenylmethoxycarbonyl chemistries (3). The peptide was purified by reversed-phase HPLC and characterized by Edman degradation and matrix-assisted laser desorption time of flight mass spectroscopy (3).

Chemicals: A 4% paraformaldehyde solution in phosphate buffered saline (PBS) was prepared from a 16% paraformaldehyde stock (Electron Microscopy Sciences, Hatfield, PA). Peptide stocks of 5 mM or 8 mM were prepared in deionized water just prior to use. Unless otherwise indicated, chemicals used were reagent grade obtained from Sigma Aldrich (St. Louis, MO).

Cell culture: MDCK cells were obtained from Dr. Lawrence Sullivan (University of Kansas Medical Center, Kansas City, KS) and maintained in culture as described previously (1, 2). Cells were grown on 25 cm^2 flasks (Corning Incorporated, Corning, NY) with a medium containing a 1:1 mixture of Dulbecco's modified Eagle medium and Nutrient F12 (GIBCO, Invitrogen, Carlsbad, CA), 5% heat inactivated fetal bovine serum (Atlanta Biologicals, Atlanta, GA) and 1% penicillin and streptomycin. Cells were maintained in a humidified incubator with 5% CO_2 at 37˚C. Cultures that were 90 to100% confluent were treated with 0.25% trypsin and 2.6 mM EDTA (GIBCO) and gentle mechanical force was used to dislodge cells from the surface. Approximately $5*10^5$ cells were seeded onto 1.13cm^2 permeable supports (Snapwell, Costar, Corning Incorporated). A tenth of the cells were also seeded onto flasks to further passage. The media were refreshed every alternate day.

Electrical Measurements: I_{sc} and transepithelial electrical potential were measured using a modified Ussing Chamber (model DCV9, Navicyte, San Diego, CA) as described previously (1,

2). Monolayers were bathed symmetrically with Ringer solution (in mM: 120 NaCl, 25 $NaHCO_3$, 3.3 KH_2PO_4, 0.8 K_2HPO_4, 1.2 $MgCl_2$, and 1.2 $CaCl_2$) that was prepared fresh daily, maintained at 37˚C and bubbled with 5% CO_2/ 95% O_2 to maintain pH. The monolayers were clamped to 0 mV and a 5 s 1 mV bipolar pulse was applied every 100 s using a voltage clamp (model 558C-5, University of Iowa, Dept. of Bioengineering, Iowa City, IA). Data acquisition was performed at 1 Hz using an Intel based computer and MP100A-CE interface (v. 3.2.6, BIOPAC Systems, Santa Barbara, CA). The current measured in response to the voltage pulse was used to calculate g_{te} (Ohms law, $g_{te} = \Delta I/\Delta V$).

FITC-Dextran permeability assay: Dextran permeation through the monolayer was measured as described previously (1). The medium was removed and the monolayers were washed with warmed PBS. Ringer solution was added to the basolateral (1 mL) and apical (200 µL) compartments in the Snapwell culture plate. NC-1059 or vehicle control was added to the Ringer solution on the apical side of the monolayers to result in a final concentration of 200 µM NC-1059. Monolayers were exposed to 5 mM EDTA in hypotonic Ringer solution (50 % dilution with water). Dextran (40 or 70 kDa) conjugated to FITC (0.5 mg) was added to the apical compartment of all treatments. After incubation at 37˚C for 1 hour samples were taken from the basolateral compartment for determination of fluorescence intensity (Fluorskan Ascent FL, Thermo Fisher Scientific, Waltham, MA). A series of dilutions of each size of dextran was prepared and fluorescence determined as a function of concentration. A linear regression was used to derive the slope and calculate the amount of dextran that permeated the monolayer.

Immunolabeling: MDCK monolayers were exposed to 200 µM NC-1059 for 5, 15, 30 and 60 min. NC-1074 (KKKKARSGSSQTTMTLARSGSSQTTMT), a peptide that does not elicit the changes in epithelial electrical parameters, or vehicle control was used as a negative control. In a

second set of experiments, concentration dependent effects were assessed by exposing MDCK monolayers to 100 μM or 200 μM NC-1059 for either 30 or 60 min. After the indicated treatments, the monolayers were fixed with 4% paraformaldehyde. Fixed monolayers were incubated with anti-occludin (Zymed, Carlsbad, CA) or anti-ZO-1 (Chemicon, Temecula, CA and Zymed) antibodies and with Alexa 488 conjugated phalloidin (Molecular Probes, Carlsbad, CA). In another set of experiments, MDCK monolayers were exposed to vehicle or 200 μM NC-1059 for 30 or 60 min. Monolayers were subsequently fixed and labeled with anti-E-cadherin (Hybridoma bank, University of Iowa, Iowa City, IA) or anti-β-catenin (BD Biosciences) antibodies. The secondary antibodies were conjugated to Alexa 488 (green), Alexa 594 (Red) or rhodamine (Red). TOPRO-3 (blue; Molecular Probes) was used to label the nucleus. Images were acquired using a confocal microscope (LSM 510, Carl Zeiss AG, Jena, Germany). Optical sections (0.8 μm) were obtained along the Z-axis from the apical to basolateral aspect of the cells to make a Z-stack. 3-D projection was used to obtain a composite view of selected regions within the Z-stack.

Immunoblotting: Proteins were extracted from MDCK monolayers following exposure to 100 or 200 μM NC-1059 or vehicle control for 30 or 60 min. Monolayers were subject to lysis using RIPA buffer (composition: 150 mM NaCl, 10 mM HEPES, 2 mM EDTA, 1% Triton X-100, 0.2% SDS, 0.5% sodium deoxycholate) with protease inhibitor cocktail III (Calbiochem, San Diego, CA) and Halt phosphatase inhibitor cocktail (Pierce, Rockford, IL) and the lysate was passed repeatedly through a 21 gauge needle. The lysate was incubated at 4˚C for 1 hour and then centrifuged at 4˚C and 14,000g for 15 min. The supernatant was collected and protein concentration determined using the bicinchoninic acid (BCA) method using albumin as standard (Pierce). The supernatants were mixed with 5x Lamelli sample buffer (250 mM Tris base, 40%

glycerol, 0.8% SDS, 20% β- mercaptoethanol and 0.01% bromophenol blue) and equal amounts of protein (15 to 35 μg) for each treatment were loaded onto 4-15% gel (Biorad, Hercules, CA) and resolved at a 140 mV for 1 hour using a running buffer (25 mM Tris Base, 200 mM Glycine, 0.1 % SDS). Proteins were transferred onto Immobilon–P transfer membrane (Millipore, Billerica, MA) overnight at 350 mA with transblot buffer (25 mM Tris base, 192 mM glycine, 20% v/v methanol). The membranes were blocked with 5% blotting grade milk (Biorad) in TBS (20 mM Tris base, 0.8% NaCl, pH 7.6) with 0.1% Tween-20 for 2 hours. Subsequently, the membranes were probed with either anti-occludin Mab (BD Biosciences, San Jose, CA), anti-ZO-1 Mab (Zymed), anti-E-cadherin (Hybridoma bank, University of Iowa, Iowa City, IA), anti-β-catenin (BD Biosciences) or anti-GAPDH Mab (Abcam, Cambridge, MA). HRP conjugated anti-rabbit and anti-mouse secondary antibodies (Amersham Biosciences, Piscataway, NJ) were used for detection. Chemiluminiscent substrate Super Signal West Pico and Femto (Pierce) were used for development. Images were obtained using the Kodak Imaging System (Kodak Image Station 4000 R, Kodak, Rochester, NY) and densitometric analysis (Kodak molecular imaging software v 4.5.0) was used to compare labeling intensity. Normalized intensity is the net intensity of the signal detected for each epitope and each treatment presented as a percentage of the net intensity detected for the corresponding GAPDH immunoreactivity in each lane.

Recovery experiments: Monolayers were mounted into modified Ussing chambers and I_{sc} and g_{te} measured as described. Monolayers were exposed to 100 or 200 μM NC-1059 or vehicle (Ringer solution) for 60 min and returned to the incubator for either 24 or 48 hours before g_{te} was assessed again. Each set of monolayers was fixed subsequently with 4% paraformaldehyde and labeled with anti-occludin and anti-ZO-1 antibodies as described.

Data analysis: All numerical results are reported as mean ± SEM. All graphs and regression fits were completed using Sigmaplot 2000 (v 6.0, SPSS Inc, Richmond, CA) and/or Excel (v 11.8, Microsoft Corp, Redmond, WA). The student's t-test (Sigmaplot) and ANOVA (Excel) were used for statistical analysis where required. The time course for NC-1059 induced changes in g_{te} was determined by fitting a sigmoidal function (Eqn. 1) to values of g_{te} that were calculated every one hundred seconds throughout each experiment using the time of NC-1059 exposure as the starting point (i.e, t=0).

$$g_{te} = g_{te\min} + \frac{\Delta g_{te\max}}{1 + e^{-\left[\frac{t-t_0}{b}\right]}} \qquad \textbf{Eqn. 1}$$

In Eqn. 1, $g_{te\ \min}$ is the baseline conductance and $\Delta g_{te\ \max}$ is the peak change in conductance reached during the recording for each NC-1059 concentration. b is inversely proportional to the slope at half $\Delta g_{te\ \max}$ and t_0 is the time taken to reach half $\Delta g_{te\ \max}$. The data used for the fit were restricted to ~ 300 s after the peak g_{te} was reached.

Results:

NC-1059 induces a concentration dependent change in g_{te}.

The average change in the g_{te} in response to 100 and 200 μM NC-1059 as a function of time is provided in Fig. 1. The graph reveals that the conductance increased with peptide exposure from a value of 0.56 ± 0.09 mS cm^{-2} to a maximal value in about 30 min and remained elevated throughout the experiment. A significant increase in g_{te} was observed with 100 μM (8.52 ± 1.17 mS cm^{-2}) and several fold greater response was observed with 200 μM (32.32 ± 1.18 mS cm^{-2}) NC-1059. The results indicated that the half-maximal response occurred more quickly as indicated by lag time (t_0) and slope (b) with exposure to 200 μM (t_0 = 14.60 ± 0.57 and b = 4.71 ± 0.51 min) as compared to 100 μM NC-1059 (t_0 = 23.36 ± 0.97and b = 7.01 ± 0.97 min).

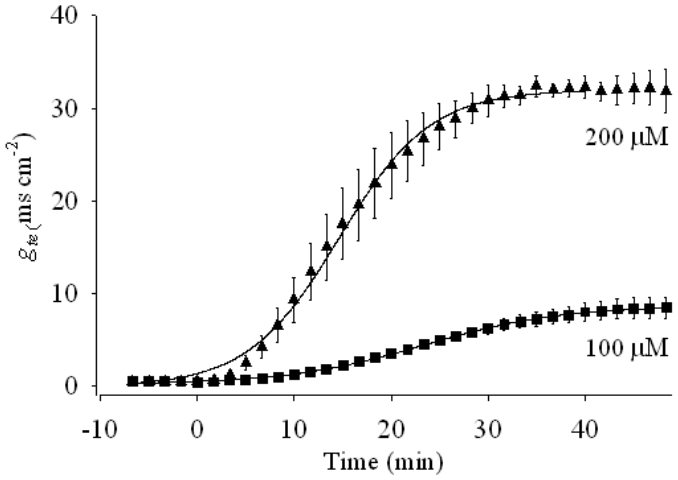

Figure 3.1: NC-1059 induces a concentration dependent change in g_{te}.

The figure shows the average change in g_{te} with 100 μM (■) and 200 μM (▲) NC-1059 as a function of time. The solid lines represent the best fit to Eqn. 1 to each data set. Results are summarized from n=3.

g_{te} is a composite measure of the transcellular and paracellular conductances. The substantial increase in g_{te} after exposure to NC-1059 is consistent with the introduction of ion channels in the apical membrane and suggests that a paracellular route is opened as reported previously (1). g_{te} is a measure of the movement of ions (< 100 kDa) although larger solutes might also permeate. Previously published observations indicate that exposure of MDCK monolayers to 60 μM NC-1059 resulted in a 5 fold increase in permeation of 9.5 kDa dextran (1). Permeation of molecules as > 77 kDa was not enhanced by the presence of NC-1059 (1). However, further experiments conducted with other epithelial cell types showed that 200 μM NC-1059 enhanced permeation of 40 and 70 kDa dextran (30). Hence experiments were conducted to measure permeation of intermediate sizes of dextran across MDCK monolayers, in the presence of NC-1059.

NC-1059 allows for the permeation of 40 and 70 kDa dextran across MDCK monolayers.

Dextran permeation across monolayers exposed to vehicle, 200 μM NC-1059 or EDTA over duration of 1 hour was measured (Fig. 2). Monolayers exposed to EDTA showed a large enhancement in permeation for both 40 and 70 kDa dextran relative to vehicle treated monolayers. NC-1059 also enhanced permeation of 40 and 70 kDa dextran relative to vehicle treated monolayers. However the fold enhancement is small compared to EDTA, a compound that has a disruptive effect on epithelia. These results support observations made with other cell types (30) and indicate that the paracellular route is partially opened to allow permeation by various size dextans across MDCK monolayers.

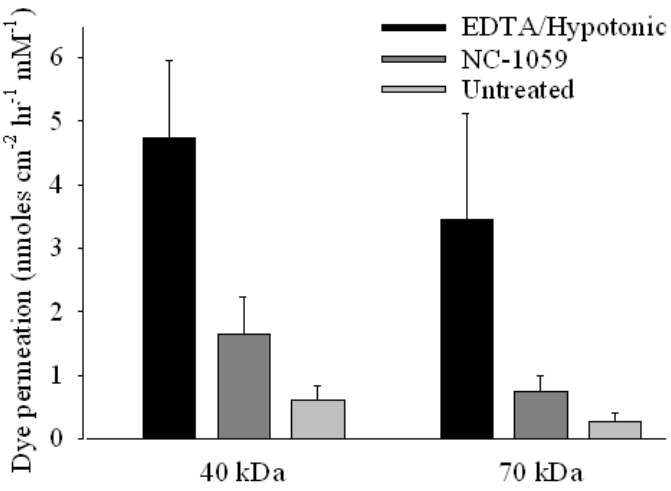

Figure 3.2: NC-1059 allows for the movement of uncharged molecules across MDCK epithelial monolayers.

FITC conjugated dextran of 40 and 70 kDa was added to the apical compartment and appearance of fluorescence in the basolateral compartment was quantified in the presence of one of three treatments (EDTA, NC-1059 and vehicle control as described in methods). Results are summarized from n=3.

The cell cytoskeleton, particularly its key component actin, along with associated junctional proteins regulates movement of ions and solutes through the paracellular route. Therefore tests were conducted to determine the effect of NC-1059 on the distribution and abundance of actin and the junctional proteins, occludin and ZO-1.

NC-1059 exposure causes a reorganization of actin: Experiments were conducted to determine the effect of NC-1059 on actin organization as a function of time (Fig. 3A). Images of the F-actin labeled monolayers were obtained as optical sections along the Z-axis. Sections of the Z-stack were divided into apical, middle and basal regions and each panel presented in the figure is a composite projection of these 4-6 optical sections. F-actin fibers are present throughout all

portions of all cells in the monolayer. Each cell is clearly circumscribed by the perijunctional actomyosin ring in the apical region. There is also central punctate staining of F-actin fibers in the apical region. The middle and basal sections show cortical actin filaments. In the most basal sections, actin filaments appear bundled and might constitute stress fibers. Exposure of the monolayer to 200 μM NC-1059 for 5 min showed little change in the F-actin labeling along the entire depth of the monolayer. The intensity of the labeling of central actin fibers and perijunctional actomyosin ring in some areas was clearly reduced at 15 min. The images (Fig. 3A) clearly show regions of the monolayer in which the apical sections exhibited no labeling while adjacent cells remained fully circumscribed. After 30 min of NC-1059 exposure an overall decrease in intensity of F-actin labeling was observed in the apical, middle and basal sections of the Z-stack. Relative to the 15 minute time point, larger regions of the monolayer were devoid of F-actin labeling especially at the apical regions. At the same time, the labeling of the perijunctional actomyosin actin ring was intensified in the remaining cells. After 60 min of NC-1059 exposure the labeling of apical actin fibers was dramatically reduced. There was a reduction in the punctate labeling of F-actin fibers apically and also a pronounced decrease in intensity of labeling of the perijunctional actomyosin actin ring. There was also a pronounced reduction in the labeling of fibers in the middle and basal portions of the cells. The reduction in the intensity of labeling both at the perijunctional actomyosin ring and F-actin fibers throughout the Z-stack suggested a disruption in the organization of the actin cytoskeleton in NC-1059 treated monolayers. Monolayers exposed to 200 μM NC-1074, a scrambled sequence of NK_4-M2GlyR that does not elicit any changes in ion transport, showed a labeling pattern for F-actin comparable to vehicle exposed monolayers. This suggests that the effect on actin organization was specific to the NC-1059 sequence.

NC-1059 has a concentration dependent effect on g_{te} and it is likely that the effect of NC-1059 on actin organization might also follow a concentration dependent pattern. The effect of 100 and 200 μM NC-1059 on actin organization in MDCK monolayers reveal that there is no discernable difference in the effect of both concentrations on actin organization (Fig. 3B). Exposure of monolayers to 100 μM NC-1059 for 30 min caused a reduction in the labeling of the actin fibers along all regions of the Z-stack. There was a decrease in the intensity at the perijunctional actomyosin ring and reduction in the central F-actin fibers along the apical sections. There was also reduction in labeling of the actin fibers along the middle and basal sections. Large areas showed a pronounced decrease in intensity of F-actin labeling, both centrally and along the perijunctional actomyosin ring. However, some cells exhibited an enhanced intensity especially along the perijunctional actomyosin ring. After 60 min of exposure with 100 μM NC-1059, there was a significant decrease in intensity and labeling of F-actin throughout most cells. The results observed with 200 μM NC-1059 were consistent with observations made in the previous experiment at the corresponding time points. The middle and basal sections show a further decrease in labeling intensity after 60 min of exposure with both concentrations. However it might be noted that after 60 min of exposure to 200 μM NC-1059, the labeling of the preijuntional actomyosin ring although substantially decreased in intensity, is still circumscribing all cells.

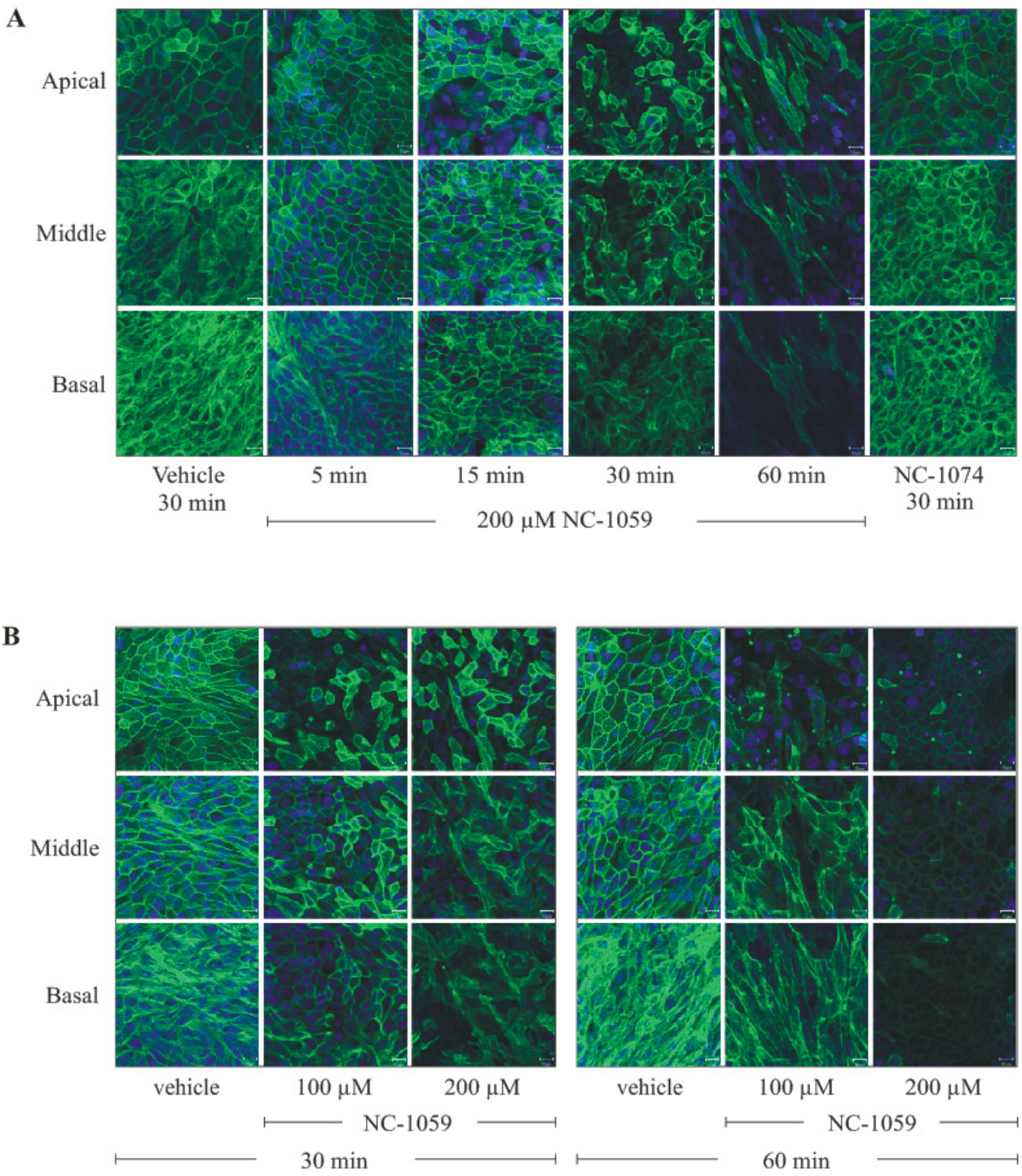

Figure 3.3: NC-1059 causes a reorganization of actin.

A) Time course of the effects of NC-1059 on actin organization. Panels show images of monolayers labeled with Alexa conjugated phalloidin. Images show typical F-actin labeling in

monolayers that were exposed to vehicle for 30 min or treated with 200 μM NC-1059 for 5, 15, 30 or 60 min or 200 μM NC-1074 for 30 min. Images were obtained as Z-stacks using confocal microscopy. Images shown above are the 3-D projection of the respective Z-stacks. **B)** Effect of 100 and 200 μM NC-1059 on actin organization: Monolayers were exposed to vehicle or 100 or 200 μM NC-1059 for 30 or 60 min and labeled with Alexa conjugated phalloidin. Images were obtained as Z-stacks using confocal microscopy. Images shown above are the 3-D projection of the respective Z-stacks. In both figures, the results are a typical example of n=4 and from paired monolayers.

NC-1059 alters the distribution of occludin and ZO-1: ZO-1 and occludin associate directly and indirectly with actin, respectively (7, 8, 24). Thus reorganization in the actin cytoskeleton may alter the localization of occludin and ZO-1, which could account for changes in the integrity of the paracellular barrier.

NC-1059 exposure was associated with diminished immunoreactivity of junctional proteins ZO-1 and occludin, with a more pronounced effect on ZO-1 (Fig. 4A). Monolayers that were exposed to vehicle and labeled with anti-occludin (green) and anti-ZO-1 (red) antibodies showed strong immunoreactivity in the apical region of the MDCK monolayers. ZO-1 and occludin localized at the tight junctions along cell-cell contact regions, as expected, and the proteins appeared to colocalize, as shown in the merged image. Exposure of MDCK monolayers to 200 μM NC-1059 for 5 min and 15 min showed apparent reduction in the intensity of labeling relative to vehicle treated monolayers. A pronounced reduction in ZO-1 immunoreactivity was observed within 30 min of exposure. After 30 min of exposure there was not only a reduction in intensity of ZO-1 labeling, but there appeared to be an absence of labeling in several areas of the monolayer. Occludin immunoreactivity appeared to be slightly reduced in intensity, albeit to a less pronounced extent when compared to ZO-1. After 60 min, immunoreactivity to ZO-1 was negligible and the labeling for occludin appeared to be discontinuous with a pronounced reduction in intensity. Immunoreactivity to anti-occludin and anti-ZO-1 antibodies in monolayers that were exposed to 200 μM NC-1074 for 30 min was comparable to vehicle.

The decrease in immunoreactivity of the junctional proteins followed a concentration dependent pattern in MDCK monolayers (Fig. 4B). Monolayers were exposed to 100 and 200 μM NC-1059 or vehicle for 30 or 60 min. Monolayers that were vehicle treated for 30 or 60 min showed comparable pattern of labeling for both occludin and ZO-1 immunoreactivity. Exposure to 200

μM NC-1059 resulted in substantially diminished immunoreactivity for occludin and ZO-1 within 30 min. Monolayers exposed to 100 μM NC-1059 for 30 min showed immunolabeling for both ZO-1 and occludin comparable to a monolayer that was exposed only to vehicle for 30 min. After 60 min of treatment both 100 and 200 μM NC-1059 showed a pronounced decrease in ZO-1 immunoreactivity and a discontinuous pattern of labeling for occludin. The immunolabeled images suggested a concentration dependent effect on the localization of the junctional proteins such as occludin and ZO-1. The immunolabeling results suggest that the distribution of the junctional proteins is altered. The decreased immunoreactivity at the apical junction could be due to change in localization or reduction in the overall abundance of these proteins.

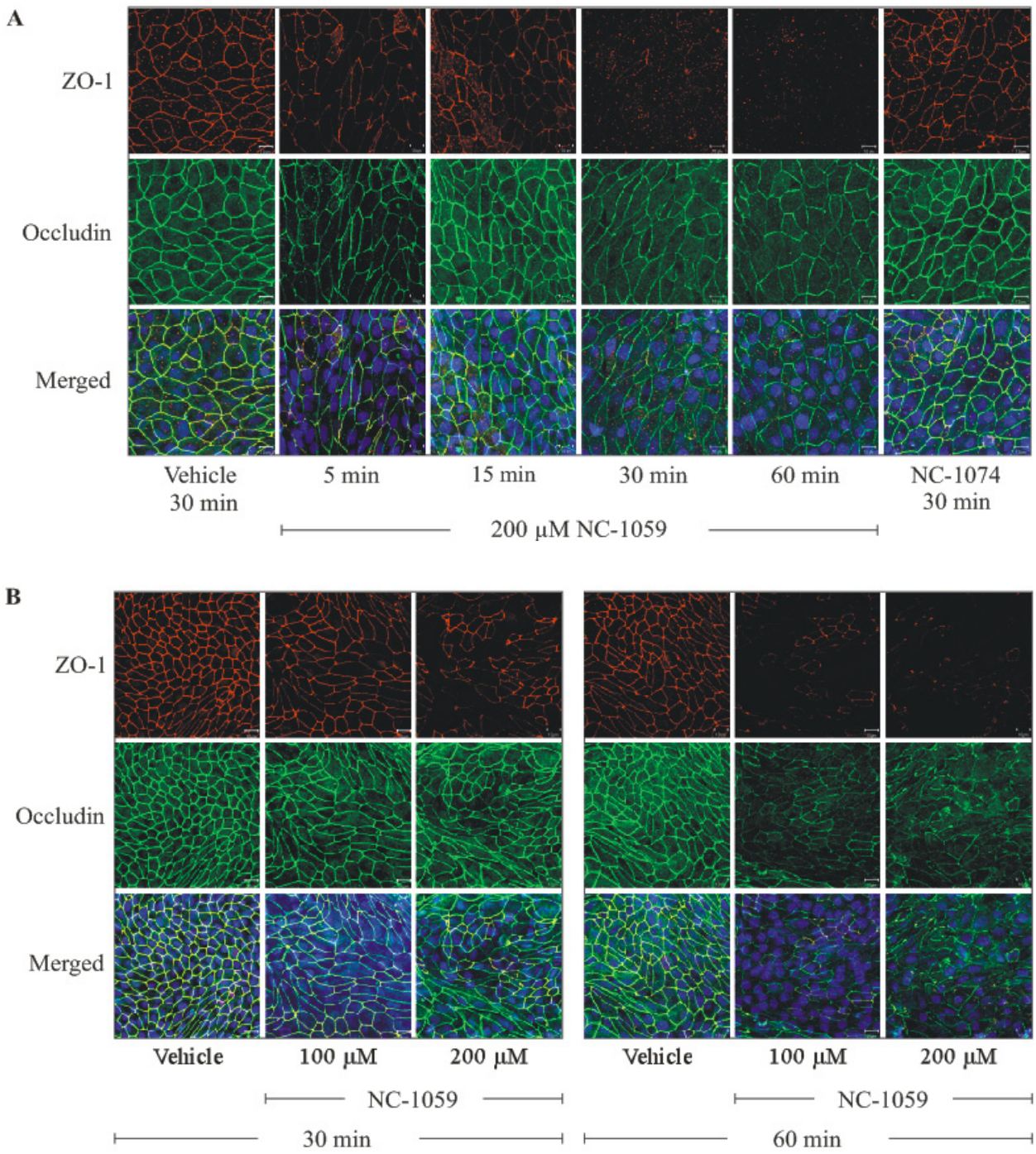

Figure 3.4: NC-1059 decreases ZO-1 and occludin immunoreactivity as a function of time and concentration.

A) Time course of the effects of NC-1059 on ZO-1 and occludin localization. Monolayers exposed to Ringer solution only for 30 min or to Ringer solution and 200 µM NC-1059 for 5, 15, 30 or 60 min were labeled with anti-ZO-1 (red, top panel) and anti-occludin antibodies (green,

middle panel). NC-1074 is a peptide that has no effect on transepithelial resistance and is used as a negative control. The bottom panels show the merged image with labeling for the nucleus in blue. **B)** Concentration dependent effects of NC-1059 on occludin and ZO-1 localization. Monolayers were exposed to vehicle or exposed to 100 or 200 μM NC-1059 for 30 and 60 min and subsequently labeled with anti-ZO-1 (red, top panel) and anti-occludin (green, middle panel) antibodies. All images were obtained as Z-stacks using confocal microscopy. Images shown are the 3-D projection of the respective Z-stacks. In both figures the results are a typical representation of n=4 and results presented represent data from paired monolayers.

NC-1059 decreases the occludin and ZO-1 cellular abundance in a concentration dependent manner: Immunoblotting was used to quantify the effect of 100 and 200 μM NC-1059 on the abundance of occludin and ZO-1. Fig. 5A is a typical immunoblot of protein extracted after apical exposure to 100 or 200 μM NC-1059 or vehicle for 30 or 60 min and labeled with anti ZO-1 antibodies. Immunoblotting showed a decrease in the intensity of ZO-1 bands, after 60 min of NC-1059 exposure relative to vehicle only. The average ZO-1 levels normalized to GAPDH, which was used as a loading control, are presented in Fig. 5B. The results showed a concentration dependent decrease in ZO-1 immunoreactivity after 30 min that was reduced further after 60 min of NC-1059 exposure. The intensity of vehicle exposed ZO-1 bands was comparable after 30 and 60 min. The loss of ZO-1 immunoreactivity was greater with 200 μM NC-1059 as compared to 100 μM NC-1059.

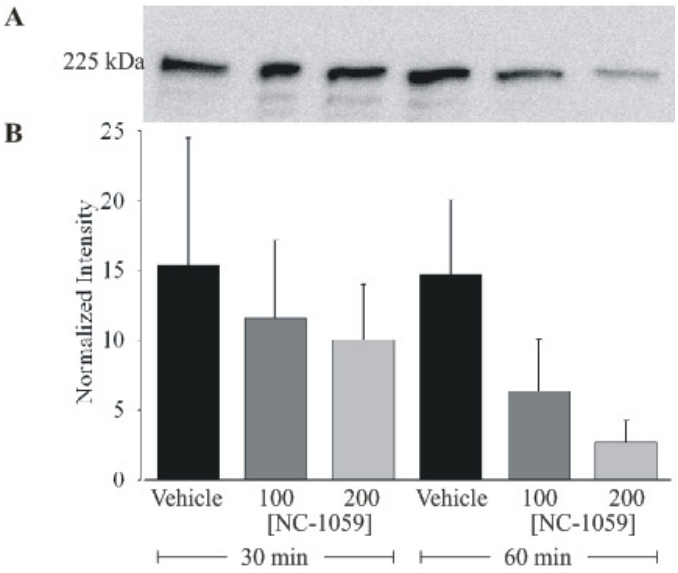

Figure 3.5: NC-1059 decreases cellular abundance of ZO-1 in a time and concentration dependent manner.

A) Typical immunoblot showing ZO-1 protein levels in monolayers that were exposed to vehicle or 100 or 200 μM NC-1059 for 30 or 60 min. **B)** Average ZO-1 immunoreactivity determined by densitometry and normalized to intensity of the corresponding GAPDH, in monolayers that were exposed to vehicle or 100 or 200 μM NC-1059 for 30 or 60 min (results are summarized from n=3).

A typical immunoblot (Fig. 6A) reveals a decrease in occludin immunoreactivity after 60 minutes of exposure to 100 and 200 μM NC-1059 relative to monolayers exposed to vehicle only for the same period of time. The intensity of the bands in the case of NC-1059 exposed monolayers decreased after 30 minutes and showed further reduction at 60 min as compared to vehicle treated. The immunoblot reveals a time and concentration dependent effect of the peptide on occludin immunoreactivity. The summarized results (Fig. 6B) show a 2 to 3 fold decrease in the occludin immunoreactivity, after 30 min of exposure to 100 or 200 μM NC-1059, which is reduced further after 60 min. The results show a trend that is consistent with time and concentration dependent changes in cellular occludin abundance after exposure to NC-1059.

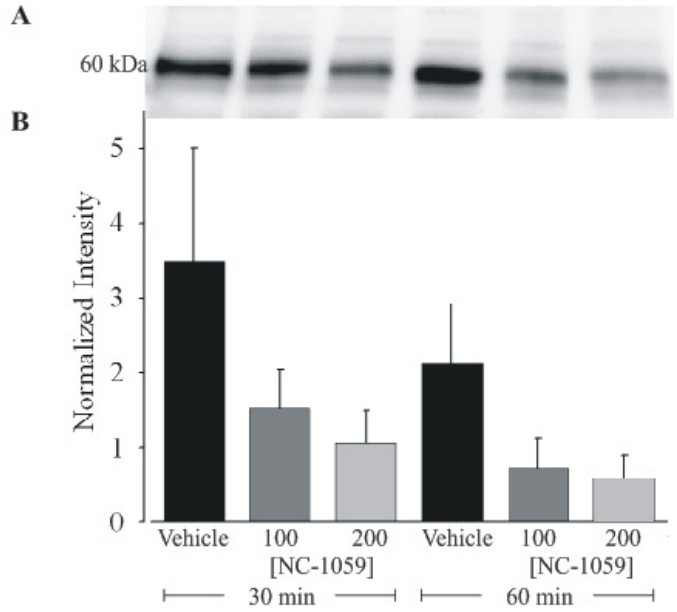

Figure 3.6: NC-1059 decreases cellular abundance of occludin in a time and concentration dependent manner.

A) Typical immunoblot showing occludin protein levels in monolayers that were exposed to vehicle or 100 or 200 μM NC-1059 for 30 or 60 min. **B)** Average immunoreactivity of occludin was determined by densitometry and normalized to corresponding GAPDH intensity in monolayers that were exposed to vehicle or 100 or 200 μM NC-1059 for 30 or 60 min (results are summarized from n=3).

Monolayers recover g_{te} and localization of tight junction proteins: The g_{te} of MDCK monolayers treated with 100 μM NC-1059 was observed to return to pretreatment levels 48 hours after exposure (1). Hence experiments were conducted to compare the pattern of recovery in g_{te} in monolayers treated with 100 and 200 μM NC-1059. Additionally, monolayers treated with 200 μM NC-1059 were labeled with anti-occludin and anti-ZO-1 antibodies to correlate the recovery in g_{te} with localization of junctional proteins.

The increase in g_{te} observed upon exposure to 100 and 200 μM returned to pretreatment levels over duration of 48 hours (Fig. 7). Monolayers were exposed to 100 or 200 μM NC-1059, or vehicle for 60 minutes. Monolayers were then placed back in typical culture conditions for 24 or 48 hours. The results summarized from 3 experiments showed a significant increase in g_{te} after exposure to 100 or 200 μM for 60 min. The change in g_{te} in the presence of 200 μM NC-1059 was four fold greater than with 100 μM. In monolayers exposed to 100 μM and recovered for 24 hours there was a 87% recovery in the g_{te} towards pretreatment levels. g_{te} recovered by at least 90% in the case of the 200 μM exposed monolayers. However in both cases, the g_{te} still remained significantly greater than pretreatment. In 48 hours the g_{te} decreased further. The majority of the recovery occurs within 24 hours and after 48 hours, the values are not significantly different from pretreatment.

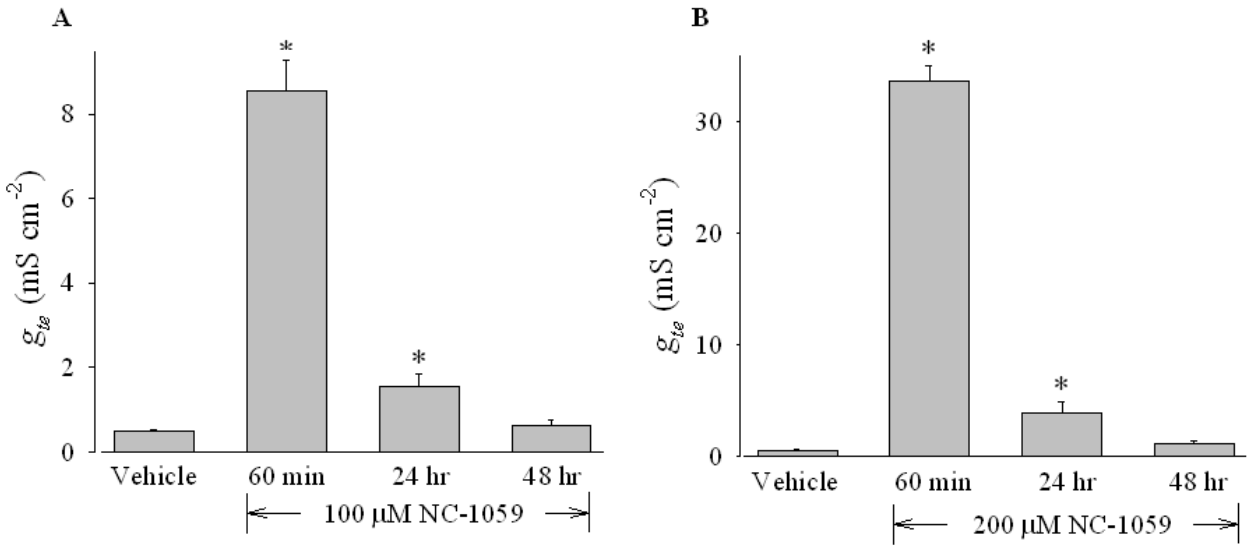

Figure 3.7: Monolayers exposed to 100 and 200 µM NC-1059 recover to pretreatment g_{te} within 48 hours.

Recovery in g_{te} after exposure to 100 µM (**A**) or 200 µM (**B**) NC-1059. Monolayers were exposed to vehicle or NC-1059 for 60 min in the Ussing chamber and returned to the incubator. g_{te} was subsequently measured after 24 hours and 48 hours post treatment for each pair (vehicle and NC-1059 treated) of monolayers and results are summarized from n = 3 (* $p<0.05$).

Occludin and ZO-1 are localized at the tight junctions within 24 hours following exposure to NC-1059. The localization pattern after 48 hours is indistinguishable from vehicle treated monolayers (Fig. 8). MDCK monolayers that were exposed to vehicle show that occludin and ZO-1 are localized as expected along the apical region of cell-cell contacts. MDCK monolayers that were exposed to 200 µM NC-1059 for 60 min showed reduced ZO-1 and occludin immunoreactivity along the apical cell-cell contacts. NC-1059 treated monolayers that were recovered for 24 hours showed greater intensity of the ZO-1 labeling at the tight junctions

similar to vehicle treated conditions. The intensity of occludin labeling was also recovered as compared to treatment with NC-1059 at 60 min but appeared to be less pronounced as compared to the vehicle exposed monolayers. After 48 hours, ZO-1 immunolabeling showed a pattern and intensity comparable to control conditions, which suggests that localization of ZO-1 to the tight junctions was fully restored. Occludin localization along cell-cell contacts also appeared to be more pronounced after 48 hours of recovery.

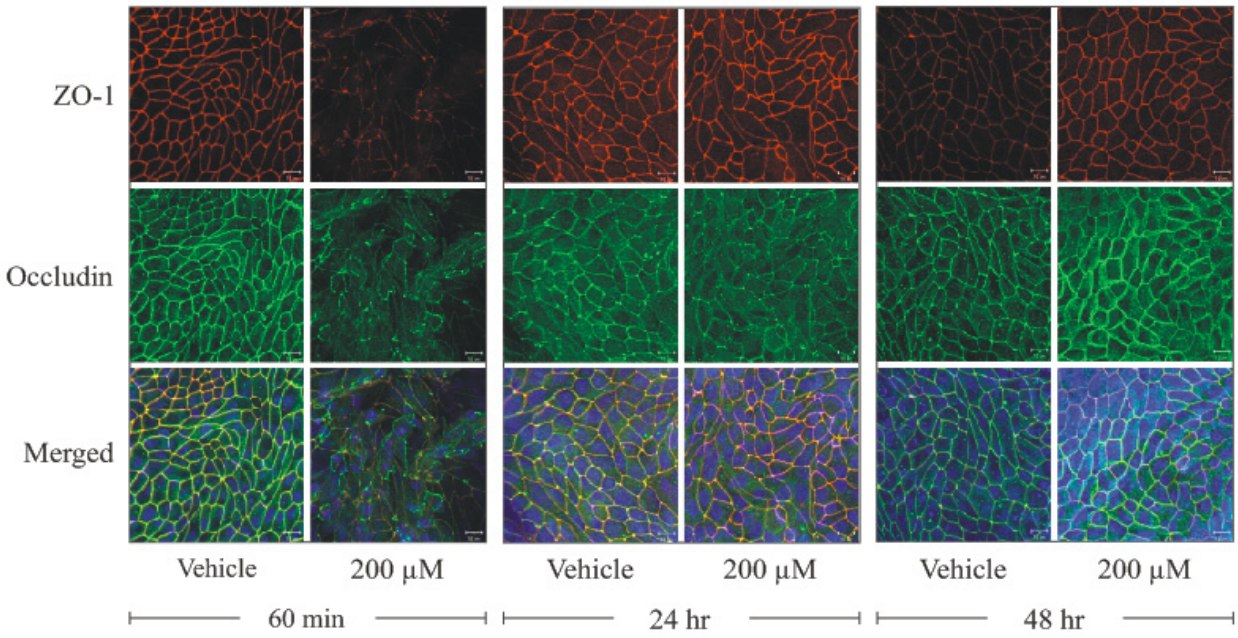

Figure 3.8: Immunoreactivity of occludin and ZO-1 at the tight junctions recovers within 24 hours.

Monolayers exposed to vehicle or 200 µM NC-1059 for 60 min. Monolayers were either fixed at 60 min or returned to the incubator for 24 or 48 hours, and fixed subsequently. Monolayers were then labeled with anti-occludin (green) and anti-ZO-1 (red) antibodies. Images were obtained as Z-stacks using confocal microscopy. Images shown above are the 3-D projection of the respective Z-stacks. Results are a typical representation of n=2..

NC-1059 alters the distribution of E-cadherin and β-catenin: NC-1059 caused a decrease in immunoreactivity of the adheren junction proteins E-cadherin and β-catenin (Fig. 9). Monolayers were exposed to 200 μM NC-1059 or vehicle (Ringer solution) for 30 or 60 minutes. Monolayers were subsequently fixed and labeled with anti-E-cadherin and anti-β-catenin antibodies. An orthogonal view showing the central optical slice (0.8 μM) and labeling along the x and y axis is presented for each condition. Monolayers that were vehicle treated for 30 or 60 minutes showed a reticular pattern of labeling along cell-cell contacts for E-cadherin and β-catenin, which is consistent with the localization of these proteins at the adheren junction. Exposure to 200 μM NC-1059 for 30 min resulted in decreased immunoreactivity of both E-cadherin and β-catenin and the labeling pattern appeared to be diffuse. After 60 minutes of exposure to 200 μM NC-1059, immnuoreactivity of E-cadherin and β-catenin was diminished further.

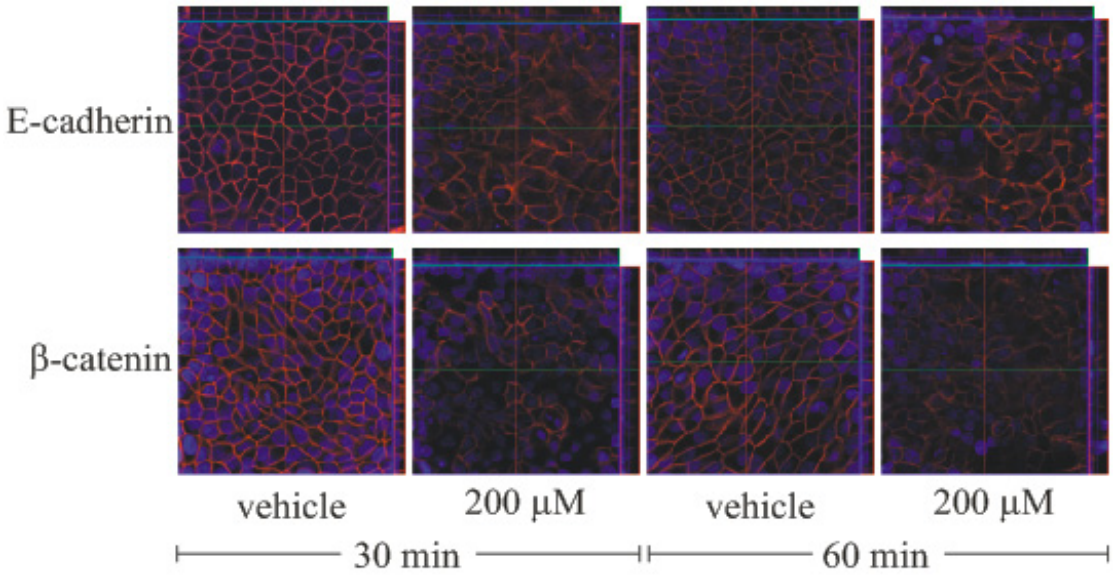

Figure 3.9: NC-1059 alters distribution of distribution of E-cadherin and β-catenin.

A) Monolayers were exposed to 200 μM NC-1059 or vehicle (Ringer solution) for 30 or 60 minutes and labeled with anti-E-cadherin (red, top panel), and anti-β-catenin (red, bottom panel) antibodies. Images are presented as an orthogonal view showing a single optical slice (0.8 μM) of the Z-stack and the labeling along x and y axis. Results are typical of n=2.

NC-1059 alters abundance of junctional proteins: NC-1059 reduced the cellular abundance of junctional proteins, E-cadherin and also has a modest affect on β-catenin abundance. Typical immunoblots of monolayers exposed to vehicle, 100 and 200 μM NC-1059 for 30 or 60 minutes and immunolabeled for E-cadherin and β-catenin, are represented in Fig. 10. A reduction in intensity of the E-cadherin after exposure to 100 and 200 M NC-1059 is observed after 60 min (Fig. 10A). The decrease in intensity appears to be greater with 200 μM NC-1059. Additionally a faint ~80 kDa band is observed that might be a breakdown product of E-cadherin. There is no

visually discernable effect of NC-1059 in the intensity of the bands as compared to vehicle treated monolayers in typical immunoblots shown for β-catenin (Fig. 10B). Nonetheless the effect on cellular abundance of β-catenin (Fig. 10B) is modest with a decrease in immunoreactivity seen only at 60 minutes which is less than 2 fold as compared to vehicle treated. The abundance of E-cadherin decreases with time and shows a concentration dependent trend (Fig. 10A). A 2 fold difference in E-cadherin immunoreactivity is observed after 60 min of NC-1059 exposure.

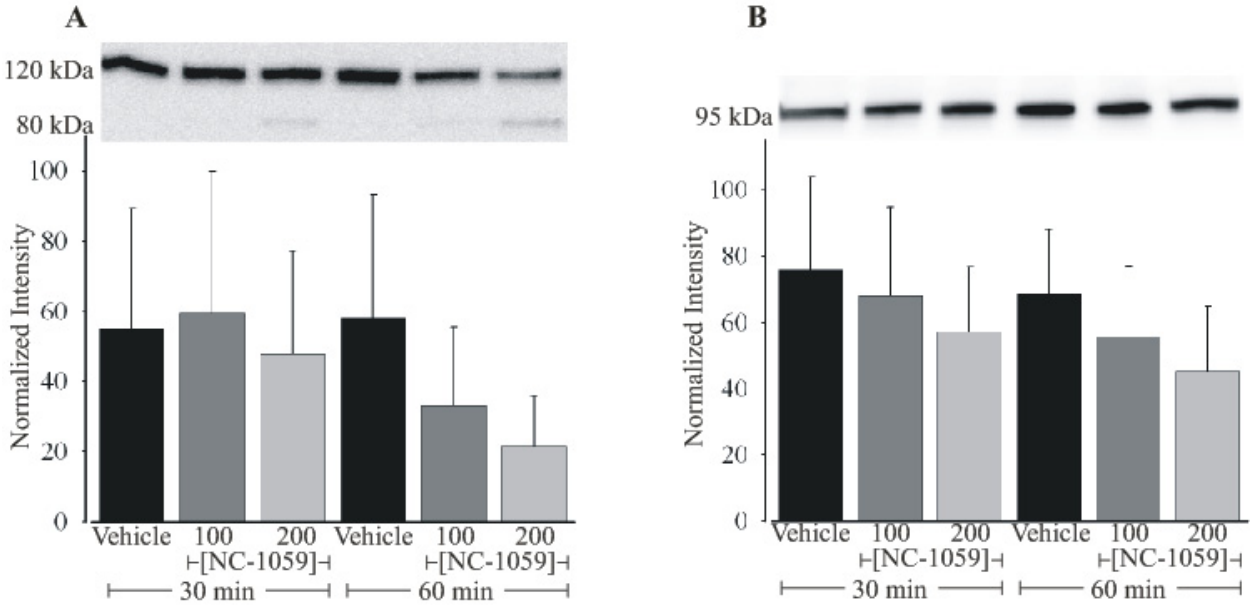

Figure 3.10: NC-1059 affects cellular abundance of E-cadherin and β-catenin.

Typical and summarized results from immunoblots of monolayers exposed to vehicle, 100 or 200 μM NC-1059 for 30 or 60 min and labeled for **A)** E-cadherin or **B)** β-catenin is shown above. (Results are summarized from n=3).

Discussion:

The results demonstrate that the NC-1059 induces an increase in paracellular permeability that is associated with a change in organization of the actin cytoskeleton and a decrease in abundance of occludin and ZO-1 at the tight junctions. NC-1059 enhances g_{te} and solute permeability through a paracellular route in MDCK monolayers in a concentration dependent manner. The effects of NC-1059 on g_{te} and localization or abundance of the junctional proteins are transient insofar as the g_{te} and localization of junctional proteins showed substantial recovery within 24 hours and complete recovery in 48 hours.

Apical exposure to NC-1059 caused a large increase in g_{te} in a concentration dependent manner. The rate of change in g_{te} and maximal g_{te} were significantly greater with 200 μM NC-1059 compared to 100 μM NC-1059. Previous studies showed that 60 μM NC-1059 enhanced permeability to dextran although 60 μM did not enhance passage of dextrans as large as 77 kDa (1). However current results show that 200 μM NC-1059 enhanced the permeation of both 40 and 70 kDa dextran several fold as compared to untreated monolayers. Permeation across epithelial barriers is the rate limiting step in the delivery of many drugs and since NC-1059 can enhance permeation of molecules as large as 70 kDa, it might provide the opportunity to develop a co-therapeutic to enhance localized delivery of several antibiotics and especially antivirals which are typically larger.

Apical exposure to 200 μM NC-1059 caused a reorganization of actin that was detectable as early as 15 min after exposure. There was a pronounced decrease in the intensity of labeling of F-actin after 30 min of NC-1059 exposure. Actin reorganization with both 100 and 200 μM NC-1059 followed a similar time course. F-actin is the polymerized form of actin and G-actin is the

monomeric form. The polymerization is a reversible reaction and the two forms exist in equilibrium at a critical concentration of G-actin (17). Loss of F-actin labeling suggests that there might be an NC-1059 induced depolymerization of F-actin. This could be due to an increase in the rate of depolymerization or destabilization of the F-actin structure as is the case with compounds such as cytochalasin (17). Based on observations under physiological conditions, it was proposed that the contraction of the perijunctional actomyosin ring might play a role in enhancing permeability through the paracellular route (18, 34). Extracellular molecules such as cytochalasins (19), protamines (25) and ZOT (9) are among several molecules that have been observed to enhance permeability by altering the organization of actin and specifically the perijunctional actomyosin ring. The NC-1059 induced increase in g_{te} is associated with the rearrangement of actin, which might be a common mechanism associated with increase in paracellular permeability.

NC-1059 treated MDCK monolayers show reduced immunoreactivity to antibodies against occludin and ZO-1, which suggests that NC-1059 causes a change in the distribution or expression of occludin and ZO-1. The distribution of ZO-1 appears to be altered to larger extent by 200 μM NC-1059 than by 100 μM NC-1059 at the 30 minute time point. There is little change in occludin at 30 min. Western blotting indicates NC-1059 decreases protein levels of both occludin and ZO-1, which likely reflects enhanced breakdown or reduced synthesis in the junctional proteins. The loss of ZO-1, as indicated by immunoblotting also follows a concentration dependent trend. ZO-1 is a MAGUK protein that has several protein-protein interaction domains and hence serves as a scaffold for the interaction of junctional proteins and the actin cytoskeleton (7, 11). ZO-1 interacts with occludin through its GUK domain and with actin through its C-terminus (12, 16). Additionally occludin interacts with actin directly (24).

Hence the NC-1059 mediated change in actin organization might cause in the loss of localization of occludin and ZO-1 at the tight junctions through its direct and indirect interactions with these proteins leading to disruption of barrier integrity.

NC-1059 has an effect on distribution and cellular abundance of the adheren junction proteins, E-cadherin and β-catenin. Although the intensity of β-catenin localized at the adheren junctions is diminished, the effect of NC-1059 on overall abundance is modest. This suggests that, the protein might be accumulating in the cytosol. Immunoblot of E-cadherin shows the appearance of a single breakdown product suggesting that E-cadherin is cleaved by a specific protease. Breakdown of E-cadherin has been reported in the case of ATP depletion (4) and also implicated in the effects on paracellular permeability by the zinc metalloprotease, *Bacteroides fragilis* toxin (27, 37) The detection of an 80 kDa fragment is unusual since metalloproteases cause ectodomain shedding with loss of the 80 kDa fragment and detection of only a 30-40 kDa fragment in other systems (38). Nevertheless the results are consistent with a protease activity.

The effect of NC-1059 is transient. Despite the loss of F-actin, especially in the basal region of the cells, the monolayers remained adherent and the g_{te} recovered to pretreatment levels within 48 hours. After 24 hours there was obvious recovery of ZO-1 localization to the cell periphery in the monolayers and occludin also recovered, although to a lesser extent. Recovery could involve either synthesis of new protein or recruitment from a preexisting or recycling pool. The reduction in overall immunoreactivity in western blots argues against recycling of protein. Moreover the recovery in g_{te} to pretreatment values requires more than 24 hours, which suggest that recovery might require synthesis and assembly of the junctional proteins. Localization of junctional proteins after 48 hours is comparable to untreated monolayers. ZO-1 is proposed to be an early

player in the assembly of junctional proteins (21). Hence recovery in ZO-1 might be significant in the recovery of $g_{te.}$

The transient effect of NC-1059 on modulating barrier function is particularly significant in developing a co-therapeutic to enhance delivery of drugs across epithelial barriers. "Absorption enhancers" are being developed to deliver clinically relevant therapeutics across epithelial barriers. Molecules that are hydrophilic and or large in size cannot easily permeate epithelial barriers. Systemic drug delivery requires larger doses of drugs and is therefore associated with potential side effects (33). Several barrier epithelia such as intestinal, airway and corneal / conjuctival epithelia are potential targets for localized drug delivery (6, 13). Results presented in this paper show that NC-1059 enhances the permeation of molecules as large as 70 kDa across MDCK epithelial monolayers. The effects on permeability can be generalized to several other epithelial cell lines derived from a variety of sources (30). NC-1059 reversibly alters the organization of actin and localization of junctional proteins, which may account for the enhanced permeability. Hence NC-1059 has potential to be developed as an absorption enhancer for therapeutic agents.

Acknowledgements: We extend thanks to Dr. Rebecca Quesnell and Dr. Yasuaki Hiromasa for technical assistance. This article is contribution # 08-209-J from the Kansas Agriculture Station, Manhattan, KS-66506.

This study is supported by GM 074096 to JMT and P20 RRO17686 (COBRE confocal facility).

References

1. **Broughman JR, Brandt RM, Hastings C, Iwamoto T, Tomich JM, and Schultz BD.** Channel-forming peptide modulates transepithelial electrical conductance and solute permeability. *Am J Physiol Cell Physiol* 286: C1312-1323, 2004.

2. **Broughman JR, Mitchell KE, Sedlacek RL, Iwamoto T, Tomich JM, and Schultz BD.** NH(2)-terminal modification of a channel-forming peptide increases capacity for epithelial anion secretion. *Am J Physiol Cell Physiol* 280: C451-458, 2001.

3. **Broughman JR, Shank LP, Prakash O, Schultz BD, Iwamoto T, Tomich JM, and Mitchell K.** Structural implications of placing cationic residues at either the NH2- or COOH-terminus in a pore-forming synthetic peptide. *J Membr Biol* 190: 93-103, 2002.

4. **Bush KT, Tsukamoto T, and Nigam SK.** Selective degradation of E-cadherin and dissolution of E-cadherin-catenin complexes in epithelial ischemia. *Am J Physiol Renal Physiol* 278: F847-852, 2000.

5. **Chung NP, Mruk D, Mo MY, Lee WM, and Cheng CY.** A 22-amino acid synthetic peptide corresponding to the second extracellular loop of rat occludin perturbs the blood-testis barrier and disrupts spermatogenesis reversibly in vivo. *Biol Reprod* 65: 1340-1351, 2001.

6. **Edward A and Prausnitz MR.** Predicted permeability of the cornea to topical drugs. *Pharm Res* 18: 1497-1508, 2001.

7. **Fanning AS, Jameson BJ, Jesaitis LA, and Anderson JM.** The tight junction protein ZO-1 establishes a link between the transmembrane protein occludin and the actin cytoskeleton. *J Biol Chem* 273: 29745-29753, 1998.

8. **Fanning AS, Ma TY, and Anderson JM.** Isolation and functional characterization of the actin binding region in the tight junction protein ZO-1. *FASEB J* 16: 1835-1837, 2002.

9. **Fasano A, Fiorentini C, Donelli G, Uzzau S, Kaper JB, Margaretten K, Ding X, Guandalini S, Comstock L, and Goldblum SE.** Zonula occludens toxin modulates tight junctions through protein kinase C-dependent actin reorganization, in vitro. *J Clin Invest* 96: 710-720, 1995.

10. **Fasano A, Uzzau S, Fiore C, and Margaretten K.** The enterotoxic effect of zonula occludens toxin on rabbit small intestine involves the paracellular pathway. *Gastroenterology* 112: 839-846, 1997.

11. **Funke L, Dakoji S, and Bredt DS.** Membrane-associated guanylate kinases regulate adhesion and plasticity at cell junctions. *Annu Rev Biochem* 74: 219-245, 2005.

12. **Furuse M, Itoh M, Hirase T, Nagafuchi A, Yonemura S, and Tsukita S.** Direct association of occludin with ZO-1 and its possible involvement in the localization of occludin at tight junctions. *J Cell Biol* 127: 1617-1626, 1994.

13. **Ghandehari H, Smith PL, Ellens H, Yeh PY, and Kopecek J.** Size-dependent permeability of hydrophilic probes across rabbit colonic epithelium. *J Pharmacol Exp Ther* 280: 747-753, 1997.

14. **Gumbiner BM.** Regulation of cadherin-mediated adhesion in morphogenesis. *Nat Rev Mol Cell Biol* 6: 622-634, 2005.

15. **Hartsock A and Nelson WJ.** Adherens and tight junctions: Structure, function and connections to the actin cytoskeleton. *Biochim Biophys Acta*, 2007.

16. **Li Y, Fanning AS, Anderson JM, and Lavie A.** Structure of the conserved cytoplasmic C-terminal domain of occludin: identification of the ZO-1 binding surface. *J Mol Biol* 352: 151-164, 2005.

17. **Lodish H, Baltimore D, Berk A, Zipursky LS, Matsudara P, and Darnell J.** *Molecular Cell Biology*. New York: W.H.Freeman and Company, 1995.

18. **Madara JL.** Regulation of the movement of solutes across tight junctions. *Annu Rev Physiol* 60: 143-159, 1998.

19. **Madara JL, Barenberg D, and Carlson S.** Effects of cytochalasin D on occluding junctions of intestinal absorptive cells: further evidence that the cytoskeleton may influence paracellular permeability and junctional charge selectivity. *J Cell Biol* 102: 2125-2136, 1986.

20. **McLaughlin J, Padfield PJ, Burt JP, and O'Neill CA.** Ochratoxin A increases permeability through tight junctions by removal of specific claudin isoforms. *Am J Physiol Cell Physiol* 287: C1412-1417, 2004.

21. **McNeil E, Capaldo CT, and Macara IG.** Zonula occludens-1 function in the assembly of tight junctions in Madin-Darby canine kidney epithelial cells. *Mol Biol Cell* 17: 1922-1932, 2006.

22. **Moore R, Pothoulakis C, LaMont JT, Carlson S, and Madara JL.** C. difficile toxin A increases intestinal permeability and induces Cl- secretion. *Am J Physiol* 259: G165-172, 1990.

23. **Nava P, Lopez S, Arias CF, Islas S, and Gonzalez-Mariscal L.** The rotavirus surface protein VP8 modulates the gate and fence function of tight junctions in epithelial cells. *J Cell Sci* 117: 5509-5519, 2004.

24. **Paris L, Tonutti L, Vannini C, and Bazzoni G.** Structural organization of the tight junctions. *Biochim Biophys Acta*, 2007.

25. **Peixoto EB and Collares-Buzato CB.** Protamine-induced epithelial barrier disruption involves rearrangement of cytoskeleton and decreased tight junction-associated protein expression in cultured MDCK strains. *Cell Struct Funct* 29: 165-178, 2005.

26. **Rajasekaran AK, Hojo M, Huima T, and Rodriguez-Boulan E.** Catenins and zonula occludens-1 form a complex during early stages in the assembly of tight junctions. *J Cell Biol* 132: 451-463, 1996.

27. **Richard JF, Petit L, Gibert M, Marvaud JC, Bouchaud C, and Popoff MR.** Bacterial toxins modifying the actin cytoskeleton. *Int Microbiol* 2: 185-194, 1999.

\28. **Schipper NG, Varum KM, and Artursson P.** Chitosans as absorption enhancers for poorly absorbable drugs. 1: Influence of molecular weight and degree of acetylation on drug transport across human intestinal epithelial (Caco-2) cells. *Pharm Res* 13: 1686-1692, 1996.

29. **Schneeberger EE and Lynch RD.** The tight junction: a multifunctional complex. *Am J Physiol Cell Physiol* 286: C1213-1228, 2004.

30. **Somasekharan S, Iwamoto T, Tomich JM, and Schultz BD.** Epithelial Barrier Modulation by a Channel Forming Peptide. Manuscript has been submitted for review and is anticipated that it will be published prior to this article. However in the event that it will not be accepted, the intext citation will be changed to unpublished observations. The manuscript is available to reviewers upon request., 2008*.

31. **Tavelin S, Hashimoto K, Malkinson J, Lazorova L, Toth I, and Artursson P.** A new principle for tight junction modulation based on occludin peptides. *Mol Pharmacol* 64: 1530-1540, 2003.

32. **Tomich JM, Wallace D, Henderson K, Mitchell KE, Radke G, Brandt R, Ambler CA, Scott AJ, Grantham J, Sullivan L, and Iwamoto T.** Aqueous solubilization of transmembrane peptide sequences with retention of membrane insertion and function. *Biophys J* 74: 256-267, 1998.

33. **Torchilin VP.** Drug targeting. *Eur J Pharm Sci* 11 Suppl 2: S81-91, 2000.

34. **Turner JR, Rill BK, Carlson SL, Carnes D, Kerner R, Mrsny RJ, and Madara JL.** Physiological regulation of epithelial tight junctions is associated with myosin light-chain phosphorylation. *Am J Physiol Cell Physiol* 273: C1378-1385, 1997.

35. **Wallace DP, Tomich JM, Iwamoto T, Henderson K, Grantham JJ, and Sullivan LP.** A synthetic peptide derived from glycine-gated Cl- channel induces transepithelial Cl- and fluid secretion. *Am J Physiol Cell Physiol* 272: C1672-1679, 1997.

36. **Wong V and Gumbiner BM.** A synthetic peptide corresponding to the extracellular domain of occludin perturbs the tight junction permeability barrier. *J Cell Biol* 136: 399-409, 1997.

37. **Wu S, Lim KC, Huang J, Saidi RF, and Sears CL.** Bacteroides fragilis enterotoxin cleaves the zonula adherens protein, E-cadherin. *Proc Natl Acad Sci U S A* 95: 14979-14984, 1998.

38. **Wu S, Rhee KJ, Zhang M, Franco A, and Sears CL.** Bacteroides fragilis toxin stimulates intestinal epithelial cell shedding and gamma-secretase-dependent E-cadherin cleavage. *J Cell Sci* 120: 1944-1952, 2007.

39. **Wu S, Shin J, Zhang G, Cohen M, Franco A, and Sears CL.** The Bacteroides fragilis toxin binds to a specific intestinal epithelial cell receptor. *Infect Immun* 74: 5382-5390, 2006.

Summary and Conclusions

NC-1059 is a synthetic channel forming peptide that reversibly modulates epithelial barrier function. Therefore it has potential to be developed into a co-therapeutic that can enhance the absorption of drugs in a localized manner across epithelial barriers.

NC-1059 increased short circuit current (I_{sc}) and transepithelial conductance (g_{te}) in a concentration dependent manner across several epithelial monolayers. The changes in the electrical parameters are consistent with the association of NC-1059 with the membrane to form ion channels that result in an increase in anion secretion or cation absorption. The increased g_{te} also suggest an effect on paracellular conductance. Although the effects of NC-1059 varied depending upon cell type, these results suggest that NC-1059 can alter the electrical properties of most epithelia.

The effect of NC-1059 on g_{te} is accompanied by an increase in paracellular permeability. Although there is no clear correlation between the paracellular permeability and $g_{te,}$ it appears that a large increase in g_{te} results in a significant increase in permeability even of large dextrans. Dextran permeability is enhanced to varying extents in different epithelia. Also, permeability is size dependent and size selectivity is maintained after NC-1059 exposure but not after exposure to EDTA. EDTA is reported to cause a pronounced disruption of the junctional proteins. Based on the differences in permeability, it is clear that the mechanisms that mediate the effects of NC-1059 are less disruptive than EDTA and probably involve select junctional proteins.

NC-1059 is distinct from zona occludens toxin (ZOT) in that the effects of ZOT are reportedly limited to certain epithelia. ZOT and compounds derived from ZOT such as ΔG lack activity in

colon (Di Pierro et al., 2001; Fasano et al., 1995). NC-1059 has significant effects on a colonic cell line (T-84). This suggests that NC-1059 might be useful in enhancing permeability across epithelia, separate from already discovered compounds.

The effects on paracellular permeability suggested a mechanism that includes changes in the organization of molecules that compose or regulate the tight junctions. NC-1059 induced increases in g_{te} and permeability are accompanied by a reorganization of actin, which begins within the first 15 minutes of exposure and pronounced effects are observed in less than 60 minutes. NC-1059 also affects distribution and abundance of tight junction proteins occludin and ZO-1. There is a pronounced effect on ZO-1 localization and these effects follow a similar time course as F-actin disruption. NC-1059 has an effect on the distribution and cellular abundance of the adheren junction proteins, E-cadherin and β-catenin. NC-1059 causes a time and concentration dependent decrease in the abundance of E-cadherin, with immunoblots suggesting a possible breakdown of E-cadherin.

It is clear that breakdown of E-cadherin, redistribution of β-catenin, F-actin rearrangement and disruption of tight junction proteins ZO-1 and occludin are inter-related events and are either regulated by identical mechanisms or pathways with significant cross talk. Taken together the results suggest that NC-1059 mediated increase in paracellular permeability might activate biochemical pathways common to several molecules that modulate barrier function. Small G proteins have a significant role in regulating F-actin organization and junctional proteins. The reorganization of actin accompanied by disruption of tight junction proteins caused by activation or inactivation of Rho and Rac also affects localization of E-cadherin in MDCK monolayers (Jou, Schneeberger & Nelson, 1998). It is possible that the reorganization of actin and possibly subsequent loss in junctional proteins induced by NC-1059, could involve Rho/Rac activity.

The most significant observation is that the effects of NC-1059 on epithelial permeability are reversible. The majority of the g_{te} recovers within 24 hours along with the localization of junctional proteins particularly ZO-1. ZO-1 is involved in tight junction assembly and hence localization of ZO-1 at the tight junctions suggests reassembly of the tight junctions. In studies where E-cadherin was degraded as seen with ATP depletion or *Bacteroides fragilis* toxin (BFT), the effects were reversible and synthesis of E-cadherin was involved in recovery (Wu et al., 1998; Wu et al., 2006). The reversible modulation of the junctional proteins that enhances paracellular permeability is an encouraging discovery in the development of an absorption enhancer.

References

Di Pierro, M., Lu, R., Uzzau, S., Wang, W., Margaretten, K., Pazzani, C., Maimone, F., Fasano, A. 2001. Zonula occludens toxin structure-function analysis. Identification of the fragment biologically active on tight junctions and of the zonulin receptor binding domain. *J Biol Chem* **276:**19160-5

Fasano, A., Fiorentini, C., Donelli, G., Uzzau, S., Kaper, J.B., Margaretten, K., Ding, X., Guandalini, S., Comstock, L., Goldblum, S.E. 1995. Zonula occludens toxin modulates tight junctions through protein kinase C-dependent actin reorganization, in vitro. *J Clin Invest* **96:**710-20

Jou, T.S., Schneeberger, E.E., Nelson, W.J. 1998. Structural and functional regulation of tight junctions by RhoA and Rac1 small GTPases. *J Cell Biol* **142:**101-15

Wu, S., Lim, K.C., Huang, J., Saidi, R.F., Sears, C.L. 1998. Bacteroides fragilis enterotoxin cleaves the zonula adherens protein, E-cadherin. *Proc Natl Acad Sci U S A* **95:**14979-84

Wu, S., Shin, J., Zhang, G., Cohen, M., Franco, A., Sears, C.L. 2006. The Bacteroides fragilis toxin binds to a specific intestinal epithelial cell receptor. *Infect Immun* **74:**5382-90